Characterization of the Mechanisms Involved in Maintenance of Apical Trafficking and Polarity in Intestinal Epithelial Cells

By

Byron Andrew Clarence Omar Knowles

Dissertation

Submitted to the Faculty of the

Graduate School of Vanderbilt University

in partial fulfillment of the requirements

for the degree of

DOCTOR OF PHILOSOPHY

in

Cell and Developmental Biology

August, 2014

Nashville, Tennessee

Approved by:

Matthew J. Tyska, Ph.D.

Robert Coffey, M.D.

Albert Reynolds, Ph.D.

David Bader, Ph.D.

James R. Goldenring, M.D., Ph.D.

To my amazing mother who always pushed me to be better

even when I got the highest grade on the exam

and

To my brother, Brenric, who always believed in me

ACKNOWLEDGEMENTS

I would like to thank my advisor, James R. Goldenring M.D., Ph.D. for helping me to become a scientist and cell biologist, no matter how much I tried to be a clinician. Jim has always provided me with support, and has always been available, even at his home, for one on one chats about science and life. From my first day in the Goldenring lab, I learned something new, and I have continued to learn new things every day since then. As I began my training I became very ill, and I contemplated giving up on science all together. But, Jim was incredibly encouraging and helped me to get better and was always available to make sure I was okay. I could not imagine doing my training in a better lab, thank you Jim.

I would also like to thank my committee members: my chair Matthew Tyska, Ph.D., Robert Coffey, M.D., David Bader, Ph.D., and Albert Reynolds, Ph.D. My committee has always provided beneficial comments and useful criticism of my work, and has consistently helped to make my work better. Dr. Reynolds has always been very stoic in my committee meetings, but his questions have been consistently insightful and helped to illuminate flaws in parts of my research. Dr. Coffey and the Coffey lab work closely with the Goldenring laboratory through the Epithelial Biology Center, and they have always been available for reagents and help with designing projects. My chair Dr. Tyska and his lab have also helped with several projects, and we have been collaborating since I joined the Goldenring lab. I would like to give special thanks to Dr. Bader for all the great talks we have had. They have helped me make it to the next experiment. My training would have been incomplete without the guidance of my

committee. I would be remiss if I did not thank Elaine Caine for all the reminders, organizing most of my Ph.D. training, and the words of encouragement.

The Goldenring lab has become like a second family to me, and every member of the lab has helped me to do at least one experiment or another in the past 4 years. I would like to first thank Dr. Victoria Weis. Tori has helped me with almost all of the projects that I started since I joined the lab, and slowly like Lex Luthor and Superman our friendship grew into “arch rivalry”. She has always been willing to read proposals and random papers, and have given me a lot of helpful feedback. Dr. Ki Taek Nam and Dr. Eunyoung Choi have consistently helped with mouse work, and have helped me to become a better animal scientist. Christine Pope-Petersen has been my workout buddy and little sister in the lab since she joined, and we have had great talks about all facets of life. Dr. Sousa has helped with designing primers for RT-PCR, and has always provided helpful feedback. Cathy Caldwell has been a great lab manager, and has been helping me with cell culture since I joined the lab. Dr. Joseph Roland has helped with every facet of my project, and I would not have been able to do many parts of my project without the constructs that he designed. I would also like to thank Zack Bradshaw and Yixi Tu who worked for Dr. Joseph Roland. Under Joe’s guidance they have helped to trouble shoot actin pull-down experiments for MYO5B constructs. The AKAP group consisting of Dr. Mason and Dr. Kolobova has also provided endless support. Finally, the Rab group of which I slowly became a member has helped with numerous parts of my work. Kenya Avant-Mitchell who was like a big sister to me is sadly no longer in our lab, but she has helped with numerous western blots along with Dr. Krishnan. Dr. Williams, my second big sister in the lab, has always helped with

numerous projects and she has continued to help with electron microscopy preparation and imaging as a staff scientist at VUMC Cell Imaging Shared Resource. Dr. Schafer, Dr. Franklin, and Dr. Lapierre have always been available for questions about experiments, and have helped continuously in many parts of my research.

I would also like to thank my funding sources. This work has been supported by the NIH grant RO1 DK70856 to J.R.G. This work was also supported by core resources specifically, the VUMC Cell Imaging Shared Resource, Translational Pathology Shared Resource, VUMC Digital Histology Shared Resource, and the shared resources of the Vanderbilt Epithelial Biology Center.

I would like to thank my family both here in Nashville and in the Bahamas for always believing in me, and helping me to be a better person. Specifically, I would like to thank my fiancée Rachel for all of the long nights, and for helping out when I wasn't able to do much of anything besides stare at the computer screen. I would also like to thank my brother Brenric who is always there for me no matter what I ask him to do. Finally, I would like to thank my mom "Mrs. Knowles" for never letting me get away with anything. You have all helped me to become the person I am, and I hope that I will always make you proud.

TABLE OF CONTENTS

Page

LIST OF TABLES

Table **Page**

LIST OF FIGURES

Figure **Page**

CHAPTER I

To the apical membrane and back: Vesicle trafficking and the establishment of polarity in epithelial cells

Adapted From: Knowles, B.C. and Goldenring, J.R. (2014). “To the apical membrane and back: Vesicle trafficking and the establishment of polarity in epithelial cells.” Review in progress. Physiology.

A definition of polarity

The concept of polarity depends greatly on context. At its most basic level in the context of general cell biology, polarity constitutes directed, purposeful movement within a cell. Under this concept, there likely is no eukaryotic system without aspects of polarity or polarized function. For example, budding yeast utilizes trafficking to a specific region of the plasma membrane to form the expanding bud. Phagocytes move directionally by polarizing their transport and cytoskeletal systems to deliver membrane and then retrieve it from a leading edge. Neurons elaborate highly polarized dendritic and axonal processes that define neuronal circuitry. However, for the purpose of this chapter, we will focus on the most organized example of polarity: the assembly of highly polarized epithelial mucosal cell layers. These polarized mucosal sheets provide a tight barrier between the external world and the internal milieu in animals (Rodriguez-Boulan and Macara 2014). In the following pages, we will review the mechanisms that are required to maintain the polarized epithelial mucosa in normal physiology and pathophysiology.

Defining polarity in epithelial cells

The ability to preserve and recycle limited resources is vital to the proper function of all tissue types. In epithelial cells, this is especially apparent in recycling across apical and basolateral domains in polarized cells to establish electrochemical gradients and recover receptors (Forte and Zhu 2010). Vesicle membrane trafficking and recycling underlies these diverse cellular processes, and is the primary process responsible for asymmetric distribution and maintenance of the plasma membrane proteins that leads to proper lumen development and cellular polarity (Bryant, Datta et al. 2010). Cellular polarity is demarcated by distinct apical and basolateral domains that are functionally divided. How epithelial cells set up apical and basolateral domains is not entirely understood, but continuous dynamic apical trafficking is necessary to establish polarized epithelial cells. Proteins destined for the plasma membrane are trafficked to the correct cell surface through a dynamic interplay of *de novo* protein synthesis and membrane recycling, with the trans-golgi network (TGN) and early endosomes serving as the main sorting stations, respectively (Ikonen and Simons 1998). Vesicular trafficking is initiated by budding of vesicles from these sorting stations, followed by targeted trafficking of vesicles, and vesicle fusion. The apical recycling endosome serves as the arena in which this dynamic interplay between the TGN and early endosomes occurs. Together, these processes establish normal apical and basolateral plasma membrane surfaces through the action of intracellular trafficking on dynamic cytoskeletal highways, utilizing membrane trafficking regulators including Rab, Rho, Rap, and Arf small GTPases and their effectors (Rodriguez-Boulan and Powell 1992). Maintenance of these polarized cells requires continuous apical and basolateral

recycling, the arrangement of adherens junctions to connect neighboring cells, and the tight junctions fence to prevent the random diffusion of proteins and lipids across apical and basolateral domains on the plasma membrane (Nelson, Wilson et al. 1992; Marrs, Andersson-Fisone et al. 1995; Yeaman, Grindstaff et al. 1999). Notably, dominant negative mutations or loss of vesicular trafficking, apical recycling, adherens junction, or tight junction proteins lead to significant polarity deficits in a wide array of epithelial cell types (Furuse, Hata et al. 2002; Capaldo and Macara 2007; Bryant, Datta et al. 2010; Sakamori, Das et al. 2012; Sato, Iwano et al. 2014).

Plasma membrane composition is determined by vesicle trafficking: lessons from non-polarized cell systems

Vesicle trafficking of proteins and lipids has been extensively studied in HeLa and other non-polarized cells over the past three decades. Indeed the insights gleaned from initial work in these cell lines set the framework for research in polarized epithelial cells. In non-polarized cells after initial synthesis, cargo destined for the plasma membrane is sorted through the TGN. This process is facilitated by the aggregation of proteins and formation of discrete sub-domains via Arf activation, which recruits trafficking machinery including: adaptor proteins, clathrin, phosphatidylinositol-4-kinase, Rab6, and GRIP-golgins. Then in conjunction with the proteins sorting signals the trafficking machinery determines the ultimate destination of proteins (De Matteis and Godi 2004). Phosphatidylinositol-4-phosphate (PtdIns(4)P) that is catalyzed by phosphatidylinositol-4-kinase recruits clathrin and clathrin-associated adapter proteins (APs) to the TGN, which aid in the targeting of specific vesicles and cargo to their ultimate destination (Bonifacino 2014).

In general, protein sorting is mediated by either the structure of the protein or the structure of its receptors with the adapter protein complex. Protein sorting signals are small internal peptide motifs that determine if proteins should be sorted to the plasma membrane, organelles, or vesicles (Pandey 2010). In addition, other determinants, including lipid composition, membrane curvatures, and small GTPases, ensure that cargo is trafficked to specific locations. The regulation of many trafficking pathways are not well characterized, but Rab-dependent trafficking pathways have been studied extensively. For example, Rab6 organizes the TGN and promotes the trafficking of

exocytic vesicles through its effector kinesin-1 (Grigoriev, Splinter et al. 2007). Rabs act as organizers of multi-protein trafficking complexes, thereby determining the localization and targeting of discrete vesicle populations (Novick and Zerial 1997).

Endocytosis utilizes Rabs to determine cargo fate

Endocytosis at the plasma membrane internalizes transmembrane proteins, receptors, lipids, and extracellular fluids either constitutively or through ligand-induced internalization (Grant and Donaldson 2009). This process can involve several endocytic pathways including: clathrin-dependent endocytosis, clathrin-independent endocytosis (including caveolae), macropinocytosis, and phagocytosis. In an analogous role to Arfs on the TGN, Rabs, in particular Rab4 and Rab5, recruit trafficking machinery to the early endosomes to generate phosphatidylinositol-3-phosphate (PtdIns(3)P), which in turn recruits EEA1 and PIKFyve proteins (Stenmark, Aasland et al. 2002). These proteins can interact directly with syntaxin-6 and syntaxin-13 to facilitate homotypic fusion or vesicle fission with the aid of phosphatidylinositol-3,5-phosphate (Mills, Jones et al. 1998; Lawe, Chawla et al. 2002; Cabezas, Pattni et al. 2006). Consequently, constitutive activation of Rab5 using a Rab5-Q79L mutant causes the accumulation of enlarged early endosomal vesicles (Stenmark, Parton et al. 1994). In addition, EHD family proteins work with Rab4 and Rab5 to regulate early endosome trafficking (Sharma, Naslavsky et al. 2008). Trafficking from the early endosome to the plasma membrane, recycling endosome, lysosome, or TGN requires sorting signals. Sorting nexins (SNX1, SNX2, SNX5, and SNX6) are recruited to the early endosome and facilitate retromer formation and transport through Rab5-dependent pathways in conjunction with EHD1 and EHD3, which aid in the transport of cargo to the TGN

(Naslavsky, Boehm et al. 2004; Mari, Bujny et al. 2008; Rojas, van Vlijmen et al. 2008). Once at the TGN, Rab31, a member of the Rab5 subfamily, facilitates trafficking of cargo from the TGN back to the early endosome, while Rab13 and Rab14 promote trafficking to the common recyling endosome (CRE) (Kajiho, Sakurai et al. 2011). Final attachment and fusion of vesicles to the plasma membrane and to other vesicles is facilitated by cargo-specific vesicle-Soluble NSF Attachment Protein REceptors (SNAREs). Specific combinations of SNAREs from both membranes form the core of the SNARE complex and these partners dictate the specificity of membrane fusion. The SNARE core complex proteins must be targeted to appropriate vesicles and plasma membrane surfaces by trafficking machinery, and failure to target these proteins disrupts vesicular trafficking in polarized cells (Reales, Sharma et al. 2011).

In the early endosomes, Rab4 sub-domains either target cargo back to the plasma membrane (fast-recycling) or to Rab11 positive recycling vesicles with the support of EHD3 and EHD4 (slow-recycling) (Hopkins and Trowbridge 1983; Ward, Martinez et al. 2005). This process is best illustrated by transferrin (Tfn) and transferrin receptor (TfnR), which are the most well studied ligand and transmembrane receptor pair to utilize recycling endosomes in non-polarized cells. TfnR binds to Tfn on the cell surface and clathrin-dependent endocytosis is initiated, which delivers the Tfn/TfnR complex to the early endosome. The Tfn/TfnR complex is then slated for fast recycling back to the plasma membrane, slow recycling via the recycling endosomes, or targeted to the lysosomes through Rab7-dependent pathways via degradation signals and ubiquitination (Lakadamyali, Rust et al. 2006; Girard, Chmiest et al. 2014). Expression

in non-polarized cells of dominant negative (Rab11aS25N) Rab11a inhibits recycling of Tfn/TfnR complex (Ullrich, Reinsch et al. 1996).

Adding a further level of complexity, Rab11 Family Interacting Proteins (Rab11-FIPs) further define recycling endosome sub-domains (Baetz and Goldenring 2013). Rab11-FIPs can bind to multiple Rabs, which may allow them to act as mediators of handoff between vesicles during vesicle trafficking from one vesicle to another. For example, Rab11-FIP1C binds both Rab11a and Rab14, and Rab11-FIP3 binds to Rab11a and Arf6. Thus, the Rab11-FIPs may provide a mechanism for Rab-mediated handoff between the TGN and the recycling endosome (Hickson, Matheson et al. 2003; Fielding, Schonteich et al. 2005; Kelly, Horgan et al. 2010; Qi, Williams et al. 2013).

Rab11-FIPs are one of the most well characterized families of Rab effectors (Hales, Griner et al. 2001). Rab11-FIPs interact mainly with GTP-bound Rab11 family members (Rab11a, Rab11b, and Rab25), but individual Rab11-FIPs also interact with Rab8a, Rab14, Arf6, MYO5A, MYO5B, SNX18, dynein, and kinesin-2 (Horgan, Hanscom et al. 2010; Ducharme, Ham et al. 2011; Willenborg, Jing et al. 2011; Baetz and Goldenring 2013). Interestingly, MYO5B functions as a direct effector for Rab11 family members and also directly interacts with Rab11-FIP2 (Schafer, Baetz et al. 2014). Overexpression of Rab11-FIP1B, Rab11-FIP1C, and Rab11-FIP3 can change the localization of Rab11a-positive vesicles and elicits tubulation of these vesicles in HeLa cells (Baetz and Goldenring 2013). This suggests Rab11-FIPs can regulate sub-domain formation and the velocity of cargo movement, since tubulation of vesicles indicates the slowing down of vesicle movement. Rabs that interact with Rab11-FIPs may act as the limiting reagent in vesicle trafficking, and the Rab11-FIPs might

competitively bind to Rabs along the trafficking pathway facilitating directed movement of various vesicles. These networks created by the Rabs and linked together by the Rab11-FIPs and other effectors provide a broadly dynamic staging point for regulating the flow of cargo toward and away from the plasma membrane through the recycling endosome (Goldenring 2013).

Myosin V in protein trafficking and recycling

In vertebrates, there are three isoforms of myosin-V: myosin-Va (MYO5A), myosin-Vb (MYO5B), and myosin-Vc (MYO5C) (Pastural, Barrat et al. 1997; Rodriguez and Cheney 2002; Velvarska and Niessing 2013). The heavy chains of class V myosins function as homodimers that are activated by calcium binding to the calmodulin on its IQ domains and cargo binding to the tail domains. These motors have three distinct domains that work together to generate movement that allows transport of cargo bound to the tail domain. Each head of class V myosins travel along F-actin by taking 74 nm steps, and moves at a velocity between 200-450nm/s for 2-2.4μm without detaching (highly processive motor) (De La Cruz, Wells et al. 1999; Mehta, Rock et al. 1999; Rief, Rock et al. 2000; Pierobon, Achouri et al. 2009). The slow movement of myosin-V gave rise to the theory that it may act as a dynamic tether for cargo bound to the tail domain by tread-milling in place on F-actin (De La Cruz, Wells et al. 1999; Mehta, Rock et al. 1999; Rief, Rock et al. 2000; Provance, Addison et al. 2008; Pierobon, Achouri et al. 2009; Schafer, Baetz et al. 2014). All three of these isoforms can bind to both Rab8a and Rab8a, but only MYO5A and MYO5B can bind to Rab11 family members. Interestingly, MYO5A has a unique binding region exon F for Rab27. Previous work using dominant negative tail constructs of MYO5B, illustrated that MYO5B is required

for trafficking transferrin, transferrin receptor, and MHC class I in HeLa cells (Lapierre, Kumar et al. 2001; Brock, Goldenring et al. 2003; Cresawn, Potter et al. 2007; Roland, Kenworthy et al. 2007; Roland, Lapierre et al. 2009). Mutations in MYO5A or MYO5B cause Griscelli syndrome type 1 or Microvillus Inclusion Disease (MVID), respectively (Takagishi and Murata 2006; Erickson, Larson-Thome et al. 2008; Muller, Hess et al. 2008). Mutations in MYO5C do not cause any known disease, but it plays an important role in secretory granule trafficking (Rodriguez and Cheney 2002; Marchelletta, Jacobs et al. 2008). As a whole, the isoforms of myosin-V are very diverse in their function and tend to play a variety of roles in different cell types.

Through its interactions with Rabs, MYO5B plays a crucial role in vesicle recycling, and has profound effects on the activity of recycling endosomes (Bryant and Mostov 2008). For example, insulin-stimulated translocation of vesicles containing GLUT4 is required for dietary glucose uptake into muscle and fat cells, and defects can lead to obesity and type II diabetes. In muscle cells, insulin activates Akt (also known as Protein Kinase B) which phosphorylates AS160 and TBC1D1, two GAPs for Rab8, Rab10, and Rab14. Consequently, Rab8a coupled to MYO5B traffics GLUT4 to the plasma membrane (Ishikura and Klip 2008). The rest of this chapter will focus on the apical recycling endosomes role as the decision point for endocytosis and exocytosis in conjunction with Rab small GTPases and its effectors, and how these decisions determine apical polarity in epithelial cells.

Apical and basolateral polarity is required for epithelial cell function

Polarized epithelial cells line the internal organs of the pulmonary, gastrointestinal, and genitourinary systems. The establishment of apical-basal polarization in epithelial cells requires the maintenance of stable functionally distinct apical (oriented toward the environment) and basolateral (oriented toward the internal milieu) plasma membrane domains (Figure 1). The apical and basolateral surfaces differ not only in their spatial location, but also in the enrichment of their constitutive proteins and lipids. For example, a key determinant of the apical surface identity is its enrichment in inner leaflet phosphatidylinositol-4,5-bisphosphate (PtdIns(4,5)P_2) and outer leaflet glycosphingolipids. Similarly, the basolateral surface is enriched for inner leaflet phosphatidylinositol-3,4,5-triphosphate (PtdIns(3,4,5)P_3) and outer leaflet phosphatidylcholine (Simons and van Meer 1988; Gassama-Diagne, Yu et al. 2006; Martin-Belmonte, Gassama et al. 2007). Variances in lipid composition might serve as indicators for cellular localization, because ectopic localization of PtdIns(3,4,5)P3 to the apical surface redistributes protein in MDCK cells (Gassama-Diagne, Yu et al. 2006). Interestingly, vesicles destined for either the apical or basolateral surface become similar to the surface they are being targeted to as they are trafficked toward that surface. For example, phosphatidylinositol-4-phosphates (PtdIns(4)P), enriched in the TGN, is produced via Arf recruitment of phosphatidylinositol-4-kinase. PtdIns(4)P causes the recruitment of CERT and FAPP2, which are precursors of glycosphingolipids and other lipids (De Matteis, Di Campli et al. 2007). Notably, these lipids tend to form membrane bilayers for which GPI-anchored proteins have an affinity, and may represent a possible mechanism for aggregation of these proteins before being sorted.

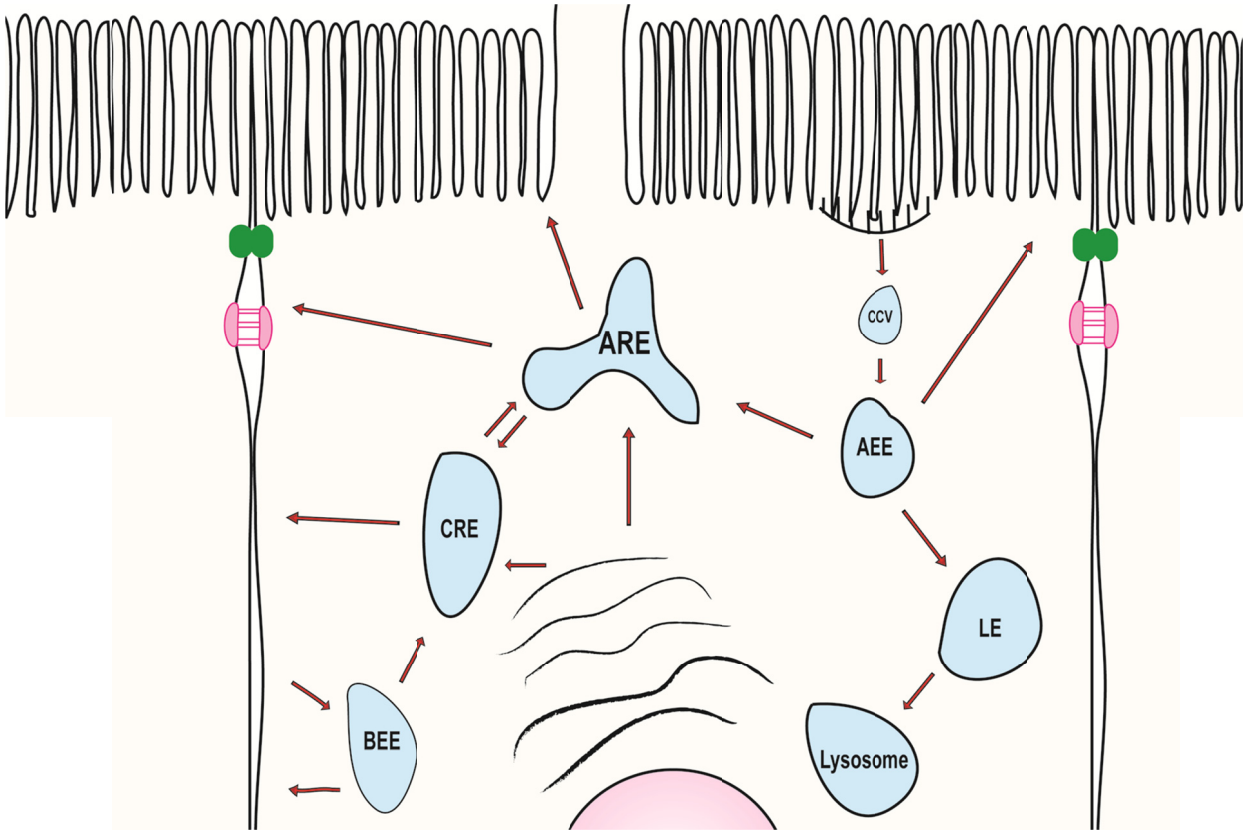

Figure 1. Dynamic trafficking through both the exocytic and endocytic trafficking pathways maintains polarity in epithelial cells.
Once apical and basolateral proteins are endocytosed sorting signals determine which trafficking routes are taken. When degradation signals and ubiquitination predominate, proteins are targeted to lysosomes through Rab7-dependent pathways. Some proteins are sorted immediately back to the plasma membrane via Rab4 sub-domains, but can also be transferred to the CRE or ARE. From these recycling endosomes, proteins are sorted back to the plasma membrane through Rab11a-dependent pathways. Proteins can also be targeted to the TGN through Rab5-dependent pathways. Newly synthesized proteins are trafficked from the TGN, which is organized by Rab6. Rab31 can facilitate trafficking from the TGN to early endosome and both Rab13 and Rab14 promote trafficking to the CRE. These vesicular trafficking networks appear to be linked together by Rab11-FIPs, which may mediate vesicle handoff between different small GTPases.

As in non-polarized cells, in polarized cells specific trafficking pathways are responsible for targeting proteins to their appropriate plasma membrane destinations. Trafficking of cargo in polarized cells is more complex than trafficking in non-polarized cells and requires the specific assembly of apical or basolateral trafficking machinery on specific sub-domains (Ikonen and Simons 1998). In general, basolateral sorting signals are found on the cytosolic tails of membrane proteins and are often based on tyrosine or di-leucine motifs (Bonifacino and Traub 2003). Apical sorting signals are highly varied and are based not only on cytosolic tail motifs, but also on post-translational lipid modifications, carbohydrate modifications, and other poorly understood signals. For example, N- and O-linked glycosylation of serine, threonine, and hydroxylysine aids in the targeting of proteins to the apical surface in part through interactions with lectins (Yeaman, Le Gall et al. 1997; Gut, Kappeler et al. 1998; Stechly, Morelle et al. 2009; Mishra, Grzybek et al. 2010).

Endocytosed cargo trafficking from the apical and basolateral early endosomes is facilitated by the recruitment of trafficking machinery to sort cargo back to the plasma membrane, recycling endosome, or TGN (Mellman 1996). Once a vesicle has been targeted to the apical or basolateral surface a number of routes can be taken. Thus, these vesicles must be directed. Trafficking from the TGN to the apical surface exploits either the direct (exocytosis) or indirect (transcytosis) route in a cell type-specific manner and utilizes AP-1A and AP-3 adapter protein complexes. For example, kidney cells generally use the direct route (Forte, Hanzel et al. 1989; Ellis, Potter et al. 2006). Conversely, enterocytes and hepatocytes utilize the indirect route extensively, but not exclusively (Hubbard, Stieger et al. 1989; Matter, Brauchbar et al. 1990). The direct

route from the TGN to the apical surface can traverse the apical recycling endosome (ARE) directly, pass through the apical early endosome (AEE), or traverse the CRE and then the ARE before finally fusing to the apical surface. The indirect route from the TGN traverses the CRE or basolateral early endosome (BEE) before fusing with the basolateral surface followed by transcytosis to the apical surface utilizing clathrin-dependent trafficking through the BEE, CRE, and finally the ARE before apical fusion.

In MDCK cells, trafficking from the TGN to the CRE is facilitated via sub-domains of trafficking machinery on the TGN organized by either Rab13 or Rab14 (Kitt, Hernandez-Deviez et al. 2008; Nokes, Fields et al. 2008). Rab effectors fine tune trafficking of cargo at each step of trafficking toward and away from the apical surface, and play key roles in membrane recycling. For example, aquaporin 2 recycling to the plasma membrane in renal collecting duct principal cells is regulated by myosin Vb (MYO5B) coupled to Rab11-FIP2 both of which are Rab11 effectors (Nedvetsky, Stefan et al. 2007). Notably, disruption of the t-SNARE syntaxin-3 (STX3) perturbs apical delivery of proteins, and it is likely a general SNARE for apical membrane fusion (Sharma, Low et al. 2006). Syntaxin-2 (STX2) may also function as an apical SNARE, but it has also been detected on the basolateral surface (Band and Kuismanen 2005). VAMP7 and VAMP8 associate with apical membrane SNAREs, and may differentially associate with vesicles through the direct or indirect pathways, respectively (Pocard, Le Bivic et al. 2007). Interestingly, syntaxin binding proteins (STXBPs) appear to regulate the specificity of the fusion event, and can promote or negate fusion between membranes (Misura, Scheller et al. 2000; Verhage, Maia et al. 2000; Rickman, Medine et al. 2007).

Vesicles that have been trafficked to the AEE through either the endocytic or exocytic pathway, as in non-polarized cells, can take one of several routes. They can utilize Rab5-mediated trafficking to the TGN, Rab4-mediated traficking back to the apical surface, or Rab4-mediated traficking to the ARE (Sonnichsen, De Renzis et al. 2000). After Rab4 facilitated handoff of cargo to the ARE, cargo can be sorted into Rab8a, Rab11a, Rab11b, or Rab25 sub-domains. Interestingly, in polarized cells overexpression of Rab25 appears to inhibit apical recycling of IgA, and suggests that Rab25 plays a role in negatively regulating apical recycling (Casanova, Wang et al. 1999). Rab15 and Rab17 are also localized to recycling endosomes, but little is known about their function on this vesicle (Lehtonen, Lehtonen et al. 1999; Strick and Elferink 2005). Unexpectedly, Tfn/TfnR complex appears to be excluded from the Rab11-positive vesicles of the ARE in polarized kidney epithelial cells; however, recent studies have shown that loss of MYO5B, an effector of Rab11, causes accumulation of Tfn/TfnR complex in the sub-apical compartment in enterocytes (Leung, Ruiz et al. 2000; Knowles, Roland et al. 2014).

Basolateral trafficking in most cell types utilizes the direct route from the TGN through the BEE or CRE using either clathrin-dependent AP-1B or clathrin-independent AP-4 adaptor protein complexes. E-cadherin, however, traverses the CRE and is then trafficked to the ARE before it is ultimately delivered to the basolateral surface (Lock and Stow 2005; Desclozeaux, Venturato et al. 2008). Increasing evidence supports an individualized approach for trafficking, and demonstrates that trafficking machinery in one cell type might serve other functions in another. For example, Rab8a and Rab10 are enriched on common recycling endosomes and facilitate AP1B-dependent

basolateral targeting of cargo in MDCK cells (Schuck, Gerl et al. 2007). Note, both Rab8a and Rab10 are also required for apical primary cilia maintenance in MDCK cells as well. In enterocytes, however, Rab8a has been found to regulate apical cargo trafficking and maintenance of the apical surface through interaction with its effector MYO5B (Roland, Kenworthy et al. 2007; Sato, Mushiake et al. 2007; Knowles, Roland et al. 2014). Presumably, Rab8a has comparable basolateral trafficking activity in enterocytes, but its function in facilitating equivalent trafficking pathways remains to be determined. Final basolateral vesicle fusion appears to be facilitated in part by the t-SNARE syntaxin-4 (STX4), as disruption of STX4 basolateral targeting by AP1B abolishes basolateral identity in MDCK cells (Reales, Sharma et al. 2011).

Assembly of apical specializations define apical polarity

The apical surface is under continuous dynamic reconstruction, and is maintained by apical vesicle trafficking and recycling. To transport cargo, the apical recycling endosome in epithelial cells utilizes Rab8a, Rab11a, Rab11b, and Rab25 along with Rab11-FIPs and other effectors particularly: MYO5A, MYO5B, Rabin8, and Exoc6 (also known as Sec15) (Mammoto, Ohtsuka et al. 1999; Lapierre, Kumar et al. 2001; Zhang, Ellis et al. 2004; Roland, Lapierre et al. 2009; Knodler, Feng et al. 2010; Feng, Knodler et al. 2012; Takahashi, Kubo et al. 2012). Long range microtubule-based trafficking to the ARE itself may be facilitated by Rab11a/Rab11-FIP5/kinesin-2 complexes (Schonteich, Wilson et al. 2008). Once vesicles fuse with the ARE, cargo may aggregate in sub-domains that are maintained in their sub-apical positions by MYO5B before being trafficked to the apical surface. MYO5B coupled to Rab8a and Rab11a-dependent trafficking is required to establish apical polarity in MDCK cells, and phosphorylation Rab11-FIP2 (Rab11 effector) by Par1b (also known as MARK2) helps to establish basolateral identity (Roland, Bryant et al. 2011; Lapierre, Avant et al. 2012). How this process regulates key determinants of polarity specifically Cdc42, aPKC, Par3, and Par6 is not fully understood. A recent study, has demonstrated that inactivating mutations in MYO5B can cause reduction in Cdc42 and leads to the redistribution of aPKC in enterocytes (Knowles, Roland et al. 2014). Studies utilizing Matrigel to form cysts from MDCK cells have also demonstrated that Rab11a controls the apical targeting of Rab8a, which through Tuba controls active Cdc42 localization (Bryant, Datta et al. 2010). Rab8a and Rab11a through a component of the exocyst, which tethers vesicles to the plasma membrane before the fusion event, specifically Exoc6,

targets Par3 to the apical surface (Bryant, Datta et al. 2010). Interestingly, Rab8a or Rab11a loss disrupted single lumen formation in MDCK cells, and expression of an Exoc6 mutant, with defective Rab11 binding had a similar phenotype (Bryant, Datta et al. 2010). Thus, Rab8a and Rab11a in part through the exocyst establish and maintain epithelial cell polarity.

In epithelial cells, aPKC/Par3/Par6 complex normally assembles at the tight junction, and together with the Crumbs and Scribble complexes regulate apical and basolateral identity. Specialized apical cytoskeletal processes that depend on apical trafficking are key components of apical identity, and appear to only be established in fully polarized cells. The F-actin dependent apical structures require continuous apical trafficking and recycling of other actin binding proteins, and as a result these structures represent a nidus of apical trafficking. For example, ezrin a member of the FERM (4.1, Ezrin, Radixin, Moesin) family binds F-actin via the C-terminal FERM domain and binds to membrane proteins, lipids, or adaptor proteins on the apical plasma membrane via its N-terminal domain (Turunen, Wahlstrom et al. 1994; Niggli, Andreoli et al. 1995; Heiska, Alfthan et al. 1998; Serrador, Vicente-Manzanares et al. 2002). Notably, MYO5B loss in enterocytes causes a reduction in apical ezrin (Knowles, Roland et al. 2014). Ezrin switches between inactive (self-associated) and active (unfolded) conformations, which is mainly facilitated by phosphorylation of threonine 567 (T567) via aPKC and Mst4 in a MYO5B-coupled Rab11a-dependent manner in enterocytes (Zhu, Zhou et al. 2007; Dhekne, Hsiao et al. 2014). Phosphorylated ezrin organizes the apical terminal web and is a key component in the elongation of established immature microvilli (Saotome, Curto et al. 2004; Gloerich, ten Klooster et al. 2012).

Interestingly, parts of basolateral identity, mainly E-cadherin from the adherens junctions, appear to depend on apical recycling endosomes for proper basolateral assembly (Lock and Stow 2005; Desclozeaux, Venturato et al. 2008). Adherens junctions are formed by E-cadherin binding directly to p120-catenin, which organizes β-catenin binding to E-cadherin and α-catenin's indirect binding to E-cadherin through β-catenin (Reynolds 2007). Through α-catenin the adherens junction is connected to the actin cytoskeleton, maintains cell shape, and allows coordinated modification of epithelial cell layers (Shapiro and Weis 2009). Interestingly, E-cadherin trafficking to the lateral plasma membrane requires MYO5B coupled Rab11a-dependent trafficking, and loss or mutation of MYO5B causes redistribution of E-cadherin to both the apical and lateral plasma membranes (Desclozeaux, Venturato et al. 2008; Knowles, Roland et al. 2014).

Rab8a and Rab11 family members are involved in the establishment and maintenance of polarity and a variety of specialized apical structures including: primary cilia, canaliculi, and microvilli. Thus, the ARE is positioned at the center of these processes, and aids in the establishment and maintenance of polarity in epithelial cells. Together with trafficking from the TGN and early endosomes, these processes provide a mechanism for re-organizing both the apical and basolateral plasma membranes, internalization of nutrients, or transmission of signals (Fuller and Simons 1986; Goh, Huang et al. 2010). This leads to the presentation of the appropriate transporter proteins, channels, and receptors on the correct surface necessary for maintaining normal epithelial physiology. Apical trafficking and recycling in polarized epithelial cells

has been studied extensively in tubular kidney epithelial cells, gastric parietal cells, and enterocytes, which will be the focus of the remainder of chapter one.

Primary cilia as a focus of kidney epithelial cell apical trafficking

Specialized apical structures such as primary cilia, canaliculi, and microvilli are essential for the function of epithelial mucosal cells and depend on continuous vesicle trafficking (Nachury, Loktev et al. 2007; Zhu, Zhou et al. 2007; Muller, Hess et al. 2008; Feng, Knodler et al. 2012). Thus, the dynamic intracellular decisions in vesicle trafficking can negatively or positively alter the physiology of epithelial cells. This is exemplified by primary cilia in tubular kidney epithelial cells, which mainly function to sense and react to external shifts in fluid pressure. Primary cilia facilitate this function by acting as mechanosensors that extend into the lumen of kidney tubules (200-300 nm wide and 5-10 μm long). When urine flows through kidney tubules the primary cilia on these cells bend, and this causes rapid Ca^{2+} influx through the polycystin-1 (PC-1)/polycystin-2 (PC-2) calcium channel, mutations of which cause autosomal dominant polycystic kidney disease (ADPKD) (Ferkol and Leigh 2012).

The primary cilium is a single, microtubule based projection that originates from the basal body and extends onto the apical surface of most differentiated mammalian cells, with the exception of enterocytes above the crypt proliferative zone. Notably, the aPKC/Par3/Par6 complex and a component of the Crumbs complex (Crumbs-3) appear to localize to the base of primary cilium, and play a role in primary cilia formation. In MDCK cells, knocking down Crumbs-3 or inhibiting aPKC with a small molecule inhibited primary ciliogenesis, and knocking down Par3 in these cells reduced the length

of primary cilia (Fan, Hurd et al. 2004; Sfakianos, Togawa et al. 2007). Primary cilia dynamically assemble and disassemble their microtubule structures (axonemes) as cells change polarity, move through the cell cycle, and respond to cellular cues, especially removal of nutrients (Dingemans 1969; Fonte, Searls et al. 1971). Interestingly, chemically induced primary cilia shedding leads to reduction of tight junction component (claudin-2), random redistribution of apically trafficked gp80 (also known as clusterin) and gp114 (also known as CEACAM), and reduction in the basolateral protein Na/K-ATPase (Overgaard, Sanzone et al. 2009). Thus, the primary cilium is intimately linked to regulators of polarity, and changes in the primary cilia leads to alteration of epithelial cell polarity.

Construction and maintenance of the primary cilia is facilitated by continuous kinesin/dynein driven intraflagellar transport (IFT) that is targeted to the structure likely through an AP-1 dependent exocytic trafficking process with the help of Rab8a- and Rab10-positive exocyst tethering complexes (Kaplan, Molla-Herman et al. 2010; Nachury, Seeley et al. 2010; Lim, Chua et al. 2011). In MDCK cells, loss of the exocyst component Exoc5 (also known as Sec10) led to shortened primary cilia, whereas overexpression of Exoc5 led to elongated primary cilia (Zuo, Guo et al. 2009). The exocyst multi-protein complex (Exoc1-Exoc8) is physically tethered to the plasma membrane via Cdc42 through Exoc1 and Exoc7 before SNARE-mediated fusion, specifically by STX3 and SNAP-25 (Mazelova, Ransom et al. 2009). Rab8a, Rab10, and Rab11a are enriched at the base of the primary cilia, and Rab11a through its effector Rabin8, which acts as a GEF for Rab8a, facilitates cilia elongation (Babbey, Bacallao et al. 2010; Knodler, Feng et al. 2010). This suggests that Rabs on the same

vesicles can recruit the GEFs for other Rabs, and could represent a crucial mechanism for the progressive activation of Rabs as vesicles are shuttled from one compartment to another during trafficking. Notably, inhibition of Rab11a function using expression of dominant-negative (Rab11a-S25N) mutants or RNA interference inhibits primary ciliogenesis (Knodler, Feng et al. 2010). Together the Rab11a/Rab11-FIP3/Arf4/ASAP1 vesicular complex is involved in targeting and trafficking cargo destined for the primary cilia (Mazelova, Astuto-Gribble et al. 2009).

Elipsa (orthologue of mammalian IFT54) may link IFT with Rab8a associated vesicular transport through shared binding of Rabaptin5 (Omori, Zhao et al. 2008; Follit, Xu et al. 2009). The complexity of this and other interactions between vesicular trafficking and IFT is still not fully understood. For example, many proteins necessary for ciliogenesis localize to the mother centriole (also known as the basal body) including the most extensively studied class of Bardet-Biedl Syndrome (BBS) proteins that form the BBSome complex (Nachury, Loktev et al. 2007). Trafficking of BBSome complex to the basal body is regulated by Rab8a and Rabin8 (Jin, White et al. 2010). Rabin8 trafficking to the mother centriole, however, precedes primary cilia membrane assembly, and TRAPP II subunits co-localize with Rabin8 and is required for Rabin8 preciliary targeting and ciliogenesis (Westlake, Baye et al. 2011). Rab11a and BBS1 bind to the same area of Rabin8, and GTP-bound Rab11 appears to promote the interaction of BBS1 to Rabin8. However, it is still poorly understood how these proteins are handed off to microtubule-based IFT after vesicular trafficking to the basal body (Figure 2).

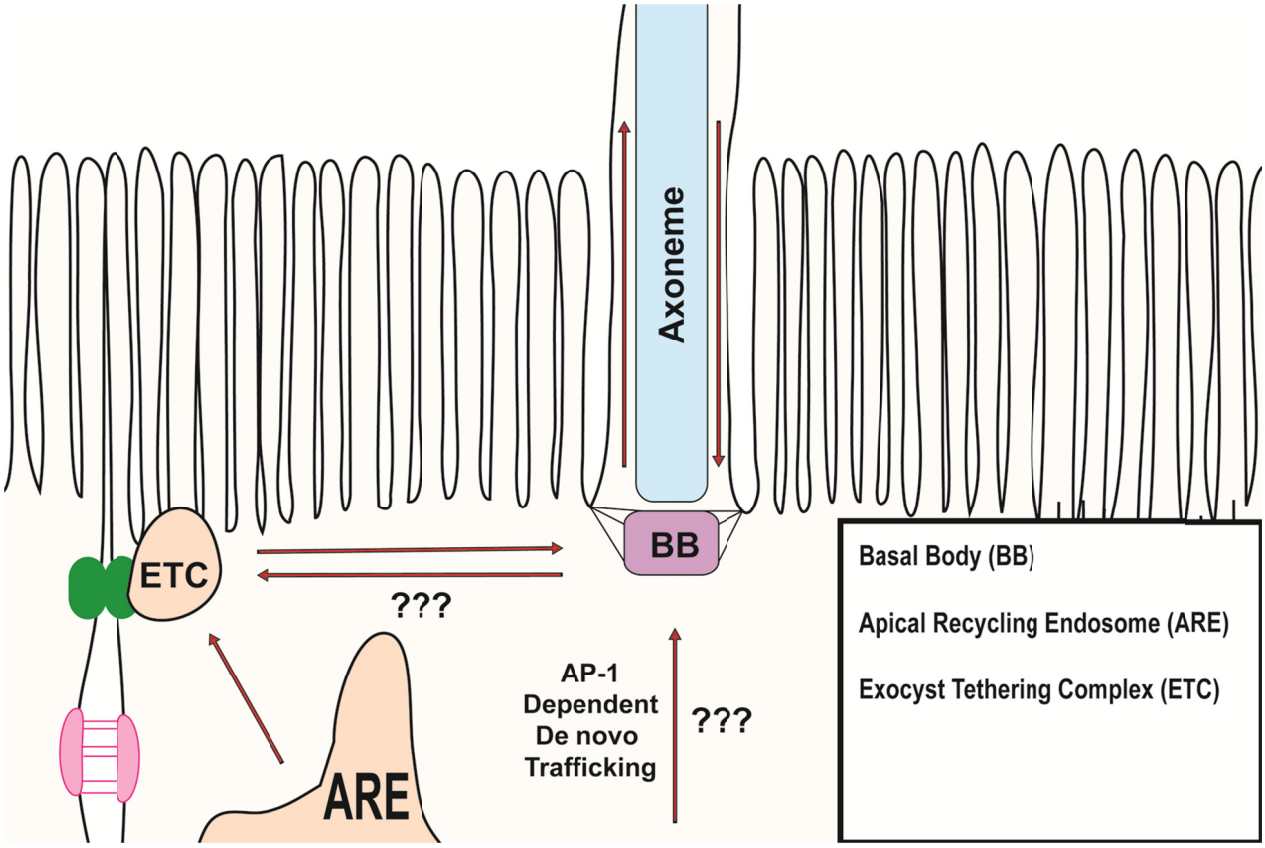

Figure 2. Primary cilia are maintained by continuous apical trafficking and recycling.
Direct targeting of newly synthesized proteins from the TGN to the primary cilia is theorized to occur through an AP-1 dependent mechanism that utilizes Rab8a and Rab10. However, this pathway has yet to be proven definitively. The exocyst is trafficked via Rab8a-, Rab10-, and Rab11a-positive vesicles to the apical surface. The exocyst complex is tethered to the plasma membrane by Cdc42, which binds to the exocyst components Exoc1 and Exoc7 before trafficking through an ill-defined mechanism to the primary cilia.

Intracellular canaliculi in parietal cell apical polarity

Gastric parietal cells were the first cellular model for regulated apical recycling as the primary pathway for movement of transmembrane proteins to the apical surface (Forte, Limlomwongse et al. 1969; Forte, Limlomwongse et al. 1969). Interestingly, these cells have the highest endogenous level of Rab11a of all polarized epithelial cells (Goldenring, Soroka et al. 1994). The main function of parietal cells is to secrete hydrochloric acid (HCl), for the sterilization of food and initiation of digestion. H/K-ATPase in parietal cells accomplishes this function by pumping protons (H^+) against an electrochemical gradient at the apical plasma membrane into the lumen of the stomach (Forte, Ganser et al. 1974). Intracellular membrane recycling in parietal cells is markedly elaborated to recycle H/K-ATPase stored intracellularly in tubulovesicular membranes, which can fuse with the extensive canalicular apical surface. In parietal cells, fusion of apical tubulovesicles to the apical canalicular surface is mediated by the core SNARE complex consisting of STX3, VAMP2, and SNAP25 (Calhoun, Lapierre et al. 1998; Karvar, Yao et al. 2002).

The secretory activity of parietal cells requires two apical structural arrangements comprising a resting and stimulated state. In the resting state, the apical surface is specialized to form apical canaliculi, which consist of an expanded apical plasma membrane with deep invaginations supported by F-actin bundles (Ammar, Nguyen et al. 2001). F-actin decorated with ezrin is vital to the function of parietal cells as inhibition by cytochalasins or latrunculin B of F-actin and/or loss of ezrin or mutation of the ezrin T567 phosphorylation site inhibits secretion of acid (Rosenfeld, McAllister et al. 1981; Yao, Thibodeau et al. 1993; Ammar, Nguyen et al. 2001; Zhou, Zhu et al. 2005).

Underneath the apical surface, an expanded ARE (Rab11a-positive vesicles) contains a resting pool of H/K-ATPase (Black, Forte et al. 1981; Goldenring, Soroka et al. 1994; Matsukawa, Nakayama et al. 2003). When stimulated by histamine or acetylcholine binding to their respective receptors on the basolateral membrane, H/K-ATPase containing vesicles fuse into apical canaliculi. This fusion event is coordinated with phosphorylation of ezrin-T567 and results in the formation of extended invaginations with increased availability of H/K-ATPase on the apical surface (Zhu, Zhou et al. 2007; Zhu, Crothers et al. 2010). Interestingly, a Rab11a dominant negative mutant (Rab11a-N124I) expressed in parietal cells inhibits acid secretion (Duman, Tyagarajan et al. 1999). After withdrawal of stimuli, H/K-ATPase is endocytosed from the apical plasma membrane, and forms vesicles that are recycled back to the ARE for future use (Sawaguchi, Aoyama et al. 2006). Concurrently, ezrin is dephosphorylated and relocated to the cytoplasm until ezrin phosphorylation is required for dynamic apical reestablishment (Figure 3) (Zhu, Crothers et al. 2010). This highly elaborated recycling pathway exemplifies a general, if amplified, pattern of Rab11a-dependent apical recycling to an F-actin and ezrin-enriched apical membrane surface.

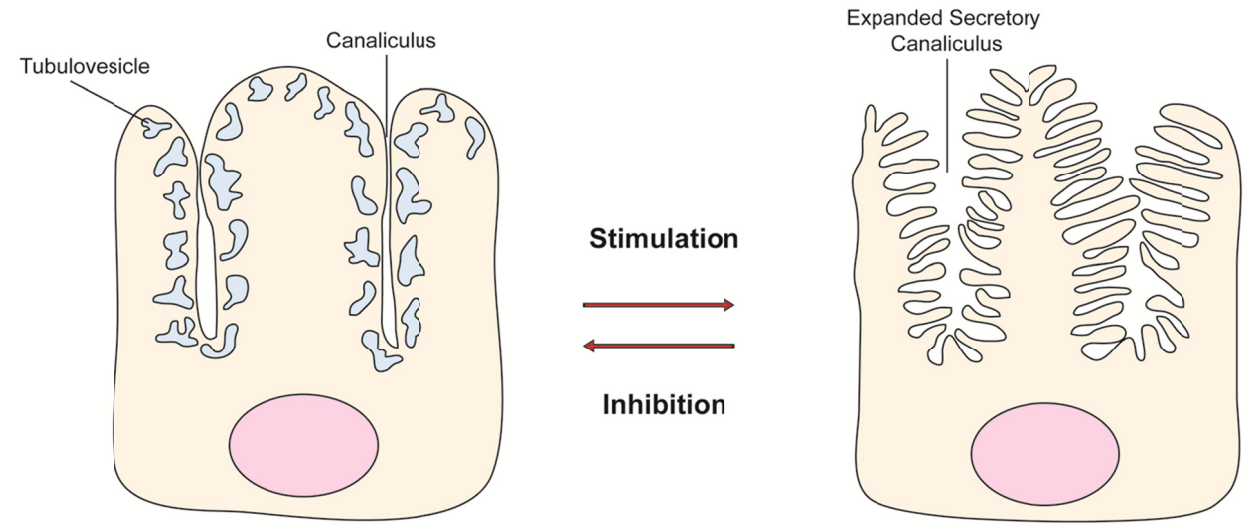

Figure 3. Stimulation of parietal cells causes fusion of H/K-ATPase vesicles to the plasma membrane through Rab11a-dependent mechanism.
Parietal cell stimulation also triggers ezrin phosphorylation and concomitant invagination of the canalicular surface.

Microvilli are indicators of enterocyte apical polarity

In normal enterocytes, a mature apical brush border can only be established in completely polarized cells, and serves as a cue for cellular polarity as a whole. Indeed, the formation of microvilli has been linked through the LKB1 (also known as Par4)-STRAD-MO25 complex to the establishment of apical polarity (ten Klooster, Jansen et al. 2009). After apical polarity is established, on the apical surface PtdIns(4,5)P2 is produced and initiates recruitment of phospholipase D1 (PLD1). PLD1 triggers an increase in phosphatidic acid, which ultimately begins a cascade of signaling events through PDZGEF that activates Rap2A and its effector TNIK on the apical surface (Gloerich, ten Klooster et al. 2012). This may trigger MYO5B-dependent recruitment of MST4 and aPKC to the apical surface, which is responsible for the phosphorylation of ezrin in enterocytes (Dhekne, Hsiao et al. 2014). Interestingly, EBP50 (ezrin binding protein 50 kDa) binds active ezrin and is phosphorylated by Protein Kinase C (PKC), which also aids in establishing epithelial polarity and microvilli formation (Garbett, LaLonde et al. 2010). EBP50 is also indirectly linked to apical trafficking through its interaction with EP164, which stabilizes Arf6-dependent trafficking and inhibits Rab8a-dependent recycling (Hokanson and Bretscher 2012). Thus, these processes link apical trafficking, establishment of apical identity, and brush border formation together as parts of overall epithelial polarization.

The primary function of enterocytes is to absorb nutrients from the lumen of the intestines, and they also play key roles in the final digestion of nutrients and host defenses. As enterocytes migrate from the villus crypt they differentiate, up-regulate, and traffic proteins necessary for microvillar assembly to the apical surface (Chang,

Chance et al. 2008). Absorption of nutrients is aided by several thousand microvilli (80nm wide and 1-2μm long) on each enterocyte that increase the surface area and consequently increase the absorptive capacity of enterocytes (Mooseker 1985). Inside the microvilli, the plus ends of F-actin filaments are located at the tips, with minus ends tethered into the terminal web, which is composed of numerous proteins including: spectrin, filamin, myosin-II, tropomyosin, villin-1, and fimbrin. Microvilli maintain constant length after initial establishment, and are under continuous dynamic assembly and disassembly with constant polymerization at the apical tip of each F-actin bundle (Mooseker and Tilney 1975). The microvilli themselves are composed of bundled F-actin cross-linked by bundling proteins and F-actin binding proteins including: ezrin, myosin-I, espin, fimbrin, and villin-1. As microvilli grow, harmonin/myosin-VIIb complex coupled to the F-actin bundle, positions Ca^{2+}-dependent inter-microvillar links that are established by protocadherin-24 and mucin-like-protocadherin to form the mature brush border (Crawley, Shifrin et al. 2014).

The mechanism behind the initial nucleation of the F-actin bundles of microvilli remains obscure, but recent studies have begun to unravel the mechanisms behind growth of microvilli after the initial nucleation event. MYO5B interaction with Rab8a promotes the initiation of microvilli growth, and MYO5B interaction with Rab11a is required for apical recycling of proteins and microvilli to the apical surface and facilitates microvilli maintenance (Knowles, Roland et al. 2014). As discussed previously, MYO5B-coupled Rab11a-dependent trafficking of MST4 and aPKC to the apical surface of enterocytes facilitate ezrin phosphorylation, which stimulates microvilli growth. Ezrin interacts with PtdIns(4,5)P2 and intracellular adhesion molecules on the apical plasma

membrane, and serves as a linker between the F-actin bundle and the apical plasma membrane (Heiska, Alfthan et al. 1998; Jayasundar, Ju et al. 2012). Consequently, ezrin knock-out mice have blunted intestinal villi, disorganized terminal web below the apical surface, and short, immature microvilli (Saotome, Curto et al. 2004). Thus, ezrin appears to be an indispensable organizer of mature brush borders. This concept is strengthened by studies utilizing knock-out mice of other constitutive microvillar proteins that have minimal effects on brush border formation in enterocytes including: villin-1 and myosin-Ia (Pinson, Dunbar et al. 1998; Tyska, Mackey et al. 2005). This is not surprising since critical functions tend to have built in redundancy to reduce the effects of otherwise detrimental loss or mutations of vital proteins. For example, myosin-Ic is redistributed from the basolateral surface to the apical surface to compensate for loss of myosin-Ia (Tyska, Mackey et al. 2005).

Phosphorylation of ezrin is integral to the formation of mature brush border in enterocytes. In enterocytes, ezrin loss may not be compensated for because the expression of FERM proteins is tissue specific. Compensation at its best, however, is imperfect. For example, villin-1 knock-out mice have impaired ability to remodel microvilli in response to cellular cues, but relatively normal microvilli (Ferrary, Cohen-Tannoudji et al. 1999). Multiple F-actin bundling proteins can bind to the F-actin scaffold of microvilli to regulate these bundles, which is an essential process. However, phosphorylated ezrin recruitment appears to be the rate limiting step in microvillar growth. Eps8L1a, a member of the Eps8 family of F-actin capping and bundling proteins, appears to work downstream of phosphorylated ezrin to regulate microvillar length. Indeed, loss of Eps8L1a causes unregulated microvillar growth, while

overexpression of Eps8L1a causes short immature microvillar development in LLC-PK1 cells (Zwaenepoel, Naba et al. 2012).

MYO5B in concert with Rab8a and Rab11a regulates the polarity of intestinal epithelial cells. The construction and maintenance of microvilli coincides with coordinated Rab8a- and Rab11a-dependent apical trafficking coupled to MYO5B, which facilitates proper microvilli growth through trafficking of key microvillar components (Figure 4) (Sato, Mushiake et al. 2007; Knowles, Roland et al. 2014). Most notably, recent studies have revealed that enterocytes might recycle microvilli from the apical surface, and defects in polarity or Rab11a-dependent MYO5B coupled pathway can halt this process (Vega-Salas, Salas et al. 1988; Achler, Filmer et al. 1989; Gilbert and Rodriguez-Boulan 1991; Knowles, Roland et al. 2014). This is not surprising since both Rab5 and Rab11a have been implicated as major regulators of actin cytoskeleton dynamics, and have been linked to the mediation of macropinocytosis, the only endocytic event that could facilitate this process (Lanzetti, Palamidessi et al. 2004; Wang, Kerr et al. 2010; Holubcova, Howard et al. 2013).

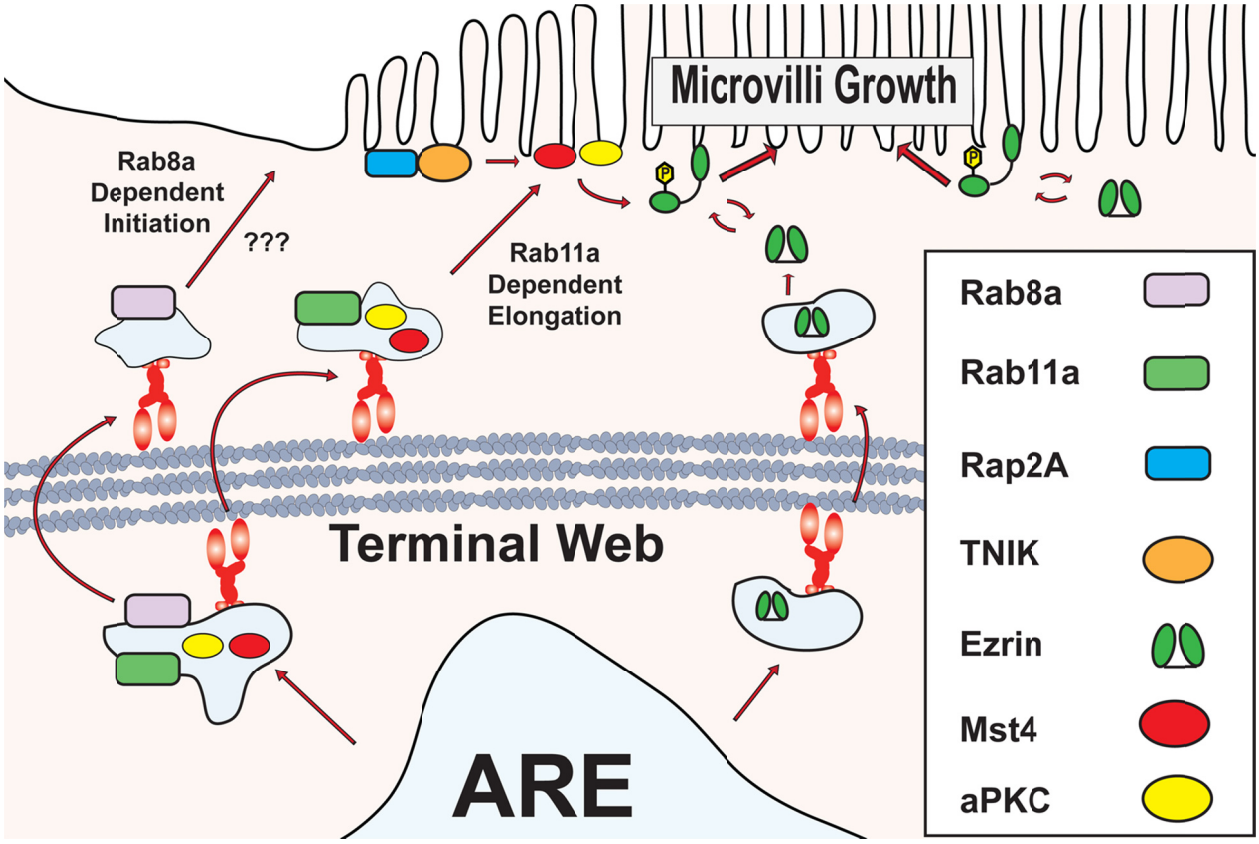

Figure 4. MYO5B in conjunction with Rab8a and Rab11a appears to play a key role in the initiation and growth of microvilli.
MYO5B in conjunction with Rab8a-dependent trafficking may be involved in the initiation of microvilli growth in enterocytes. However, no studies have uncovered the mechanism by which Rab8a mediates nucleation of microvilli. Recent studies have revealed that MYO5B may traffic ezrin, Mst4, and aPKC to the apical surface through a Rab11a-dependent trafficking pathway. Ezrin is in turn phosphorylated by Mst4 and aPKC, which stimulates microvilli growth.

Defects in apical polarity define mucosal disease pathology

Apical trafficking and recycling of cargo in polarized epithelial cells is integral to the identity and function of these cells, and as a result mutations in key components of this system would likely be evolutionarily unviable. In the general population, however, nonsynonymous SNPs are present in every imaginable component of this system (ESP 2014)(ESP 2014)(ESP 2014)(ESP 2014)(ESP 2014). Some of which should be detrimental, but they do not appear to cause known human diseases directly. Recently, another major area of our research has focused on the effects of mutations in MYO5B and its associated apical polarity proteins on the general population. The consequences of these subtle mutations in apical recycling in the human population are hard to predict, but studies done in the past decade have begun to shed light on the extreme end of this continuum. Classically, mutations in MYO5B that disrupt the function of this motor or induce premature termination before the tail domain can cause depolarization of enterocytes and lead to Typical MVID, a neonatal diarrheal disorder (Muller, Hess et al. 2008; Ruemmele, Muller et al. 2010; Szperl, Golachowska et al. 2011; van der Velde, Dhekne et al. 2013). Recently, mutations in *STX3* and *STXBP2 (Munc18-2)* have been implicated as the causative agents for an atypical form of MVID (Muller, Hess et al. 2008; Stepensky, Bartram et al. 2013; Wiegerinck, Janecke et al. 2014).

Typical and Atypical MVID

MVID was initially characterized in 1978 in newborns experiencing chronic, unremitting, secretory diarrhea (Davidson, Cutz et al. 1978). Studies of these patient biopsies from the small intestine displayed significant villus blunting, crypt hypoplasia,

absence of microvilli, malabsorption of glucose, and defective sodium transport. In spite of enteral feeding withdrawal, the secretory diarrhea persisted in these patients. MVID treatment has not changed significantly since the first recorded cases, and this disease is currently treated initially with total parenteral nutrition (TPN) and eventually with paired small intestine and liver transplant (Oliva, Perman et al. 1994). The causative agent of this disease was discovered after Sato et al. in 2007 demonstrated that Rab8a knockout mice displayed phenotypic similarities to MVID, and Roland et al. in 2007 observed that MYO5B regulates apical recycling by localizing with Rab8a-, Rab10-, and Rab11-positive vesicles in the ARE (Roland, Kenworthy et al. 2007; Sato, Mushiake et al. 2007). Together, these studies culminated in 2008 with reports from Austria and the United States that mutations in the *MYO5B* gene caused MVID (Erickson, Larson-Thome et al. 2008; Muller, Hess et al. 2008). However, in the original report from Europe, there was one MVID patient without any *MYO5B* mutation. Nonetheless, in the past 8 years there have been 41 published mutations in the *MYO5B* gene that cause MVID in patients (van der Velde, Dhekne et al. 2013). Recently, Wiegerinck, et al. 2014 identified two patients with mutations in *STX3*, an apically targeted t-SNARE, which caused Atypical MVID (Wiegerinck, Janecke et al. 2014). The recently reported Atypical MIVD involved two patients who presented with a milder phenotype when compared with Typical MVID patients (Wiegerinck, Janecke et al. 2014). Most notably, patients developed improved tolerance for enteral feeding. This disease presentation reinforces the role of apical trafficking and vesicle fusion in maintaining apical polarity in enterocytes. Interestingly, patients with mutations in *STXBP2 (Munc18-2)*, which

regulates STX3 vesicle fusion, have persistent chronic diarrhea and intestinal histological findings consistent with Atypical MVID (Stepensky, Bartram et al. 2013).

Investigations into the cause of these enteropathies have begun to unravel key findings in regards to MYO5B function in polarized cells, where it most likely functions as a dynamic tether to maintain both Rab8a and Rab11a at their appropriate sub-apical location (Roland, Bryant et al. 2011; Knowles, Roland et al. 2014). Rab11a-positive vesicles may utilize STX3 to facilitate vesicle fusion of apically trafficked protein to the plasma membrane, and STXBP2 might act as a regulator of the final fusion event in this pathway (Carmosino, Valenti et al. 2010). Both MYO5B and STX3 in polarized epithelial cells are involved in many essential vesicular trafficking pathways in epithelial cells, but mutations in both of these proteins appear to lack, at least initially, extra-intestinal manifestations in patients (ter Beest, Chapin et al. 2005; Lapierre, Avant et al. 2007). How this compensation occurs is not understood completely, but compensation is never comprehensive and other polarized epithelial cells of the kidneys and stomach also depend heavily on proper apical trafficking. As a result, mutations in either *MYO5B* or *STX3* could lead to deficits in the primary cilia and/or parietal cells. However, MVID patients do not commonly live to an age where either of these diseases would manifest. Consequently, determining the full scope of these mutations on human homeostasis is not presently feasible.

Regarding the Future

In this chapter, we have given a thorough overview of apical trafficking and recycling, and the consequences of its disruption on polarized epithelial cell identity and function. However, many areas in this field not addressed in this chapter are currently the targets of substantial investigation. One of these areas of particular interest to human disease is viral hijacking of intracellular trafficking systems. It has been established that expression of dominant negative MYO5B in MDCK cells leads to aberrant basolateral trafficking of RSV (Brock, Goldenring et al. 2003). HIV-1 also appears to utilize this system extensively as expression of dominant negative Rab11a and MYO5B disrupts the trafficking of HIV-1 protein (Vpu) through the recycling endosome, and abolished HIV-1 particle release (Varthakavi, Smith et al. 2006). Notably, MYO5B mutations appear to persist in certain populations in spite of the detrimental effects observed in homozygous patients. Thus, heterozygous carriers of MYO5B mutations may be protected against certain viral infections. However, this is one of the many areas in MVID research that has not been examined in detail. Perhaps the most significant question in regards to global human health that is coupled to MVID research is what are the consequences of nonsynonymous SNPs in apical trafficking components in apparently healthy individuals? In regards to cell biology, many apical trafficking questions have yet to be addressed, and will likely serve as robust areas of research for at least the next decade. For example, the role of MYO5B in parietal cell physiology is not completely understood, the protein responsible for the initial nucleation of F-actin bundles of microvilli has yet to be discovered, and it is still not fully understood if recycling of the apical brush border is a naturally occurring event. The

research reported in the next four chapters has laid the framework to answer these and many other questions.

Rationale and aims of proceeding work

MYO5B plays a crucial role in apical trafficking in enterocytes, and might perform similar roles in other highly polarized enterocytes. In the second chapter, we theorized that reduction of endogenous MYO5B would lead to a decrease in microvilli and apically trafficked proteins, and this phenotype could be exacerbated by the re-introduction of mutant MYO5B. I began to characterize this in MVID patient duodenum samples and CaCo2-BBE cells, by stably knocking down MYO5B, which caused loss of microvilli, alterations in components of tight junctions, and disruption of apical and basolateral trafficking. These changes appeared to be due to relocalization of Rab8a and Rab11a, which are tethered to apical MYO5B on F-actin. In the third chapter, we theorized that loss of Rab11a would lead to disruption of apical trafficking, and cause major disruption of apical polarity in enterocytes. The consequences of Rab11a loss and associated effects on apical trafficking, polarity, and microvilli length was characterized using both stable Rab11a knock down and intestinal conditional knockout of Rab11a ($Rab11a^{fl/fl}$;villin-cre^{+}) in mice. Of particular interest, was the redistribution of STX3 into cytoplasmic vesicles, which likely caused shortened microvilli and redistribution of other components of apical trafficking. In the fourth chapter, we hypothesized that MYO5B mutation should lead to loss of polarity in other highly polarized tissue with similar effects to what was previously observed in the small intestine. In the Navajo MVID patient stomach, liver, pancreas, and large intestine we observed marked loss of polarity. Of particular interest, the stomach parietal cells loss normal apical canalicular morphology. We also observed alterations in the distribution of MYO5B and its associated Rabs (Rab8a and Rab11a), and redistribution of apical and basolateral

markers. As a whole, the studies presented here will expand our current understanding of apical trafficking's role in epithelial polarity, and the consequences of alterations in components of the apical trafficking system on human diseases.

CHAPTER II

Myosin Vb uncoupling from Rab8a and Rab11a elicits microvillus inclusion disease

Adapted From: Knowles, B. C., J. T. Roland, et al. (2014). "Myosin Vb uncoupling from RAB8A and RAB11A elicits microvillus inclusion disease." The Journal of clinical investigation.

Introduction

Microvillus Inclusion Disease (MVID) is a rare neonatal diarrheal disorder of the small intestine that arises mainly in European, Middle-Eastern, and Navajo Native American cohorts (Erickson, Larson-Thome et al. 2008; Muller, Hess et al. 2008). Recent investigations have identified putative inactivating mutations in myosin Vb (*MYO5B*) in MVID patients. In the Navajo population, MVID has an incidence of 1 case per 12,000 live births, with a single homozygous *MYO5B-P660L* (1979C>T p.Pro660Leu, exon 16) mutation responsible for all of these cases, inherited in an autosomal recessive pattern (Pohl, Shub et al. 1999; Erickson, Larson-Thome et al. 2008). Of the 41 published mutations in the MYO5B gene that contribute to MVID, 16 mutations were homozygous, 9 mutations were heterozygous, and 16 further mutations were found in patients who have compound heterozygous mutations (Erickson, Larson-Thome et al. 2008; Muller, Hess et al. 2008; Chen, Chiang et al. 2010; Ruemmele, Muller et al. 2010; Golachowska, Dael et al. 2011; Szperl, Golachowska et al. 2011; Chiang, Hsu et al. 2013; Thoeni, Vogel et al. 2013; van der Velde, Dhekne et al. 2013).

MYO5B is a highly processive motor, which functions as a homodimer that is activated by calmodulin binding. Structurally MYO5B has three distinct domains: an N-terminal motor domain, a central light chain binding domain, and the C-terminal cargo-binding tail domain. The motor domain generates force and the central calmodulin light chain binding domain acts as the lever arm. Together, these domains generate motion that allows MYO5B to function as a dynamic tether for cargo bound to the tail domain by tread-milling in place on F-actin (De La Cruz, Wells et al. 1999; Mehta, Rock et al. 1999; Rief, Rock et al. 2000; Provance, Addison et al. 2008; Pierobon, Achouri et al. 2009; Schafer, Baetz et al. 2014). MYO5B has binding regions in its tail domain for Rab8a via exon C (exon 30), Rab11 via the globular tail, and Rab10 through its alternatively spliced exon D (exon 31). It should be noted, the predominant splice variant of *MYO5B* in enterocytes lacks exon D (Roland, Lapierre et al. 2009). Mutations that disrupt the function of the motor, lever arm, calmodulin binding, Rab binding, or induce premature termination before the tail domain can lead to MVID (Muller, Hess et al. 2008; Ruemmele, Muller et al. 2010; Szperl, Golachowska et al. 2011; van der Velde, Dhekne et al. 2013).

MVID was first characterized in 1978 in newborns with chronic, unremitting diarrhea (Davidson, Cutz et al. 1978; Chehade 2005). The underlying cause of the diarrhea remains to be determined definitively, but biopsy data points to a decrease in sodium absorption that could be the result of absent microvilli or leaky tight junctions in the enterocytes of the patients' small intestine (Rhoads, Vogler et al. 1991; Arpin 1999). In these biopsy samples, pathognomonic microvillus inclusions were observed in 10% of enterocytes. No studies until now have identified conclusively the origin or nature of

these structures (Cutz, Rhoads et al. 1989; Reinshagen, Naim et al. 2002). The accumulation of PAS-positive “granules” also occurs at higher frequency in MVID patient samples than in the enterocytes of normal duodenum (van der Velde, Dhekne et al. 2013). MVID is uniformly fatal and no current pharmacotherapy exists, but it can be treated with total parenteral nutrition (TPN) or an intestinal transplant (Oliva, Perman et al. 1994).

While recent studies have identified *MYO5B* mutations in MVID, the pathophysiology remains less clear. Previous investigations have established that microvillus inclusions contain apical enterocyte proteins such as sucrase isomaltase, alkaline phosphatase, and sodium hydrogen exchanger 3 (NHE3) (Ameen and Salas 2000). In MVID patients, normally apically trafficked proteins are mislocalized sub-apically, while sodium potassium ATPase (Na/K-ATPase) basolateral localization was unaffected in the biopsy samples (Ameen and Salas 2000). In another study, CD10, which is normally associated with the brush border, accumulated on the sub-apical surface of the enterocytes in MVID patients (Groisman, Amar et al. 2002). Since the initial discovery that *MYO5B* mutations were responsible for MVID, much speculation has focused on the role of MYO5B interacting proteins in the manifestations of this disease. In previous studies, we have demonstrated that MYO5B regulates intracellular trafficking and endocytic recycling by localizing with specific Rab small GTPases (Rab8a, Rab10, and Rab11) in sub-apical vesicle populations (Roland, Bryant et al. 2011). Of interest, Rab8a knockout mice display a deficit in intestinal microvilli with prominent intracellular vacuoles that has similarities to some of the features of MVID, but no mutations in Rab8a have been associated with the disease in humans (Sato,

Mushiake et al. 2007). All of these previous investigations suggest that MVID represents a pathophysiologic window into this apical trafficking process, because it arises as a result of inactivating mutations in MYO5B predicted to elicit aberrant apical trafficking of proteins and loss of apical microvilli in intestinal enterocytes (Erickson, Larson-Thome et al. 2008). Therefore, understanding how mutations in MYO5B lead to aberrant trafficking in enterocytes should provide novel insights into the fundamental mechanisms governing plasma membrane recycling system trafficking and lay the framework for producing a viable therapeutic alternative for MVID patients.

In this study, we report that MYO5B regulates global intestinal enterocyte polarity. Using stable MYO5B knock down (KD) in CaCo2-BBE cells, we demonstrate that MYO5B loss results in a decrease in microvilli, mistrafficking of apically and basolaterally trafficked proteins, a decrease in Cdc42, and dispersal of Rab8a and Rab11a. In Navajo MVID patient samples, microvilli are decreased, apical membrane proteins are mistrafficked, and Rab8a and Rab11a are dispersed from their normal apical position. While microvillus inclusions were not observed in MYO5B knockdown cells, the re-expression in MYO5B-KD CaCo2-BBE cells of the Navajo mutation MYO5B-P660L, a mutation that slows MYO5B movement, causes the formation of microvillus inclusions. Rescue of the microvilli loss in the MYO5B-KD required intact Rab8a binding with MYO5B, while expression of a MYO5B that cannot bind Rab11a elicited microvillus inclusions. Finally, we demonstrate in CaCo2-BBE cells that microvillus inclusions arise from internalization of the apical membrane and are likely the products of macropinocytosis. Together, these studies demonstrate that loss of apical microvilli in MVID patients likely arises from a defect in Rab8a-dependent

trafficking, while deficits in the Rab11a-dependent pathways account for the formation of microvillus inclusions. The broad changes in cell polarity in enterocytes at the microvillus tips likely account for the secretory diarrhea that dominates the clinical picture in MVID patients.

Results

Loss or mutation of MYO5B causes a reduction in apical microvilli in enterocytes

Previous work has demonstrated that both truncations and non-functional motor mutations in MYO5B are associated with the MVID phenotype in neonates, including the loss of microvilli and microvillus inclusion formation (Szperl, Golachowska et al. 2011; Chiang, Hsu et al. 2013). To examine the effects of loss of MYO5B, we stably knocked down (KD) MYO5B in CaCo2-BBE cells, a sub-clone from the CaCo2 parental cell line selected specifically for the extensive microvilli that develop when grown on permeable Transwell filters (Peterson and Mooseker 1992). For this study, two lentiviral shRNA vectors targeting MYO5B and a control shRNA were used for transduction of CaCo2-BBE cells. With both shRNA MYO5B constructs, MYO5B mRNA and protein were reduced by greater than 50% compared to the control cells (data not shown). The MYO5B-KD shRNA2 expressing cell line was used for all the subsequent studies discussed below, unless stated otherwise.

Previous published work has demonstrated that CaCo2 cells completely polarize when grown on permeable filters for 14 days, and all CaCo2-BBE cell lines for this study were grown on Transwell filters for 15 days unless stated otherwise (Gilbert and Rodriguez-Boulan 1991). We examined the microvilli of these cells by staining both CaCo2-BBE cells expressing control and MYO5B-KD shRNA CaCo2-BBE cells with anti-ezrin antibodies and co-labelling with fluorescent phalloidin (Figure 5A-F, K, and L). In the control cells, we observed a normal apical brush border distribution of F-actin and ezrin (Figure 5A-C and K). By scanning electron microscopy (SEM) and transmission

electron microscopy (TEM), normal densely packed microvilli were observed in the control cells with no microvillus inclusions (Figure 5G and H). In the MYO5B-KD cells, phalloidin staining accumulated in the terminal web and apical ezrin decreased (Figure 5D-F and L). SEM and TEM studies of these cells showed sparse, shortened apical microvilli with no microvillus inclusions (Figure 5I and J). Similar results were found with MYO5B-KD cell lines expressing both shRNA vectors. Quantitation of ezrin immunofluorescence revealed a reduction in CaCo2-BBE MYO5B-KD cells, and quantitation of ezrin by western blot showed a significant decrease in total ezrin protein in the MYO5B-KD cells (Figure 5M and N).

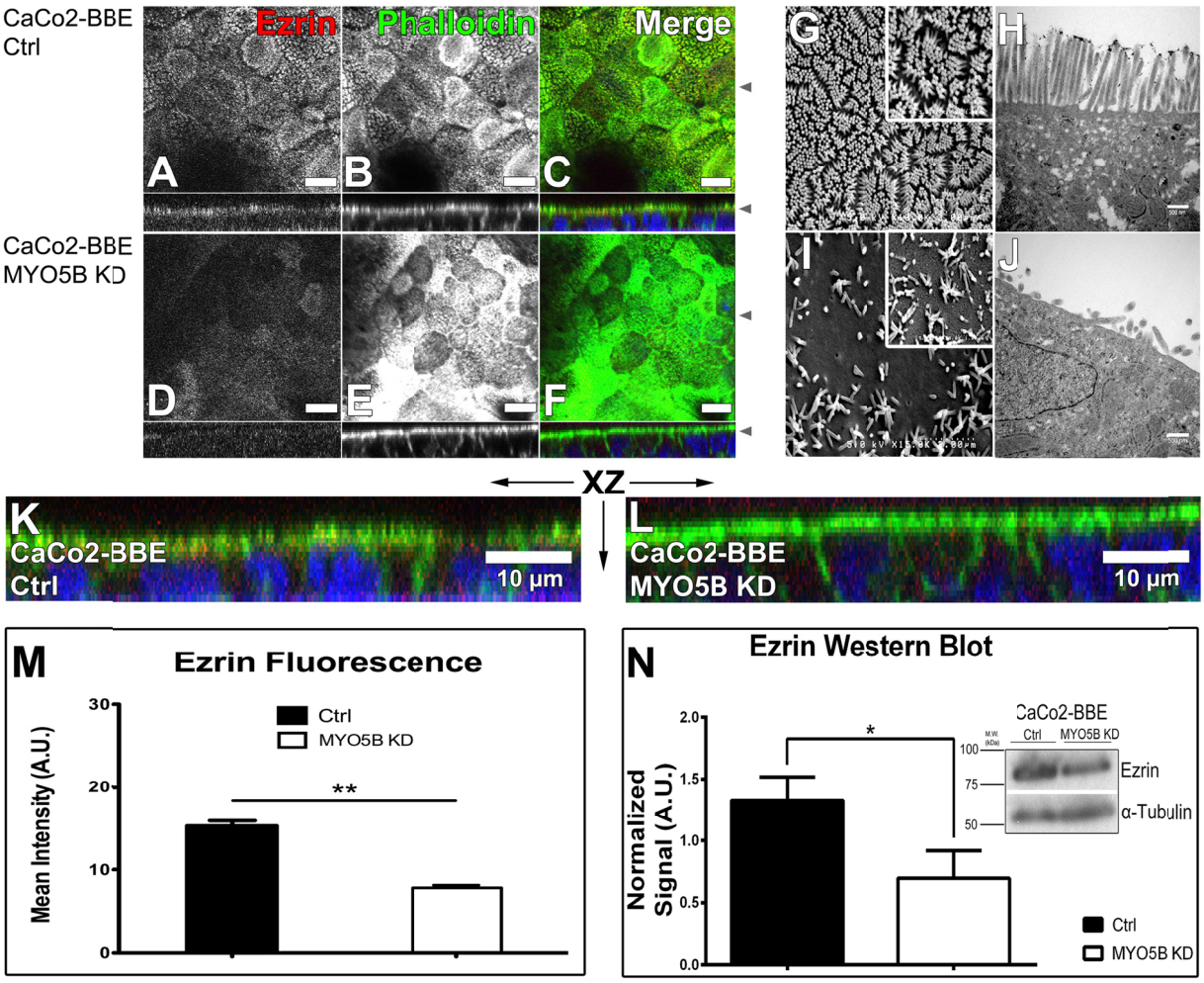

Figure 5. Confocal fluorescence imaging, SEM, and TEM of CaCo2-BBE cells demonstrating loss of microvilli with MYO5B-KD.
In panels A-F, the X-Y images are shown in the upper panels with X-Z images below each. (A and B) Immunostaining for ezrin (red) and Phalloidin F-actin (green) in control cells showed prominent staining of microvilli. Triple overlay with DAPI nuclear staining (blue) is shown in (C). (D and E) Immunostaining for ezrin (red) and Phalloidin F-actin (green) in MYO5B-KD cells showed reduced apical ezrin and an accumulation of F-actin in the subapical region. Triple overlay with DAPI nuclear staining (blue) is shown in (F). (G and H) Control cells SEM and TEM showing normal densely packed microvilli. (I and J) MYO5B-KD cells SEM and TEM showing immature sparse microvilli. (K) Control cells X-Z images from C magnified showing microvilli stained for both ezrin and F-actin. (L) CaCo2-BBE MYO5B-KD cells X-Z images from F magnified showing loss of apical microvilli stained for both ezrin and F-actin and their accumulation in the terminal web. (M) Quantitation of ezrin mean fluorescence in maximum-intensity Z-stack projections showing a reduction in CaCo2-BBE MYO5B-KD cells. (N) Ezrin western blot with quantitation showing a decrease in total ezrin in the MYO5B-KD cells. Scale bars in A-F, K, and L are 10µm, in G and I are 3µm and 1µm in the insets, and H and J are 500nm. Statistical significance is denoted by *$p \leq 0.05$ and **$p \leq 0.01$ using the Mann-Whitney-test. Error bars denote S.E.M.

To examine if the loss of microvilli was due to improper formation or a delay in formation in the MYO5B-KD cells, we examined the stages of microvillar development in both control and MYO5B-KD CaCo2-BBE cell lines. In a time series of control cells grown on Transwell filters, microvilli formed in stages and established a mature brush border by 12 days after plating (Figure 6A). In the control cells, microvilli began to bud from the plasma membrane after 2 days, initiated contact with their neighbors after 4 days, formed Tee-Pee-like structures after 6 days, and initiated the process of packing their microvilli after 8 days on Transwell filters. By western blot analysis, villin-1 was up-regulated throughout microvillar development (Figure 6B and C). In a time series for CaCo2-BBE MYO5B-KD cells, the initial stages of microvilli development were similar to those seen for the control cells. However, MYO5B-KD cells did not progress past the Tee-Pee-like stage and did not achieve microvillar packing, even when cultured for up to 20 days on Transwell filters (Figure 7A). By western blot analysis, compared to the control cells, in MYO5B-KD cells villin-1 was not up-regulated during culture on Transwell filters (Figure 7B and C).

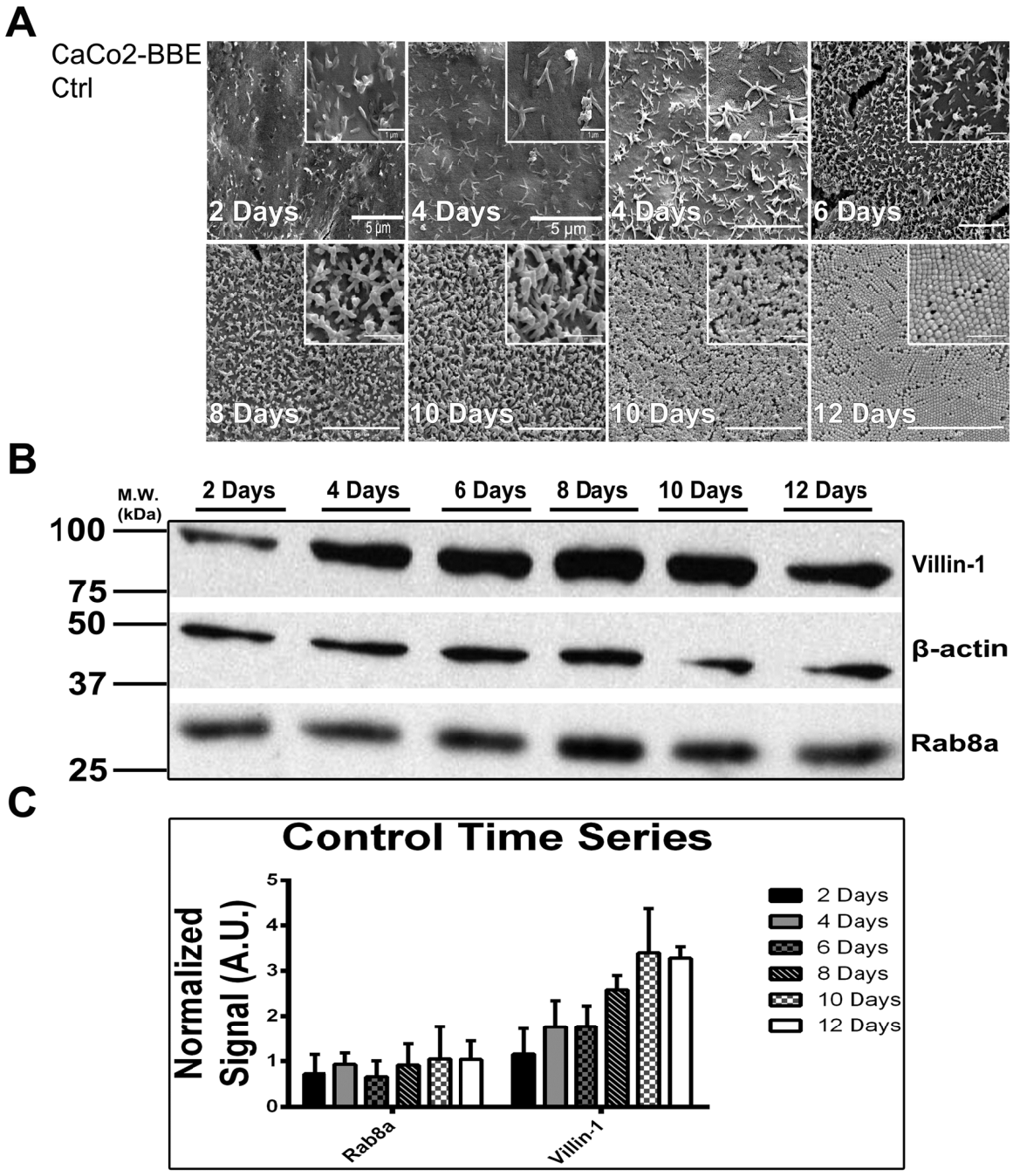

Figure 6. Scanning electron micrographs and western blots of control CaCo2-BBE cells in a time series from 2 to 12 days on Transwell filters.
(A) SEM images of cells cultured from 2 to 12 days on Transwell filters illustrate the progression of microvilli development with insets at higher magnifications. Note, the progression of microvillar packing in CaCo2-BBE control cells becomes more complex over time. Scale bars are 5µm in the panels and 1µm in the insets. (B and C) Western blots with quantitation of villin-1, β-actin, and Rab8a showing that villin-1 is up-regulated throughout microvillar development.

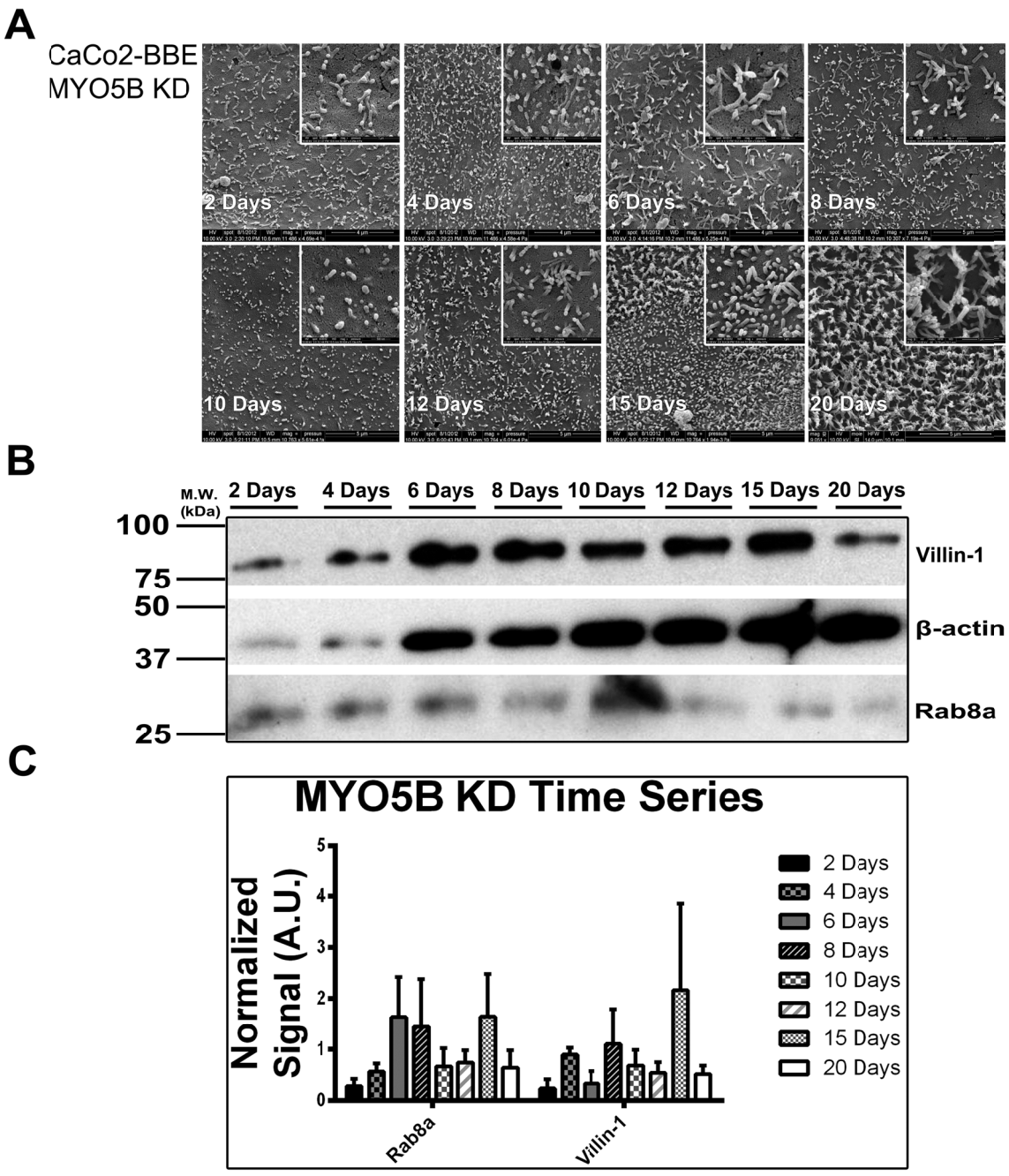

Figure 7. Scanning electron micrographs and western blots of MYO5B-KD CaCo2-BBE cells in a time series from 2 to 20 days on Transwell filters.
(A) SEM images of cells grown on Transwell filters from 2 to 20 days illustrate the progression of microvilli development with insets at higher magnifications. Note, that microvillar packing is never fully established. Scale bars in panels denoting days 2, 4, and 6 are 4μm and 1μm in the panel and its inset, respectively, except the panel denoting the inset for day 6, in which it is 500nm. Scale bars in all other panels are 5μm and 1μm in all panels and insets, respectively, except the inset for day 10, in which it is 500nm. (B and C) Western blots with quantitation of villin-1 and Rab8a that show no up-regulation of villin-1 throughout microvillar development until the 20 day time point.

A wide array of mutations in MYO5B are associated with MVID. As a result, it was unclear if the loss of MYO5B or the effect of MYO5B mutation was responsible for the MVID phenotype. Notably, we did not observe evidence for microvillus inclusions in the MYO5B-KD cells. To examine the effects of the Navajo MYO5B mutation (MYO5B-P660L) on the MVID phenotype, we immunostained Navajo MVID patient small intestine biopsy samples for ezrin and MYO5B (Figure 8A-F). In normal duodenum sections, MYO5B immunostaining was concentrated in the sub-apical region of enterocytes below the brush border, which stained strongly for ezrin (Figure 8A-C). In contrast, MVID patient samples showed a marked decrease in ezrin, dispersal of MYO5B staining, and microvillus inclusion formation in a subset of enterocytes at the tips of intestinal villi, when compared with controls (Figure 8D-F). Interestingly, the cells within the lower regions of the villi demonstrated normal ezrin staining of the apical brush border (Figure 8E). Structured illumination microscopy (SIM) of the MVID patient samples revealed an accumulation of β-actin in the terminal web and a dispersal of MYO5B from its normal sub-apical position above the terminal web (Figure 8G and H). TEM of the MVID patient samples revealed a prominent decrease in microvilli and enlarged intracellular vesicular structures (Figure 8I and J). Thus, while MYO5B-KD in CaCo2-BBE cells replicated losses in microvilli seen in MVID patients, we did not observe microvillus inclusions.

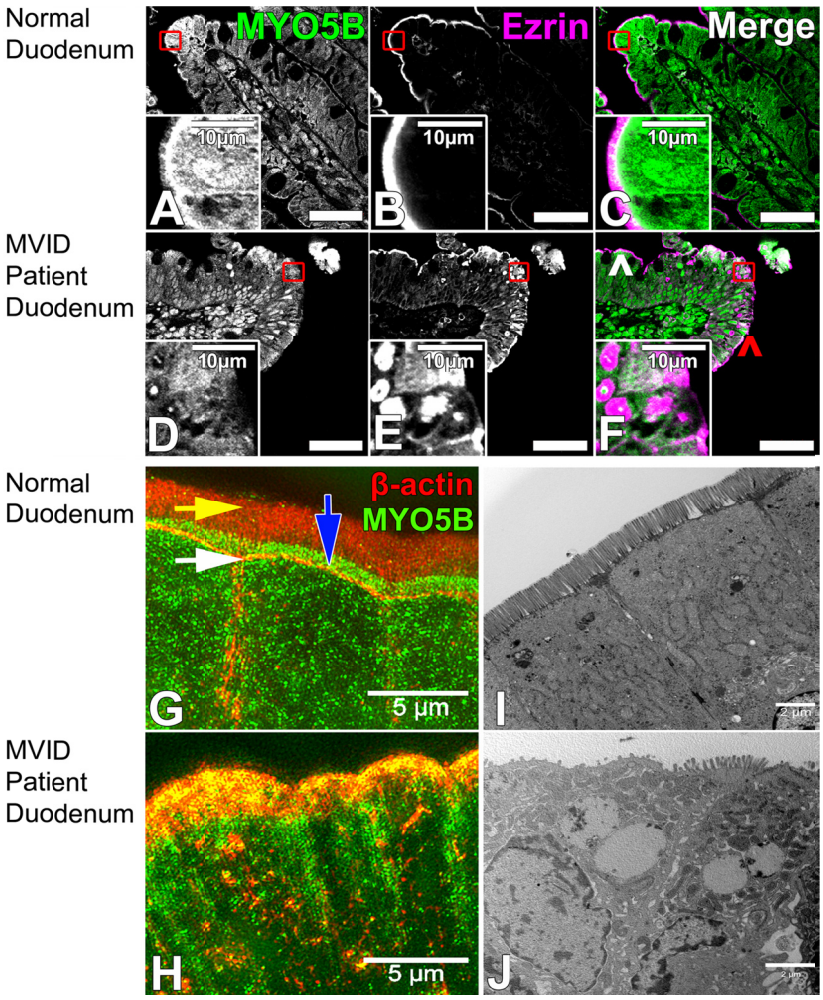

Figure 8. Immunostaining of Navajo MVID patient duodenum samples reveal that mutation of MYO5B causes loss of apical microvilli, microvillus inclusion formation, and accumulation of F-actin into the terminal web.
(A-C) Normal duodenum immunostaining for MYO5B (green) and ezrin (magenta) showed sub-apical MYO5B with increased staining at the tips of villi and ezrin localization to the brush border. (D-F) MVID patient duodenum immunostaining for MYO5B and ezrin showed dispersal of MYO5B from the subapical region of enterocytes and ezrin localization to microvillus inclusions in cells at the villus tips. Note that cells near the crypts (white ^) showed a normal apical ezrin distribution when compared to cells at the villus tips (red ^). (G) SIM imaging of β-actin (red) and MYO5B (green) in normal duodenum showed actin staining in the apical brush border (yellow arrow), discrete staining of the terminal web (white arrow), and MYO5B localization above the terminal web and below the apical surface (blue arrow). (H) SIM imaging of the MVID patient samples revealed an accumulation of β-actin (red) in the terminal web, and dispersal of MYO5B (green) from its normal sub-apical position above the terminal web. (I) TEM in normal duodenum showed normal apical microvilli. (J) TEM of the MVID patient duodenum revealed a decrease in microvilli and enlarged sub-apical vesicular structures. Scale bars in A-F are 50μm and 10μm in the panels and insets, respectively, in G-H are 5μm, and in I-J are 2μm.

Alterations in tight junctions were observed in CaCo2-BBE MYO5B-KD cells and MVID patient enterocytes

We evaluated the integrity of the tight junctions by immunostaining for claudin 1 (CLDN1), claudin 2 (CLDN2), claudin 4 (CLDN4), and ZO-1 (Figure 9A-H). Immunocytochemistry supported the loss of CLDN1 at the junctions as well as an increase in CLDN2 staining in the junctions of MYO5B-KD cells. Quantitation of CLDN1, CLDN2, CLDN4, and ZO-1 immunofluorescence showed a reduction in CLDN1 and ZO-1 and an increase in CLDN2 and CLDN4 in MYO5B-KD cells (Supplemental Figure 4I). Western blot analysis and quantitation showed that CLDN1 was down-regulated and CLDN2 was up-regulated in the MYO5B-KD cells compared with control cells (Figure 9J and K). The increase in CLDN1 and concomitant decrease in CLDN2 is indicative of a shift from a high resistance junctional complex to a leaky junction (Van Itallie and Anderson 2006). In support of this concept, the trans-epithelial electrical resistance (TEER) in MYO5B-KD cells was reduced significantly compared with control cells (Figure 9L). Interestingly, previous studies have noted that microvilli formation is correlated with TEER in CaCo2 cells (Vandrangi, Lo et al. 2013).

We next examined the effects of the MYO5B-P660L Navajo mutation on components of the tight junction by immunostaining duodenal biopsy samples from Navajo patients for CLDN1 and CLDN4 (Figure 10). Unfortunately, no CLDN2 antibody is presently available for reliable staining of human paraffin sections. CLDN1 in MVID patient samples was lost from junctions and mislocalized to the cytoplasm (Figure 10A and B). In contrast, CLDN4 maintained its normal localization in the MVID patient samples, although its expression was reduced (Figure 10C and D). These findings

suggest that loss or mutation of MYO5B in both the CaCo2-BBE cell model and MVID patients leads to alterations in junctional composition in enterocytes.

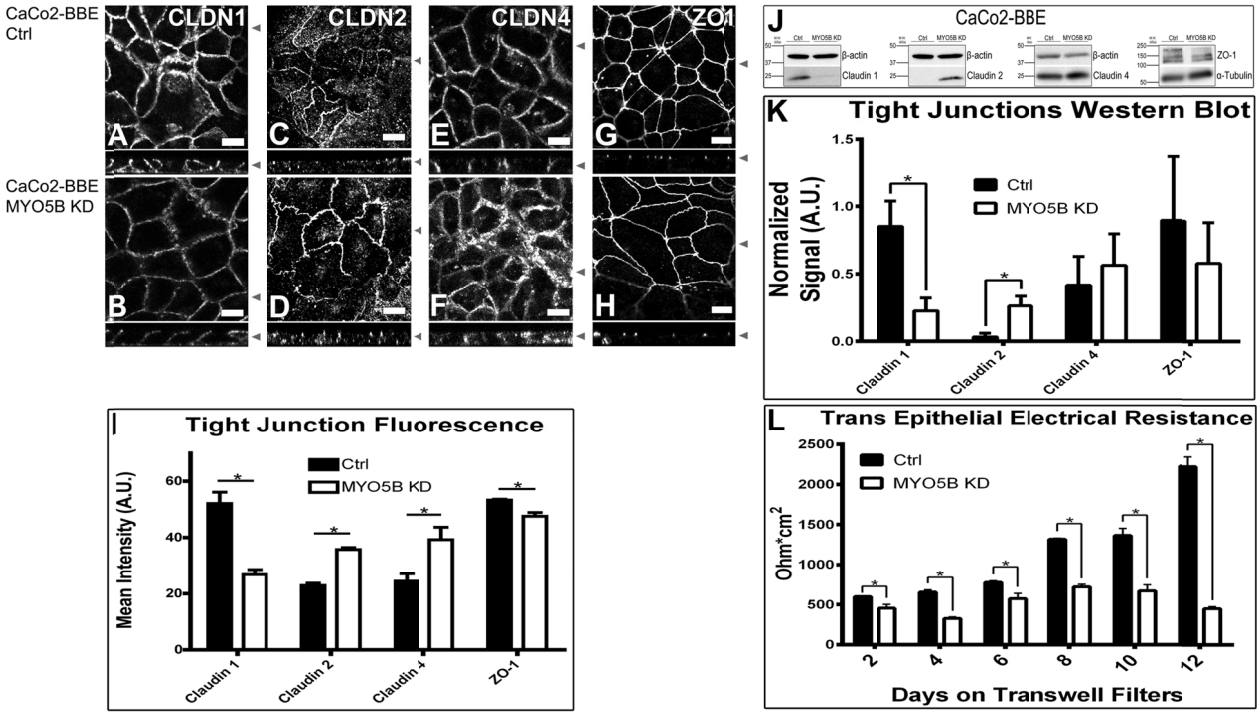

Figure 9. Junctional compartment immunofluorescence staining in CaCo2-BBE MYO5B-KD cells shows a shift in claudin staining.

In panels A-H, X-Y confocal images are shown above Z-axis reconstructions. (A-B) In control cells, CLDN1 has a lateral distribution, and in MYO5B-KD cells, CLDN1 staining is decreased but maintained a lateral distribution. (C-D) In control cells, CLDN2 has a junctional distribution, while in MYO5B-KD cells; CLDN2 staining becomes more intensely junctional than in the control cells. (E-F) In control cells, CLDN4 has a lateral distribution, and in MYO5B-KD cells, CLDN4 has a lateral cytoplasmic distribution. (G-H) In control cells, ZO-1 has a junctional distribution, and MYO5B-KD cells, ZO-1 has the same distribution as the control. (I) Quantitation of mean fluorescence of CLDN1, CLDN2, CLDN4, and ZO-1 immunofluorescence showed a reduction in CLDN1 and ZO-1 and an increase in CLDN2 and CLDN4 in MYO5B-KD cells. (J-K) Western blot analysis and quantitation of MYO5B-KD cells compared with control cells, CLDN1 was down-regulated and CLDN2 was up-regulated. It should be noted, the gel used for Rab11a in Figure 7 was stripped and re-probed for CLDN1 and CLDN2, and as a result they have the same loading controls. (L) The trans-epithelial resistance was decreased in MYO5B-KD cells. Scale bars are 10μm in all panels. Statistical significance is denoted by *p ≤ 0.05, ** p ≤ 0.01, and ***p≤ 0.001 using the Mann-Whitney-test. Error bars denote S.E.M.

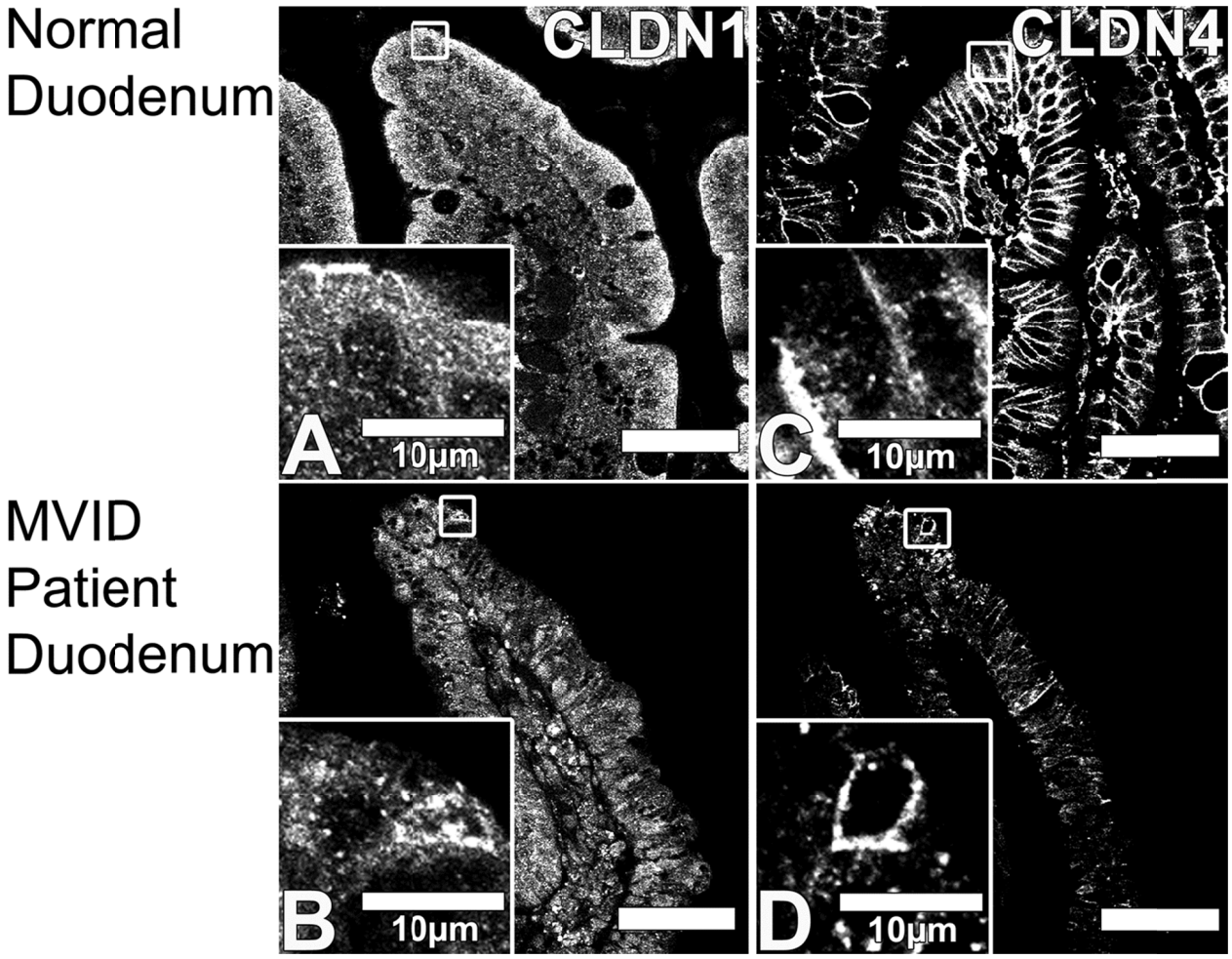

Figure 10. Junctional compartment immunofluorescence staining in MVID patient duodenum shows alterations in claudin staining.
(A-B) CLDN1 staining in normal duodenum showed a junctional distribution, while CLDN1 staining in MVID patient duodenum showed dispersal of the junction staining. (C-D) CLDN4 staining in normal duodenum showed a lateral distribution, while CLDN4 staining in MVID patient duodenum showed reduced fluorescence and lateral distribution. Scale bars are 50µm in all panels and are 10µm in all insets.

Loss of polarity in basolateral and apical compartments is observed in MYO5B-KD CaCo2-BBE cells and MVID patient enterocytes

We next examined the effects of reducing MYO5B on components of the basolateral and apical compartments in CaCo2-BBE cells. To evaluate the integrity of the basolateral compartment, we immunostained for p120-Catenin (p120), Na/K-ATPase, E-cadherin, and β-Catenin (Figure 11). In the control CaCo2-BBE cells, p120, Na/K-ATPase, and β-catenin were distributed along the basolateral membranes, while E-cadherin was confined to the junctions (Figure 11A, C, E, G, and I). In the MYO5B-KD cells, p120 and Na/K-ATPase staining was decreased at the lateral membrane by immunofluorescence (Figure 11B and D). Remarkably, E-cadherin staining in the MYO5B-KD cells was re-distributed to both apical and basolateral membranes as well as to vesicles underlying both surfaces (Figure 11F and J). Nevertheless, β-Catenin was not redistributed or decreased by immunofluorescence between these two cell lines (Figure 11G and H). Quantitation of immunofluorescence for the basolateral proteins revealed that MYO5B-KD cells showed a reduction of p120, no change in Na/K-ATPase or β-catenin, and an increase in E-cadherin (Figure 11K). Interestingly, the apical-to-basolateral ratio in MYO5B-KD cells for p120 or β-catenin showed no change. However, Na/K-ATPase shifted to the apical surface, while E-cadherin was redistributed from the junction to both the apical and basolateral surfaces (Figure 11N). Western blots analysis of p120 in MYO5B-KD cells showed isoform switching when compared to the pattern observed in the control cells (Figure 11L), which is indicative of an alteration in polarity (Fukumoto, Shintani et al. 2008; Yanagisawa, Huveldt et al. 2008). This change was not accompanied by a decrease in total p120 protein (Figure 11M). The apparent decrease

by immunofluorescence staining was likely due to the restricted specificity of the immunostaining antibody for extended carboxyl-terminal isoforms (Wu, Mariner et al. 1998). We observed no changes in Na/K-ATPase and β-catenin, and an increase in total E-cadherin (Figure 11L and M).

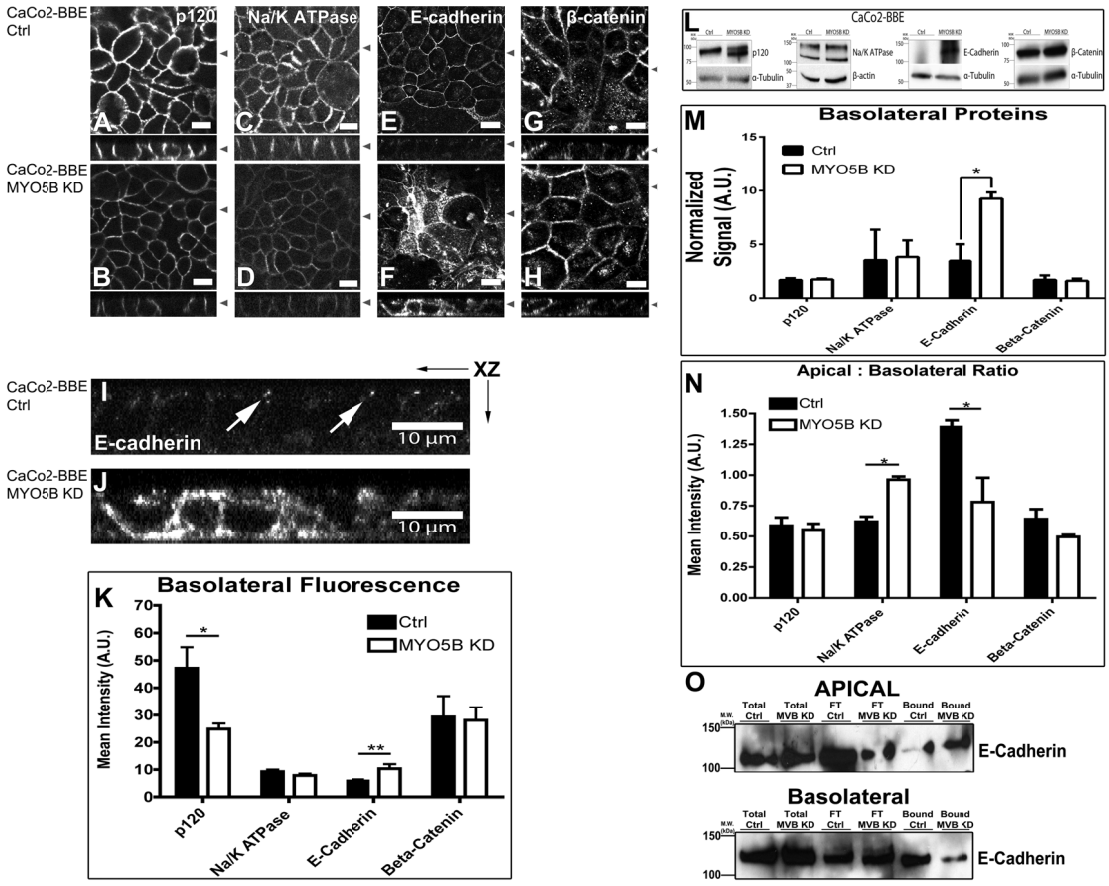

Figure 11. Loss of MYO5B in CaCo2-BBE cells causes the redistribution of basolateral markers. In panels A-H, the X-Y confocal images are shown above Z-axis reconstructions.

p120 staining in control (A) showed a lateral distribution, while MYO5B-KD (B) showed decreased p120 at the lateral membranes. Na/K-ATPase staining in control (C) showed a lateral distribution, while MYO5B-KD cells (D) showed reduction in lateral membranes. E-cadherin staining in control (E) showed a junctional distribution, X-Z images magnified in (I) junctional E-cadherin (white arrows), while MYO5B-KD (F) showed distribution along both apical and lateral membranes and internally, X-Z images magnified in (J). (G-H) In control and MYO5B-KD, β-catenin stained lateral membranes. (K) Quantitation of basolateral mean fluorescence. MYO5B-KD showed a reduction of p120 and an increase in E-cadherin. (L) Quantitation of apical-to-basolateral ratio in MYO5B-KD showed a redistribution of Na/K-ATPase to the apical surface, while E-cadherin was localized over both the apical and basolateral surfaces. (M-N) Western blot with quantitation of basolateral markers in MYO5B-KD showed an isoform switch of p120 with no decrease and an increase E-cadherin total protein. (O) Surface biotinylation of either the apical or basolateral surfaces in control and MYO5B-KD cells with Total protein, flow through from streptavidin-beads (FT), and biotinylated-streptavidin-bound protein from control (Bound-Ctrl) or MYO5B-KD (Bound-MVBKD) showed an increase in apical and a decrease in basolateral E-cadherin in the MYO5B-KD. Scale bars are 10µm in all panels. Statistical significance: *p ≤ 0.05 and **p ≤ 0.01 using the Mann-Whitney-test. Error bars denote S.E.M.

To investigate the localization of E-cadherin using a biochemical approach, we performed cell surface biotinylation of both the apical and basolateral surfaces, and analyzed the distribution of E-cadherin in proteins collected on streptavidin-coated beads (Figure 11O). Analysis of the relative distributions across biotinylated fractions demonstrated that E-cadherin in the apical bound fraction was increased in MYO5B-KD cells compared with the control cells (17.93 ± 2.15% versus 9.76 ± 3.1%), and E-cadherin in the basolateral bound fraction decreased in MYO5B-KD cells compared to control cells (12.43 ± 7.46% versus 22.8 ± 5.87%). All of these results suggest that loss of MYO5B caused aberrant trafficking of E-cadherin.

To evaluate the integrity of the basolateral compartment in MVID patient samples, we immunostained sections for p120, E-cadherin, Na/K-ATPase, and β-catenin (Figure 12). In the control duodenum biopsy samples, all four markers were distributed along the basolateral membranes (Figure 12A, C, E, and G). In the MVID patient samples, p120 and β-catenin staining was decreased at the lateral membranes by immunofluorescence, but maintained a normal lateral distribution (Figure 12B and H). E-cadherin staining in the MVID patient samples, however, was re-distributed to both the apical and basolateral surfaces (Figure 12D). Na/K-ATPase staining in the MVID patient samples was maintained with dispersal in enterocytes at the villus tips (Figure 12F).

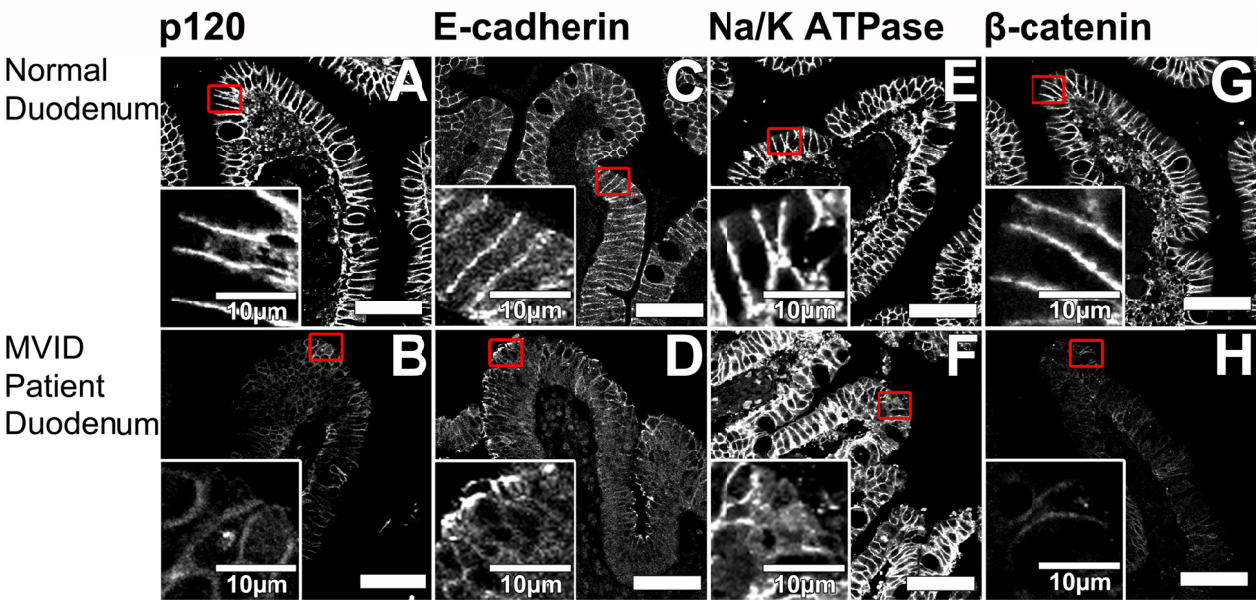

Figure 12. Immunostaining of MVID patient duodenum samples demonstrated alteration of the basolateral compartment.
(A) In normal duodenum, p120 staining showed a lateral distribution. (B) In MVID patient duodenum, p120 staining was reduced but maintained its lateral membrane localization. (C) In normal duodenum, E-cadherin staining demonstrated a lateral distribution. (D) In MVID patient duodenum, E-cadherin staining was present on both apical and lateral membranes. (E) In normal duodenum, Na/K-ATPase antibodies stained the lateral membranes. (F) In the MVID patient samples, Na/K-ATPase stained the lateral membranes with dispersal of staining in enterocytes at the villus tips. (G) In normal duodenum, β-catenin staining was present in the lateral membranes. (H) In MVID patient duodenum, β-catenin staining was decreased in the lateral membranes. Scale bars are 50μm in all panels and 10μm in the insets.

To examine the effects of MYO5B-KD on a non-structural component of the microvilli, we immunostained the CaCo2-BBE cells for dipeptidyl peptidase-4 (DPPIV). In control cells, DPPIV labeled the apical external surface of microvilli (Figure 13A-F and M). However, in the MYO5B-KD cells, DPPIV staining was reduced in the apical membranes, consistent with the loss of microvilli and we observed DPPIV staining in internal punctate vesicular structures. In the Rab8a knockout mouse, DPPIV was observed in enlarged lysosomes (Sato, Mushiake et al. 2007). To test whether DPPIV in MYO5B-KD cells was also diverted to the lysosomes, we dual immunostained the cells for DPPIV and LAMP2a. In the MYO5B-KD cells, DPPIV localized to both LAMP2a negative and also LAMP2a positive vesicles (Figure 13G-L and N). To determine the origin of the LAMP2a negative vesicles, we dual immunostained both the control and MYO5B-KD cell lines for Rab11a, which labels the apical recycling endosome (ARE), and DPPIV (Figure 13O-R). In control cells, DPPIV labeled the apical surface and Rab11a labeled punctate vesicles below the apical surface (Figure 13O). In the MYO5B-KD cells, Rab11a localized to both DPPIV-positive vesicles and vesicles that contained no DPPIV (Figure 13P-R). Quantitation of DPPIV immunofluorescence revealed a decrease in DPPIV in the MYO5B-KD cells, and by western blot analysis total protein expression of DPPIV was significantly reduced (Figure 13S and T).

To investigate the localization of DPPIV using a biochemical approach, we performed cell surface biotinylation of the apical surface and analyzed proteins collected on streptavidin-coated beads for DPPIV (Figure 13U). In the MYO5B-KD cells, we observed a loss of DPPIV from the apical membranes (7.209 ± 3.63% versus 13.42 ± 2.98% in controls) and an increase in the non-biotinylated pool of DPPIV (92.79 ±

3.63% versus 86.58 ± 2.98% in controls). All of these results suggest that DPPIV is lost from the apical membrane and localized intracellularly in part to lysosomes as well as to endosomes in MYO5B-KD cells.

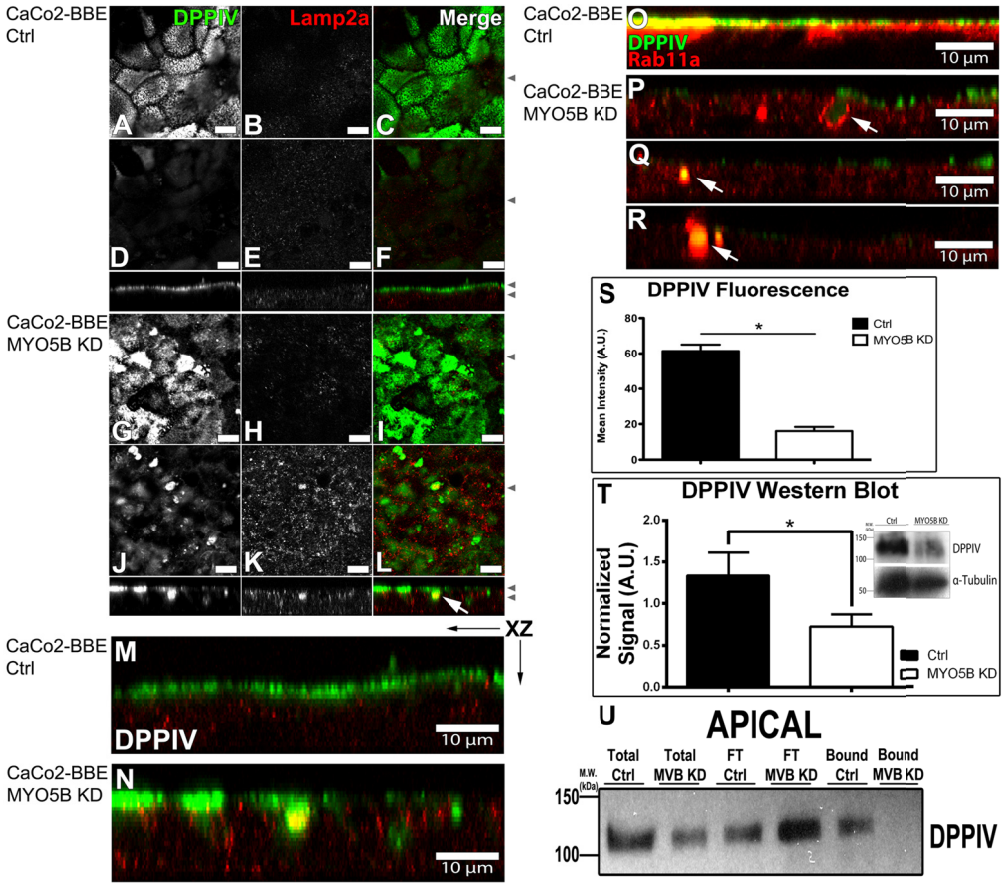

Figure 13. Co-immunostaining of DPPIV and Lamp2a in CaCo2-BBE cells with redistribution of DPPIV to large vesicles in MYO5B-KD cells.
In panels A-L, X-Y confocal images are shown above Z-axis reconstructions. Control and MYO5B-KD cells were immunostained for DPPIV (green) and LAMP2a (red). (A-F) Control cells showed a normal apical distribution of DPPIV and diffusely cytoplasmic LAMP2a. (G-L) In MYO5B-KD cells, DPPIV was seen in internal vesicles, some of which also stained for LAMP2a (white arrow). (M) Magnified X-Z images from control cells in F. (N) Magnified MYO5B-KD cell X-Z images from L showing cytoplasmic distribution of DPPIV. (O) Control cells immunostained for DPPIV (green) and Rab11a (red) showed apical DPPIV and sub-apical Rab11a. (P-R) MYO5B-KD cells, immunostained for DPPIV (green) and Rab11a (red) showed dispersal of Rab11a from the sub-apical surface and localization in large DPPIV positive vesicles (white arrows). (S) In MYO5B-KD cells, DPPIV reduction shown via mean fluorescence in maximum-intensity Z-stack projections. (T) Western blot comparing control and MYO5B-KD cell lines probed for DPPIV and α-Tubulin demonstrating reduction of DPPIV expression. (U) Apical surface biotinylation in control and MYO5B-KD cells showing DPPIV immunoreactivity in Total protein, flow through from streptavidin beads (FT), and biotinylated streptavidin-bound protein demonstrating an increase in the non-biotinylated cytoplasmic pool and a decrease in DPPIV on the apical surface in the MYO5B-KD (Bound-MVBKD) versus control (Bound-Ctrl) cells. Scale bars are 10µm in all panels. Statistical significance: *p ≤ 0.05 and **p ≤ 0.01 using the Mann-Whitney-test. Error bars denote S.E.M.

Other proteins previously reported as mistrafficked in MVID patient samples, such as transferrin receptor (CD71) and CD10, also displayed an altered distribution in MYO5B-KD cells. CD10 was observed in sub-apical and lateral puncta in the MYO5B-KD cells instead of a more diffuse pattern observed in the control cells, and quantitated CD10 fluorescence was significantly decreased (Figure 14A, B, and F). CD71 was redistributed strongly to the sub-apical region, throughout the cytoplasm, and total protein was increased in MYO5B-KD cells (Figure 14C-F). Finally, we also evaluated the pattern of transferrin trafficking in MYO5B-KD cells. Fluorescently-labeled transferrin was endocytosed from the basolateral membranes and then chased with serum for 60 minutes in both control and MYO5B-KD cells. Fluorescently-labeled transferrin was endocytosed appropriately from the basolateral membranes in both the control and MYO5B-KD cells (Figure 14G and H). In MYO5B-KD cells, fluorescently-labeled transferrin accumulated in sub-apical vesicles, rather than recycling out of the cell following serum chase as in the control cells (Figure 14I and J). Quantitation of transferrin trafficking showed no significant difference in uptake between the control and the MYO5B-KD cells, but transferrin was significantly retained in MYO5B-KD cells (Figure 14K). All of these results suggested that MYO5B-KD caused alterations in apical and basolateral trafficking.

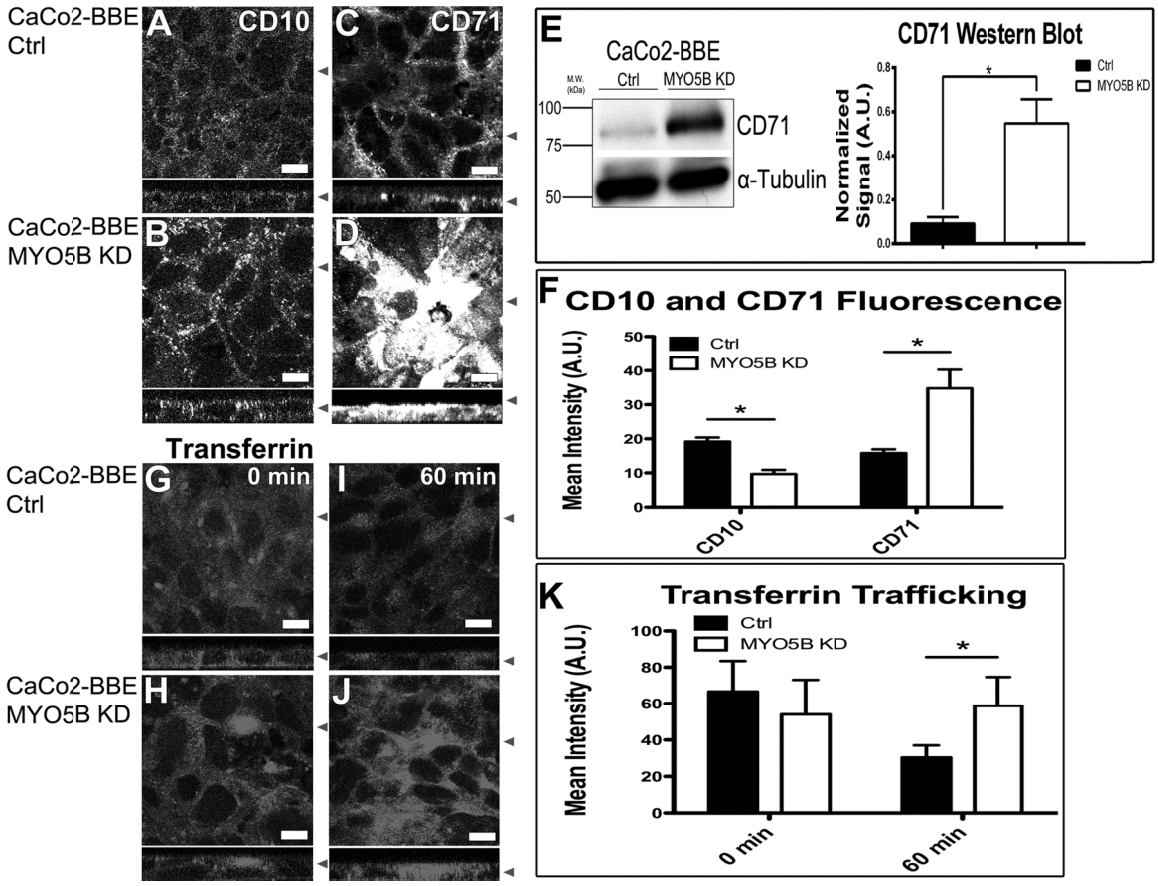

Figure 14. Deficits in apical trafficking are observed in CaCo2-BBE MYO5B-KD cells.

CD10 staining in control cells (A) was diffusely cytoplasmic and laterally distributed, while MYO5B-KD cells (B) showed concentration in both apical and lateral compartments in large punctate vesicles. In control cells (C), CD71 staining showed an apical and lateral cytoplasmic distribution, while MYO5B-KD cells (D) showed concentrated staining mainly in the sub-apical compartment with some lateral distribution. (E) Total CD71 protein was increased in MYO5B-KD cells by western blot analysis. (F) Quantitation of mean fluorescence in maximum-intensity Z-stack projections showed reduction of CD10 and increase in CD71 in MYO5B-KD cells. (G-K) Fluorescently-labeled transferrin was endocytosed from the basolateral membranes and then chased with serum for 60 minutes in both CaCo2-BBE control and MYO5B-KD cells. (G and H) Control and MYO5B-KD cells at the zero time point. (I) After 60 minutes control recycled most of the labeled transferrin out of the cells. (J) In MYO5B-KD cells fluorescently-labeled transferrin accumulated in sub-apical vesicles rather than being recycled as in control cells after 60 minutes of serum chase. (K) Quantitation of mean fluorescence in maximum-intensity Z-stack projections of transferrin showed no significant difference in uptake between the control and the MYO5B-KD cells at 0 minutes, and retention of transferrin in MYO5B-KD cells at 60 minutes. In panels (A-D and G-J), X-Y confocal images are shown above Z-axis reconstructions. Scale bars are 10μm in all panels. Statistical significance is denoted by *$p \leq 0.05$ using the Mann-Whitney-test. Error bars denote S.E.M.

To examine the effects of the Navajo MYO5B-P660L mutation on apical non-structural components of the microvilli, we immunostained the duodenal biopsy samples for CD10 and sodium glucose transporter 1 (SGLT1). In the duodenal biopsy control samples, CD10 and SGLT1 labeled the apical brush borders of enterocytes (Figure 15A and E). In contrast, Transferrin receptor (CD71) was diffusely distributed throughout the enterocytes (Figure 15C). However, in the MVID patient samples, CD10 and SGLT1 were redistributed away from the apical surface with a loss of SGLT1 (Figure 15B, D, and F). In contrast, CD71 staining was increased in both the apical and basolateral poles of enterocytes (Figure 15D). Interestingly, when DPPIV was co-stained with villin-1, they co-localized in microvillus inclusions, but DPPIV was also observed in large internal punctate vesicular structures that did not stain for villin-1 (Figure 16A-F). These findings confirmed that loss of MYO5B in CaCo2-BBE cells caused a disruption of normal apical and basolateral trafficking, and localization similar to what is observed in Navajo MVID patients' enterocytes.

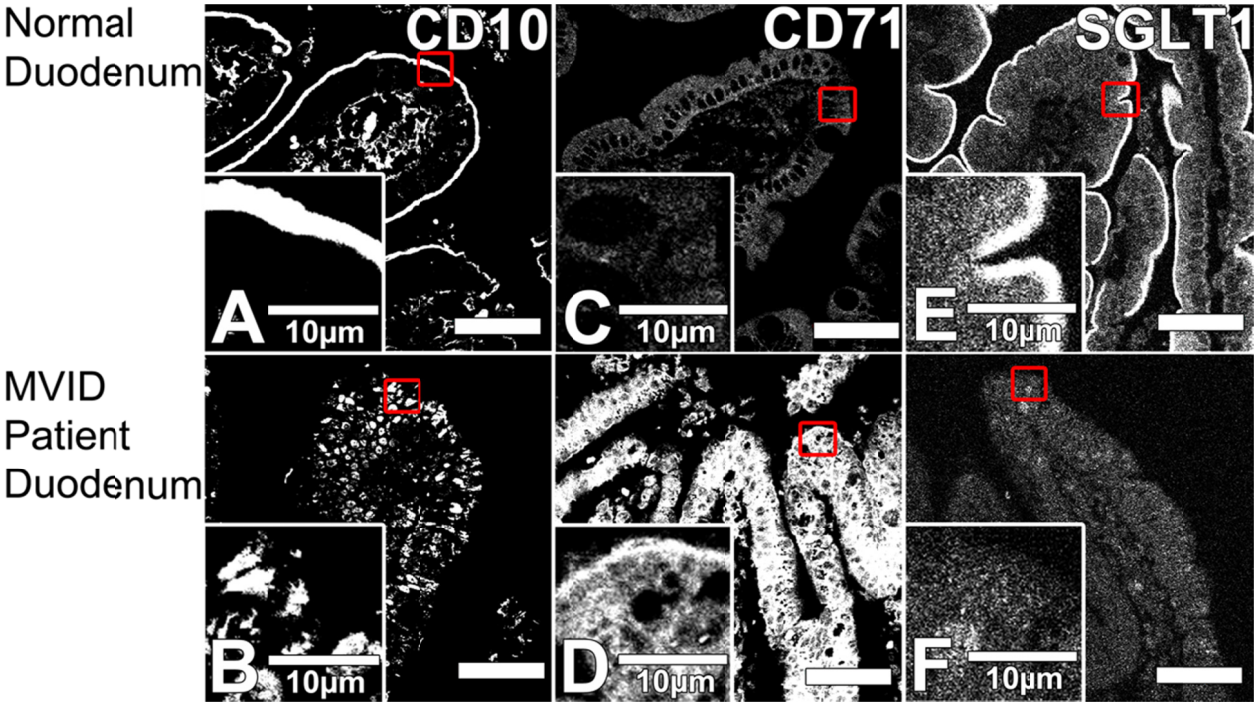

Figure 15. MVID patient duodenum samples show redistribution of apical non-structural microvillar markers to the cytoplasm.
(A) In normal duodenum, CD10 staining was localized to the brush border. (B) In MVID patient duodenum, CD10 staining was redistributed into large cytoplasmic intracellular vesicles. (C) In normal duodenum, CD71 staining was localized diffusely throughout the enterocytes. (D) In MVID patient duodenum, CD71 staining was increased and sharply redistributes to the apical surface. (E) In normal duodenum, SGLT1 was present at the apical brush border of the enterocytes. (F) In MVID patient duodenum, we observed a general loss of SGLT1 apical staining. Scale bars are 50μm in all panels and 10μm in all insets.

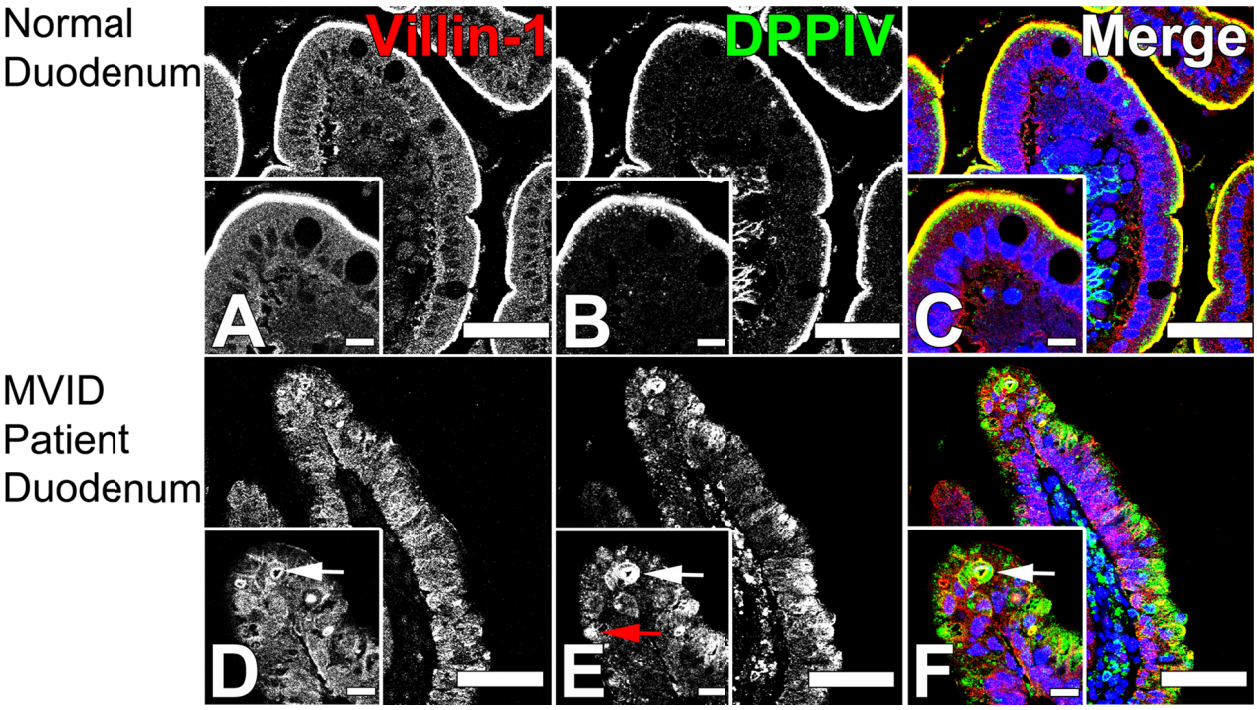

Figure 16. DPPIV is mistrafficked to intracellular vesicles and to microvillus inclusions in MVID patient samples.
(A-C) Normal duodenum villin-1 (red) and DPPIV (green) immunostaining showed localization of DPPIV and villin-1 to the brush border. Merged overlay images with DAPI nuclear staining (blue) are shown at right. (D-F) MVID patient duodenum villin-1 and DPPIV immunostaining showed mis-localization of DPPIV to microvillus inclusions (white arrows) and to large intracellular vesicles (red arrow). Merged overlay images with DAPI nuclear staining (blue) are shown at right. Scale bars are 50μm in all panels and 10μm in the insets.

Rab8a and Rab11a positive vesicles are dispersed in CaCo2-BBE MYO5B-KD cells and Navajo MVID patient enterocytes

To determine the underlying effects of MYO5B loss on trafficking to microvilli and polarity, we stained the MYO5B-KD cells for two Rab proteins that bind to MYO5B, Rab8a, and Rab11a. Both Rab8a and Rab11a were concentrated in large vesicular complexes sub-apically in the control cells, with Rab11a showing a central sub-apical distribution and Rab8a having a sub-apical and lateral distribution. In the MYO5B-KD cells, both Rab8a and Rab11a were dispersed throughout the cytoplasm away from their normal sub-apical distributions (Figure 17A-C). Maximum-intensity Z-stack projections of MYO5B-KD cells showed dispersal of both Rab8a and Rab11a into smaller vesicles located diffusely through the cell cytoplasm (Figure 17D). Quantitation of the mean total cellular fluorescence intensity demonstrated that Rab11a staining across the entire cell volume did not change for Rab11a, but was decreased for Rab8a (Figure 17E). Total Rab8a and Rab11a protein by western blot showed no change between control and MYO5B-KD cells (Figure 17F and G). All of these findings suggest that loss of MYO5B expression disrupts the normal defined sub-membrane localization of Rab8a and Rab11a.

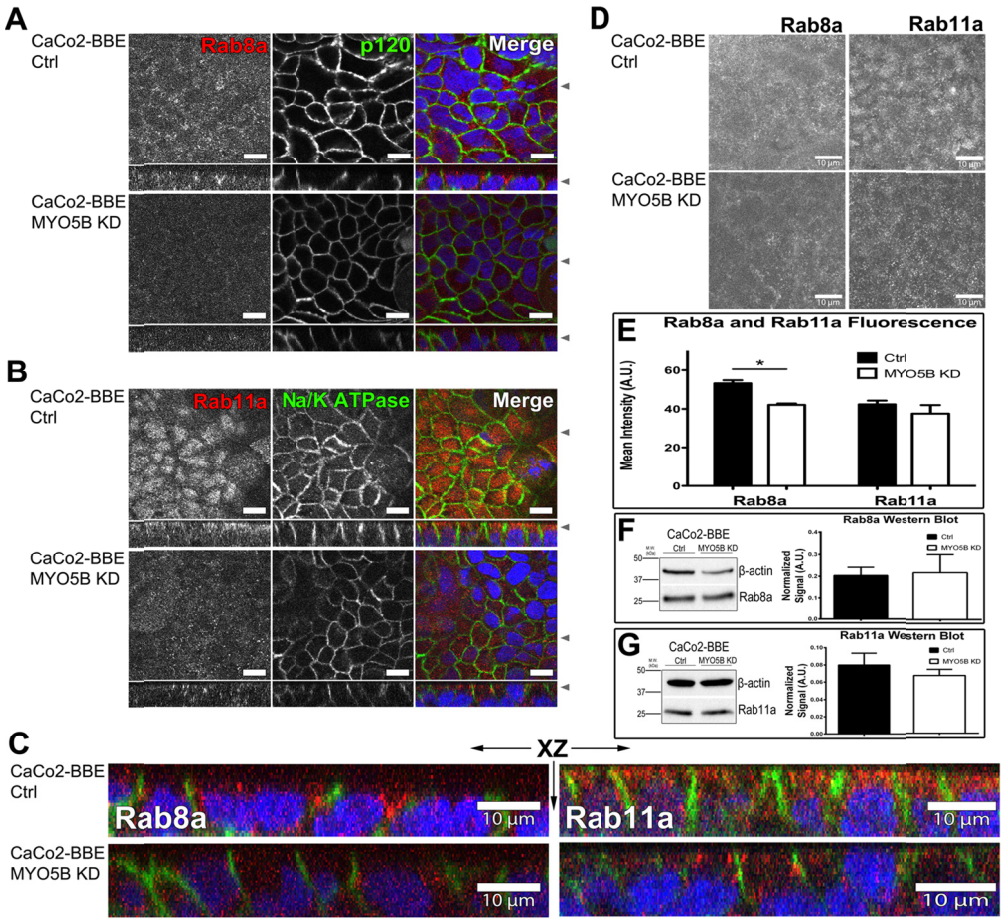

Figure 17. Rab8a and Rab11a immunofluorescence staining in MYO5B-KD cells was dispersed from the apical surface.

(A, B) X-Y confocal images are shown above Z-axis reconstructions. (A) Rab8a (red) and p120 (green) co-staining in CaCo2-BBE cells. Top: Control cells showed apical-lateral Rab8a distribution. Bottom: MYO5B-KD cells showed Rab8a dispersal throughout the cytoplasm. (B) Rab11a (red) and Na/K-ATPase (green) staining in CaCo2-BBE cells. Top: In control cells, Rab11a showed a sub-apical distribution. Bottom: In MYO5B-KD cells Rab11a was dispersed throughout the cytoplasm. (C) Left: Magnified Rab8a staining X-Z images from control and MYO5B-KD cells in A. Right: Magnified Rab11a staining X-Z images from control and MYO5B-KD cells in B. (D) Left Top: In control cells, Z-axis projection showed the normal distribution of Rab8a-positive vesicles. Left Bottom: In MYO5B-KD cells, Z-axis projection showed dispersal of Rab8a-positive vesicles. Right Top: In control cells, Rab11a Z-axis projection showed the normal distribution of Rab11a positive vesicles. Right Bottom: In MYO5B-KD cells, Rab11a Z-axis projection showed the dispersal of Rab11a-positive vesicles. (E) Quantitation of Rab8a and Rab11a mean fluorescence in maximum-intensity Z-stack projections showed a reduction in Rab8a, but no change of Rab11a in MYO5B-KD cells. (F) Western blot with quantitation of Rab8a showed no change in Rab8a in MYO5B-KD cells. (G) Western blot with quantitation of Rab11a showed no change in Rab11a in MYO5B-KD cells. Scale bars are 10µm in all panels. Statistical significance: *$p \leq 0.05$ and **$p \leq 0.01$ using the Mann-Whitney-test. Error bars denote S.E.M.

To examine the effects of loss of MYO5B on other markers of polarity, we also stained the CaCo2-BBE cells for Cdc42. Activation of Cdc42 is regulated by Rab8a via its GEF TUBA, and both Cdc42 and Rab8a-deficient mice develop aspects of the MVID phenotype (Bryant, Datta et al. 2010; Sakamori, Das et al. 2012; Melendez, Liu et al. 2013). In the control cells, we observed two distinct Cdc42 populations. In one, Cdc42 was dispersed throughout the cells, while in another Cdc42 localized to small puncta. In the MYO5B-KD cells, the punctate population was disrupted and total Cdc42 was reduced as assessed by immunofluorescence quantitation (Figure 18A and B). Total Cdc42 protein was reduced in MYO5B-KD cells, and furthermore, the active Cdc42 population was also reduced (Figure 18B and C). Immunostaining in normal duodenum showed an apical distribution of Cdc42, however, in MVID patient samples, total Cdc42 was reduced and mislocalized away from the apical surface (Figure 18D). It should be noted, atypical Protein Kinase C (aPKC) was also mislocalized in MVID patient tissue samples (Figure 18D), consistent with regulation of the localization and activation of aPKC by Cdc42 (Atwood, Chabu et al. 2007; Qin, Meisen et al. 2010). These findings, along with previous work using Cdc42-deficient mice, suggest that loss of Cdc42 contributes to the MVID phenotype.

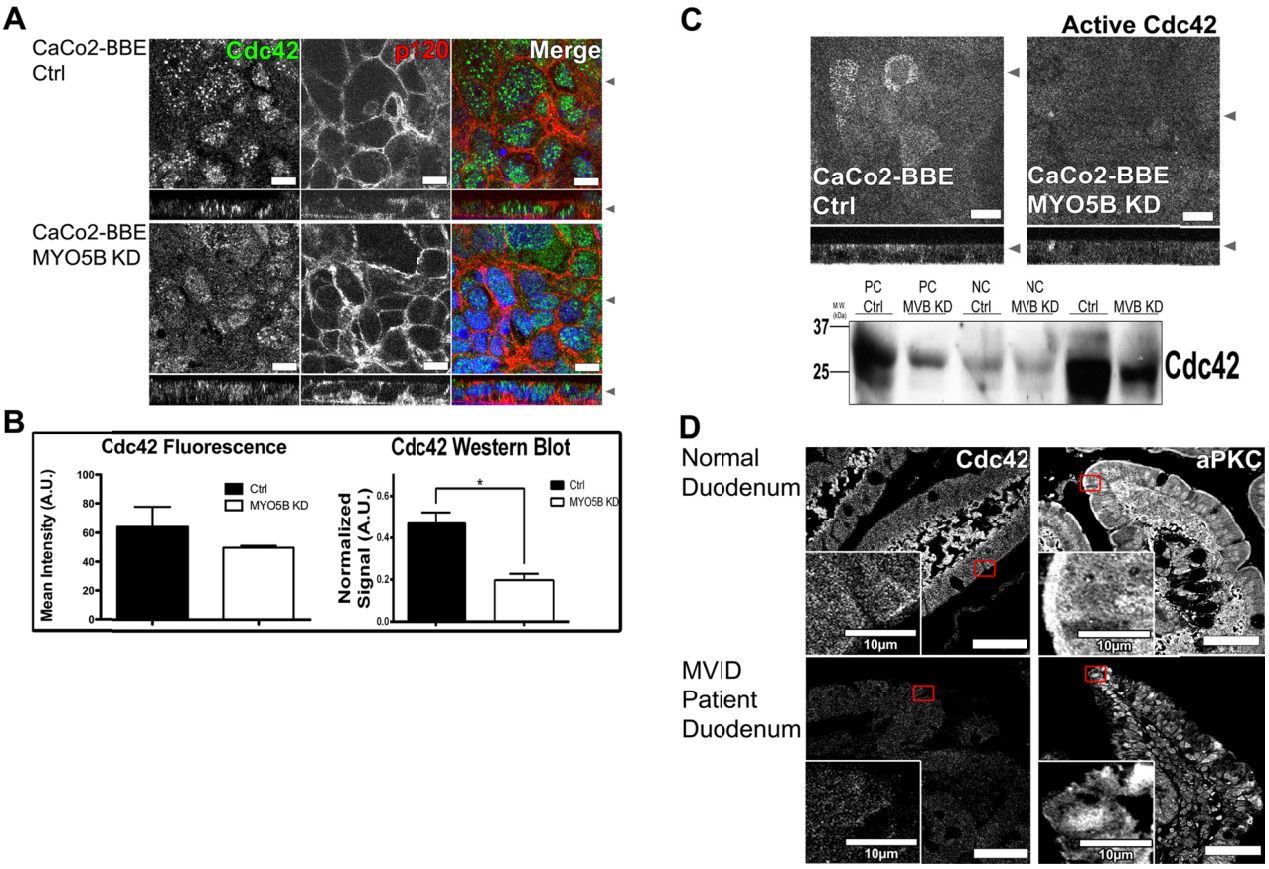

Figure 18. Cdc42 staining in CaCo2-BBE cells and MVID patient samples demonstrated loss of total Cdc42 in MYO5B-KD. In panels A and C, X-Y confocal images are shown above Z-axis reconstructions.

(A) Top: Control cells stained with Cdc42 antibodies showed two Cdc42 populations; one was dispersed throughout the cell and another existed in small discrete puncta. Bottom: MYO5B-KD cells stained with Cdc42 showed dispersal and loss of Cdc42. (B) Top-Left: Quantitation of mean fluorescence in maximum-intensity Z-stack projections of Cdc42 fluorescence. Top-Right: Western blot quantitation showed a decrease in total Cdc42 in MYO5B-KD. Bottom: Western blot showed a decrease in total Cdc42 in MYO5B-KD. (C) Top-Left: In control cells, active Cdc42 accumulated in sub-apical puncta by immunostaining. Top-Right: In MYO5B-KD cells, active Cdc42 was reduced by immunostaining. Bottom: Cdc42 activity assay of control and MYO5B-KD cells with GTPγS positive controls labeled (PC) and GDPγS negative controls labeled (NC) showed a decrease in total Cdc42 and a decrease in active Cdc42 in MYO5B-KD cells. (D) Top: In normal duodenum, Cdc42 and aPKC staining was localized to the brush border. Bottom: In MVID patient duodenum, Cdc42 was decreased and aPKC was redistributed into the cytoplasm. Scale bars in A and C are 10μm, and in D are 50μm in all panels and 10μm in the insets. Statistical significance is denoted by *p ≤ 0.05, ** p ≤ 0.01, and ***p≤ 0.001 using the Mann-Whitney-test. Error bars denote S.E.M.

To determine the underlying effects of the Navajo MYO5B mutation on trafficking to microvilli and polarity loss, we stained the MVID patient samples for Rab8a and Rab11a. Both Rab8a and Rab11a were distributed sub-apically in control duodenal biopsy samples, with Rab8a showing a sub-apical and lateral distribution and Rab11a showing a sub-apical vesicle distribution (Figure 19A and C). In the MVID patient sample, Rab8a was dispersed throughout the cytoplasm and accumulated in small puncta (Figure 19B). Moreover, in the MVID patient samples, Rab11a was dispersed throughout the cytoplasm away from its normal distribution and accumulated with increased fluorescence intensity throughout the enterocytes (Figure 19D). These findings demonstrate that loss or mutation of MYO5B leads to a disordered distribution of Rab8a and Rab11a both *in vitro* and in MVID patients, and suggest that MYO5B tethers these Rabs and their associated vesicles in the apical domain.

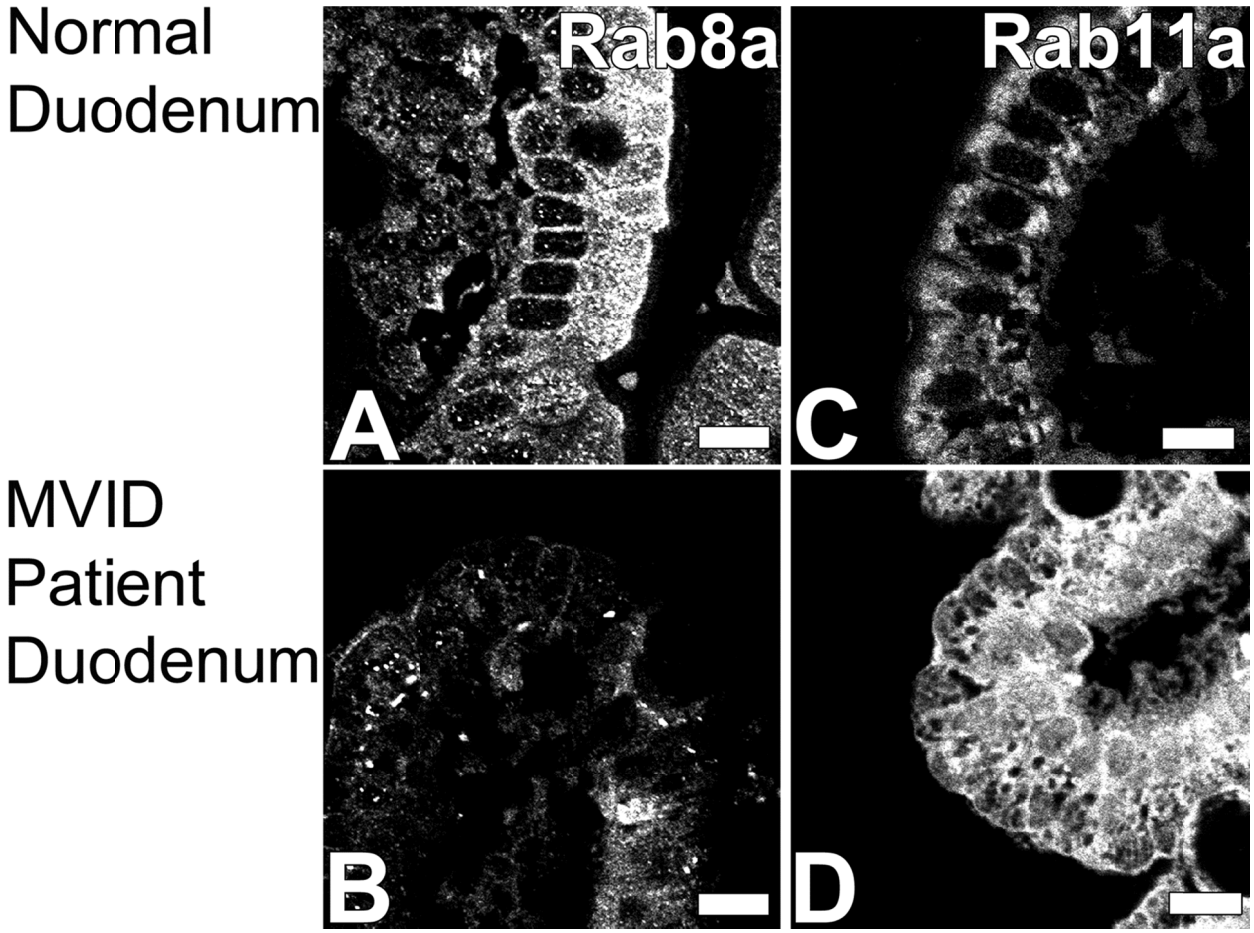

Figure 19. Both Rab8a and Rab11a are dispersed from their normal subapical distributions in MVID patient duodenum.
(A) Normal duodenum stained for Rab8a showed sub-apical-lateral localization of Rab8a. (B) Staining of MVID patient duodenum for Rab8a showed dispersal of Rab8a and accumulation of Rab8a in small puncta vesicles. (C) Normal duodenum stained for Rab11a showed sub-apical localization of Rab11a. (D) Staining of a MVID patient duodenum for Rab11a showed dispersal from the sub-apical region and accumulation of Rab11a throughout the cytoplasm. It should be noted, for visualization of Rab11a staining in the normal duodenum sample levels were adjusted independently of the MVID patient sample, because of the intense Rab11a staining in the patient sample. Scale bars are 10μm in all panels.

MYO5B-P660L mutation causes the motor to move slowly along F-actin

All of our preceding studies suggested that loss of MYO5B expression could replicate many aspects of the MVID phenotype, with the notable exception of the production of microvillus inclusions. The MYO5B-P660L mutation seen in Navajo MVID patients lies outside the actin binding region, so the functional impact of this mutation required clarification. We expressed 3x-mCitrine-MYO5B-WT or 3x-mCitrine-MYO5B-P660L in HEK cells and both proteins were precipitated by F-actin pull-down (data not shown). It should be noted, MYO5B breaks down readily because of an internal PEST site, which can be appreciated by the second band visualized in the F-actin pull-down. Previously published work has shown that MYO5B motors that move slowly along F-actin or cannot bind to F-actin are non-functional motors (Szperl, Golachowska et al. 2011). Thus, to evaluate the effects of MYO5B-P660L mutation on MYO5B dynamics in live cells, we used single molecule TIRF-FRAP microscopy. We reasoned that fluorescent myosin motors with similar actin binding properties and motor function would demonstrate comparable photo-bleaching kinetics. For these studies, we tagged synthetic MYO5B wild type (MYO5B-WT) motor domain (MYO5B-1016X) and MYO5B-P660L motor domain (the Navajo MVID mutation, MYO5B-P660L-1016X) with three tandem copies of mCitrine (3x-mCitrine) and expressed these constructs in BF16 cells (Muller, Hess et al. 2008). Previous studies have utilized this approach to measure average motor speed, the processivity of single kinesin molecules, and the life-times of myosin-1a tail/membrane interactions (Cai, McEwen et al. 2009; Mazerik and Tyska 2012). 3x-mCitrine-MYO5B-WT-1016X molecules demonstrated localization and movement towards the tips of filopodia, which indicated active forward movement along

F-actin (Figure 20A). In contrast, 3x-mCitrine-MYO5B-P660L-1016X localized with the F-actin binding protein espin, but showed negligible movement towards the tips of filopodia, which is indicative of stalled forward movement along F-actin (Figure 20A). Single molecule TIRF-FRAP imaging of 3x-mCitrine-MYO5B-WT-1016X showed that these motors were photo-bleached by 50% of the maximum intensity after 30 seconds of laser exposure in live BF16 cells (Figure 20B). In contrast, 3x-mCitrine-MYO5B-P660L-1016X photo-bleached to 20% of the maximum intensity after 30 seconds of laser exposure in live BF16 cells, consistent with a stalled motor (Figure 20B). Together, these results suggest that, while MYO5B-P660L can bind F-actin, the motor movement is consistent with a rigor-type phenotype for a non-functioning slow moving motor.

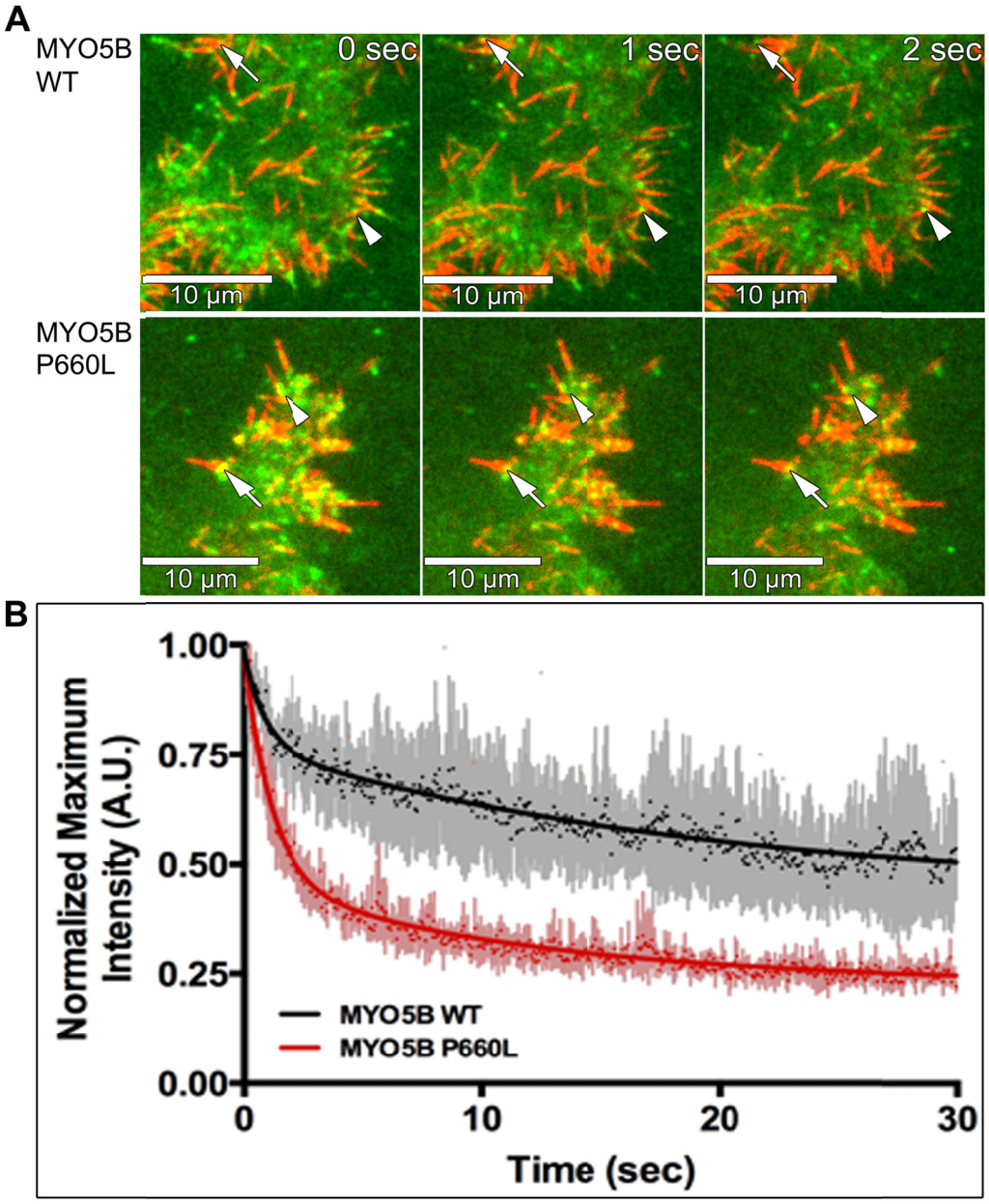

Figure 20. Single molecule TIRF-FRAP imaging showed an increase in photo-bleaching in 3x-mCitrine-MYO5B-P660L-1016X transfected constructs compared to 3x-mCitrine-MYO5B-WT-1016X, and these molecules are also stalled on filopodia.

(A) Stills of BF16 cells transfected with 3x-mCitrine-MYO5B-WT-1016x or 3x-mCitrine-MYO5B-P660L-1016x and mCherry-Espin over 2 seconds showing localization and movement of 3x-mCitrine-MYO5B-WT-1016x to the tips of filopodia (arrows). 3x-mCitrine-MYO5B-P660L-1016x, however, does not localize to the tips of filopodia and is never observed in active forward motion along F-actin filaments (arrows). Scale bars are 10µm. (B) TIRF-FRAP of 3x-mCitrine-MYO5B-WT-1016x (black) and 3x-mCitrine-MYO5B-P660L-1016x (red) showed a greater than 30% increase in photo-bleaching in the 3x-mCitrine-MYO5B-P660L-1016x transfected cells. Error bars denote S.D.

Re-expression of MYO5B-WT rescues the phenotype in MYO5B-KD cells, but MYO5B-P660L re-expression does not rescue and causes microvillus inclusion formation

To determine the specificity of MYO5B knockdown effects in CaCo2-BBE MYO5B-KD cells, we re-expressed synthetic full-length sequences for either mCherry-MYO5B-WT or mCherry-MYO5B-P660L. We stained both of these “rescued” cell lines for the microvillar markers ezrin and phalloidin (F-actin). The re-expression of mCherry-MYO5B-WT in MYO5B-KD cells restored apical microvilli, as visualized by both immunofluorescence and SEM (Figure 21A, B, and E). In contrast, the expression of mCherry-MYO5B-P660L in CaCo2-BBE MYO5B-KD cells failed to restore microvilli and induced the formation of microvillus inclusions containing F-actin-based structures with inward facing microvilli, as visualized by both immunofluorescence and SEM (Figure 21C, D, and F). Microvillus inclusions form normally in CaCo2 cells during their initial polarization on Transwell filters, but after 14 days on Transwell filters, unless induced by colchicine or nocodazole treatment, microvillus inclusions do not form (Gilbert and Rodriguez-Boulan 1991). Quantitation of microvillus inclusions in CaCo2-BBE control, MYO5B-KD, MYO5B-WT rescue, and MYO5B-P660L re-expression cells showed a significant increase in microvillus inclusions associated with MYO5B-P660L re-expression over the other control or wild type MYO5B-rescued cell lines (Figure 21H).

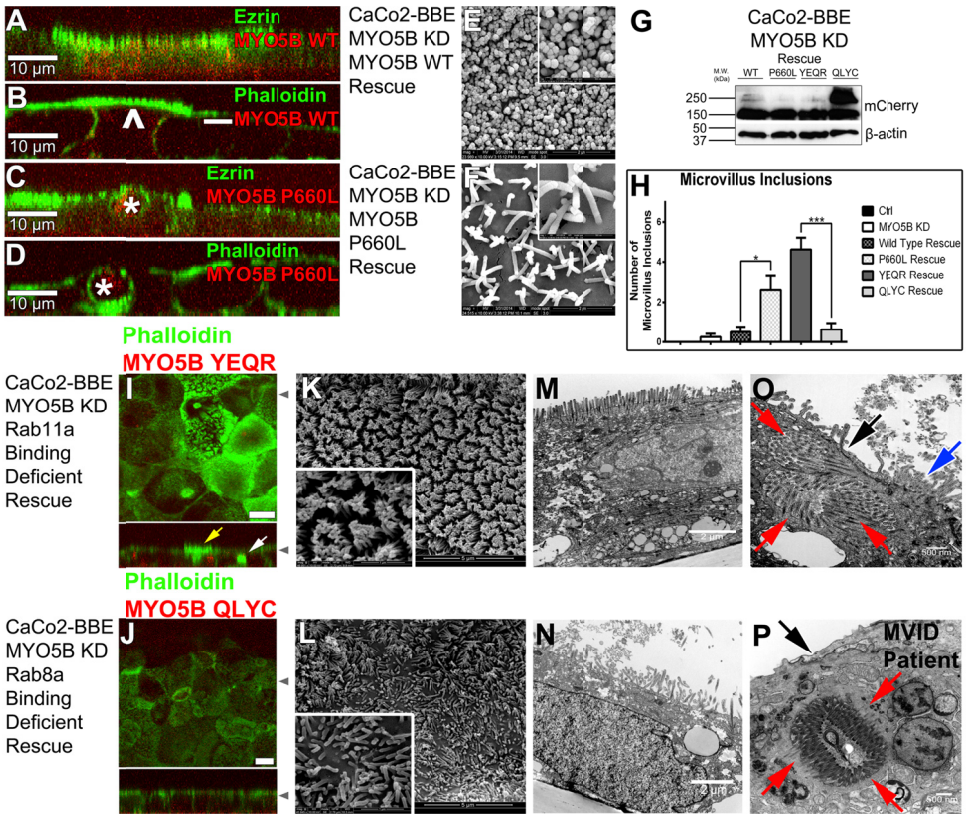

Figure 21. MYO5B-WT and MYO5B-YE/QR rescue the MYO5B-KD phenotype, while MYO5B-P660L and MYO5B-YE/QR promote microvillus inclusions.
(A) Ezrin and (B) phalloidin staining in microvilli was rescued in MYO5B-KD–expressing MYO5B-WT. Arrowhead, high expressers; –, low expressers. (C and D) Ezrin and phalloidin staining in microvilli was not rescued in MYO5B-KD–expressing MYO5B-P660L and induced microvillus inclusions (asterisks). (E and F) Scanning electron microscopy of (E) MYO5B-KD–expressing MYO5B-WT showed reestablished mature microvilli and (F) MYO5B-KD–expressing MYO5B-P660L showed immature microvilli in the tepee-like stage. (G) Western blot of rescue cell lines showed similar expression levels of mCherry. (H) Microvillus inclusions in MYO5B-KD re-expressing MYO5B-P660L and MYO5B-YE/QR were significantly higher compared with other cell lines. (I) Expression of MYO5B-YE/QR reestablished phalloidin staining of microvilli (yellow arrow) but also induced the formation of microvillus inclusions (white arrow). (J) Expression of MYO5B-QL/YC partially recovered microvilli. (K and M) Scanning electron microscopy and TEM of MYO5B-KD cells expressing MYO5B-YE/QR showed reestablished mature microvilli. (L and N) Scanning electron microscopy and TEM of MYO5B-KD cells expressing MYO5B-QL/YC showed partial rescue of non-uniform microvilli. (O) MYO5B-KD cells expressing MYO5B-YE/QR showed subapical microvillus inclusions (red arrows), with corresponding denuded microvilli (black arrow) and surrounding brush border (blue arrow). (P) MVID patient duodenum with pathognomonic microvillus inclusion (red arrows) and denuded microvilli (black arrow). Scale bar: 10 µm (A–D, I, and J); 2 µm (E and F); 500 nm (E and F, insets); 5 µm (K and L); 1 µm (K and L, insets), 2 µm (M and N); 500 nm (O and P). *P ≤ 0.05, ***P ≤ 0.001, Mann-Whitney test. Error bars denote mean ± SEM.

The mCherry-MYO5B-WT rescue of MYO5B-KD cells, partially re-established the normal distribution of CLDN1 and CLDN2 (Figure 22A). In contrast, the expression of mCherry-MYO5B-P660L in MYO5B-KD cells caused CLDN1 to be mislocalized into the cytoplasm and an increase in CLDN2 at the lateral membrane (Figure 22A). The mCherry-MYO5B-WT rescue of CaCo2-BBE MYO5B-KD cells also re-established the normal distribution of DPPIV, while the expression of mCherry-MYO5B-P660L caused mislocalization of DPPIV to microvillus inclusions and large vesicles (Figure 22B). Re-expression of mCherry-MYO5B-WT in MYO5B-KD cells restored the normal distributions of both Rab8a and Rab11a-containing vesicles (Figure 23A). In contrast, the expression of mCherry-MYO5B-P660L in CaCo2-BBE MYO5B-KD cells failed to rescue the dispersal of either Rab8a or Rab11a (Figure 23A). The failure of MYO5B-P660L to rescue suggests that this motor has lost its ability to function as a tether, likely due to loss of the ability of MYO5B-P660L to treadmill on F-actin at the speed of actin polymerization (Rafelski and Theriot 2005; Pierobon, Achouri et al. 2009; Kodera, Yamamoto et al. 2010). These findings suggest that MYO5B-P660L expression promotes microvillus inclusion formation and can recapitulate the MVID phenotype.

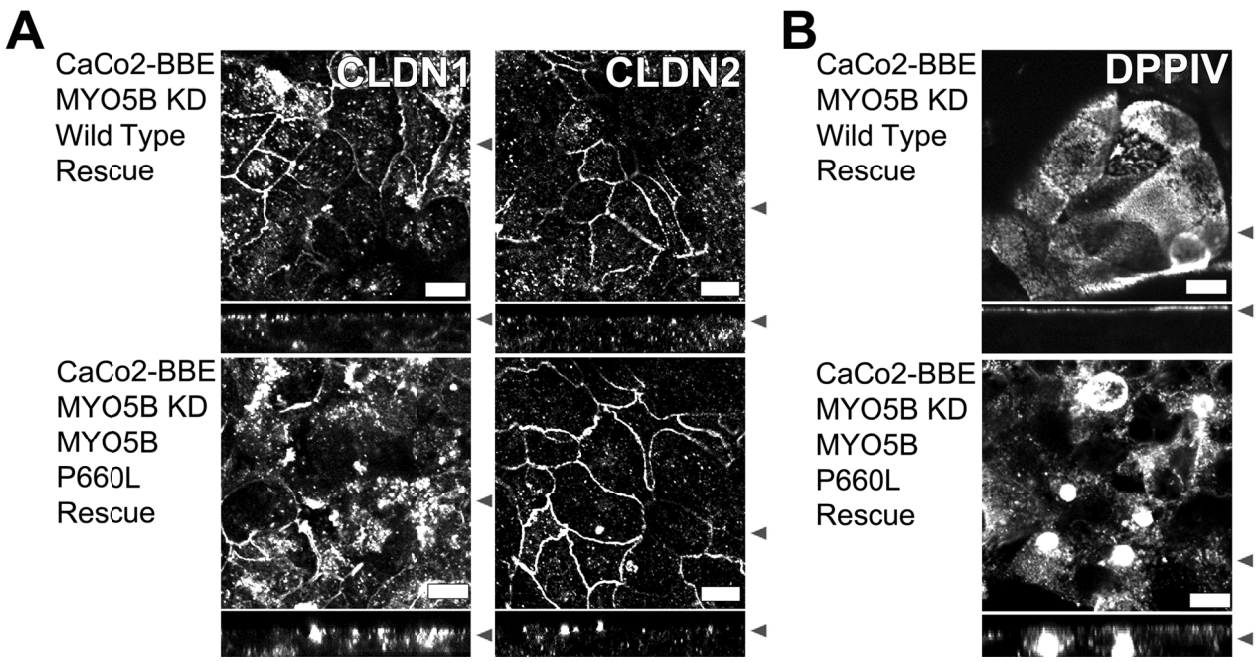

Figure 22. Re-expression of MYO5B-WT and MYO5B-P660L in CaCo2-BBE MYO5B-KD cells stained with CLDN1, CLDN2, and DPPIV.
In all panels, X-Y confocal images are shown above Z-axis reconstructions. (A) Top: MYO5B-KD cells with mCherry-MYO5B-WT re-expression showed partial recovery of normal CLDN1 and CLDN2 staining. Bottom: MYO5B-KD cells with mCherry-MYO5B-P660L expression showed exacerbation of the MYO5B-KD phenotype with internalization of CLDN1 and an increase in lateral CLDN2 staining. (B) It should be noted, for visualization of DPPIV staining in the mCherry-MYO5B-WT and mCherry-MYO5B-P660L expressing cells were adjusted independently. Top: MYO5B-KD cells with mCherry-MYO5B-WT re-expression showed recovery of normal DPPIV staining. Bottom: MYO5B-KD cells with mCherry-MYO5B-P660L expression showed exacerbation of the MYO5B-KD phenotype with DPPIV positive microvillus inclusion formation. Scale bars are 10μm in all panels.

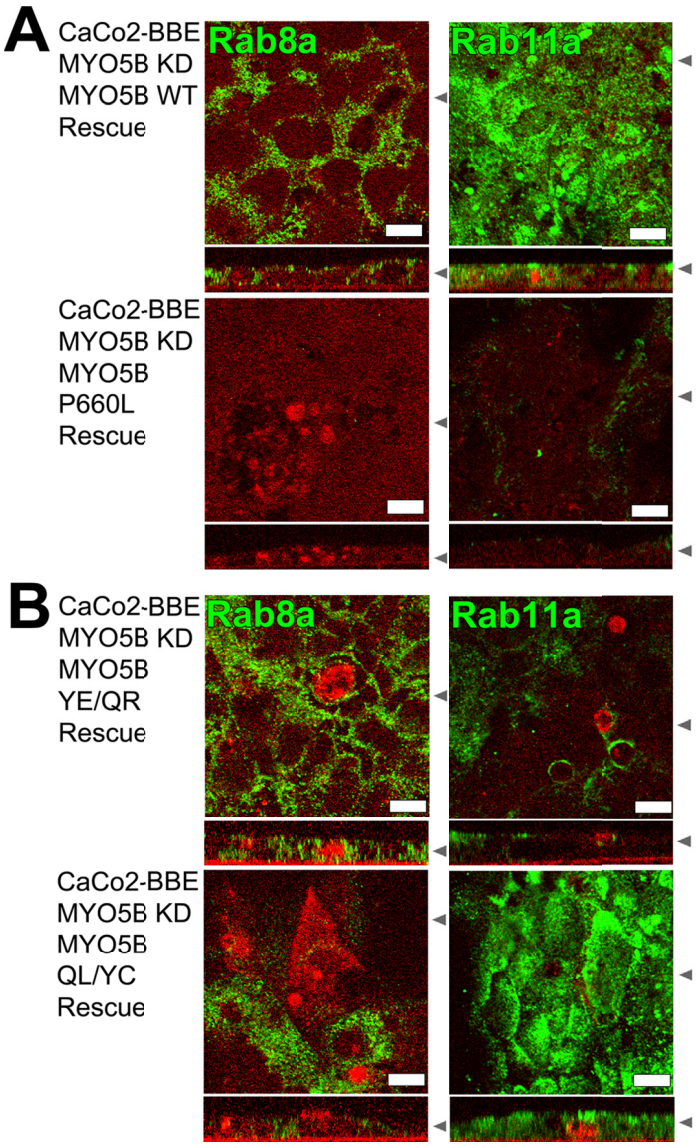

Figure 23. Rab8a and Rab11a immunostaining in MYO5B-KD cells expressing MYO5B-WT rescued Rab8a and Rab11a, MYO5B-QLYC rescued Rab11a, MYO5B-YEQR rescued Rab8a, and MYO5B-P660L does not rescue either Rab.
(A) Left-top: Expression of mCherry-MYO5B-WT (red) rescued the dispersal of Rab8a (green) in MYO5B-KD. Left-bottom: Expression of mCherry-MYO5B-P660L (red) failed to rescue the dispersal of Rab8a (green) in MYO5B-KD cells. Right-top: Expression of mCherry-MYO5B-WT (red) rescued the dispersal of Rab11a (green) in MYO5B-KD. Right-bottom: Re-expression of mCherry-MYO5B-P660L (red) failed to rescue the dispersal of Rab11a (green) in MYO5B-KD. (B) Left-top: Expression of mCherry-MYO5B-YE/QR (red) in MYO5B-KD cells rescued Rab8a (green). Left-bottom: Expression of mCherry-MYO5B-QL/YC (red) in MYO5B-KD cells did not rescue Rab8a. Right-top: Expression of mCherry-MYO5B-YE/QR (red) in MYO5B-KD cells did not rescue Rab11a (green). Left-bottom: Expression of mCherry-MYO5B-QL/YC (red) in MYO5B-KD cells rescued Rab11a. In all panels, X-Y confocal images are shown above Z-axis reconstructions. Scale bars are 10μm in all panels.

MYO5B mutant that selectively binds to Rab8a rescues the loss of microvilli in CaCo2-BBE MYO5B-KD cells

In previous work, we have identified two mutants of MYO5B that have altered interactions with critical Rab proteins (Roland, Bryant et al. 2011). MYO5B(Y1714E/Q1748R) (designated MYO5B-YE/QR) binds Rab8a, but does not interact with Rab11a. Contrastingly, MYO5B(Q1300L/Y1307C) (designated MYO5B-QL/YC) can bind to Rab11a, but does not interact with Rab8a. Thus, to determine if aspects of MYO5B loss are referable to interactions with specific Rab proteins, we evaluated the MYO5B-KD cell lines with re-expression of either mCherry-MYO5B-YE/QR or mCherry-MYO5B-QL/YC. The expression of mCherry-MYO5B-YE/QR in MYO5B-KD cell lines re-established microvilli as visualized by phalloidin staining, SEM, and TEM (Figure 21I, K, and M). However, we also observed the presence of microvillus inclusions in these cells by immunofluorescence and TEM (Figure 21I and O). It should be noted, microvillus inclusions that formed were consistent with the size seen in MVID patient samples (Figure 21O and P). Re-expression of mCherry-MYO5B-QL/YC in MYO5B-KD cells elicited incomplete rescue of microvilli, but no microvillus inclusions formed (Figure 21J, L, and N). Quantitation of microvillus inclusions in MYO5B-QL/YC and MYO5B-YE/QR rescued cells showed a significant increase in microvillus inclusions in the MYO5B-YE/QR expressing cells compared with MYO5B-QL/YC expressing cells (Figure 21H).

The expression of mCherry-MYO5B-YE/QR in MYO5B-KD cells re-established the normal pattern for Rab8a, but not Rab11a, distribution (Figure 23B). Contrastingly, the expression of mCherry-MYO5B-QL/YC in MYO5B-KD cells did not elicit the normal

Rab8a distribution, but was able to re-establish the normal distribution of Rab11a (Figure 23B). Interestingly, mCherry-MYO5B-QL/YC was able to re-establish the proper distribution of both ezrin and DPPIV, while mCherry-MYO5B-YE/QR did not rescue either (data not shown). Thus, establishment of apical microvilli appeared to involve interactions of MYO5B with Rab8a, while microvillus inclusion formation was associated with a loss of Rab11a interactions with MYO5B (Figure 24).

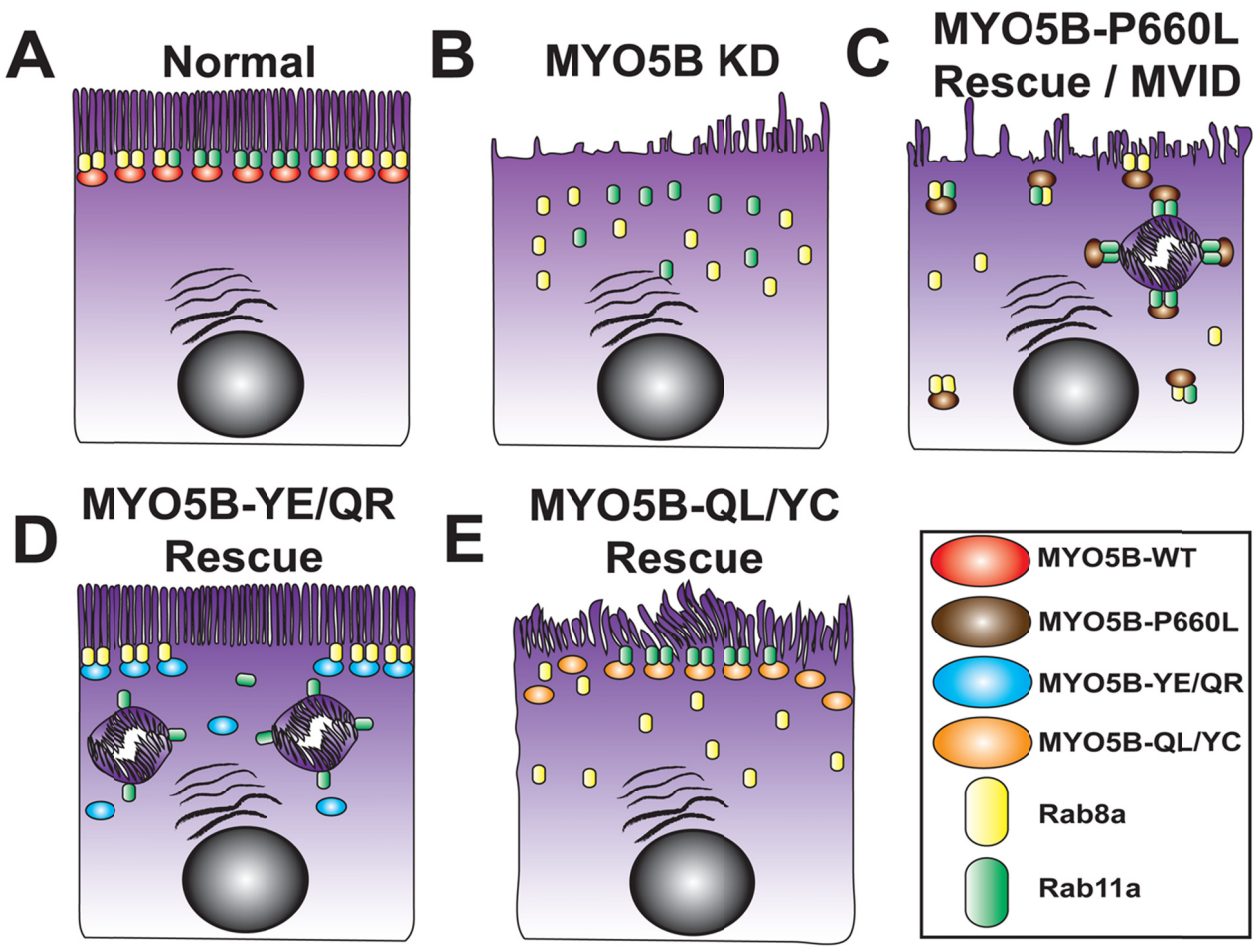

Figure 24. MYO5B interacts with both Rab8a and Rab11a to maintain normal apical brush border.
(A) Normal localization of both Rab8a and Rab11a with MYO5B permits the normal appearance of the apical brush border in enterocytes. (B) Loss of MYO5B causes the relocalization of Rab8a and Rab11a to the cytoplasm and disrupts the apical brush border. (C) Rescue of MYO5B-KD cells with MYO5B-P660L induces microvillus inclusions and exacerbates the loss of apical microvilli. (D) Rescue of MYO5B-KD cells with MYO5B-YE/QR induces microvillus inclusions, but rescues apical microvilli. (E) Rescue of MYO5B-KD cells with MYO5B-QL/YC does not rescue apical microvilli, but does not induce microvillus inclusions.

Microvillus inclusions arise from internalization of the apical surface

Microvillus inclusions could arise when either endocytosis or exocytosis is altered (Gilbert and Rodriguez-Boulan 1991). Since microvillus inclusions do not contain acid phosphatase, a lysosomal marker, it was postulated that microvillus inclusions do not originate from autophagocytosis of the apical membrane (Lake 1988). Previous investigations using organ culture of duodenal biopsies from MVID patients incubated for 5 min in PBS containing cationized ferritin suggested that microvillus inclusions originate from engulfing brush-border membrane (Reinshagen, Naim et al. 2002). We postulated that because of the large size of the microvillus inclusions only macropinocytosis could facilitate such a large endocytic event. Macropinocytosis is an actin-based endocytic process in which the plasma membrane is internalized to form large endocytic vesicles >0.2 μm in diameter, designated macropinosomes (Wang, Kerr et al. 2010). In MYO5B-YE/QR re-expressing CaCo2-BBE cells, we observed microvillus inclusions forming in a series of stages. First, we observed cells with apical membrane invaginations into the cytoplasm (Figure 25A). Other cells showed invaginations with increased size, as well as internalized inclusions where the apical membrane was completely engulfed and separated from the apical surface (Figure 25B and C). To determine the origin of these inclusions, we biotinylated the apical surface of the mCherry-MYO5B-YE/QR expressing CaCo2-BBE MYO5B-KD cells, and we, fixed and stained with phalloidin and fluorescent streptavidin after 24 hours (Figure 25D-F). We observed the presence of fluorescent-streptavidin in the microvillus inclusions in CaCo2-BBE cells expressing mCherry-MYO5B-YE/QR (Figure 25D-F). Similar results were observed in cells expressing mCherry-MYO5B-P660L (data not shown). To

examine whether microvillus inclusions in CaCo2-BBE cells represented products of macropinocytosis, we stained mCherry-MYO5B-YE/QR expressing MYO5B-KD cells with phalloidin and antibodies against sorting nexin 18 (SNX18), a marker of early macropinosome formation (Figure 25G-I) (Wang, Kerr et al. 2010). SNX18 and phalloidin double-labeling of these cells revealed that early stages of microvillus inclusion formation were marked by SNX18 staining, while more complete microvillus inclusions lost their SNX18 staining as they matured (Figure 25G-I). Interestingly, some microvillus inclusions detected in MVID patient samples triple labeled for SNX18, MYO5B, and DPPIV (Figure 26). As a whole, these results provide evidence that microvillus inclusions arise from macropinocytosis of the apical surface.

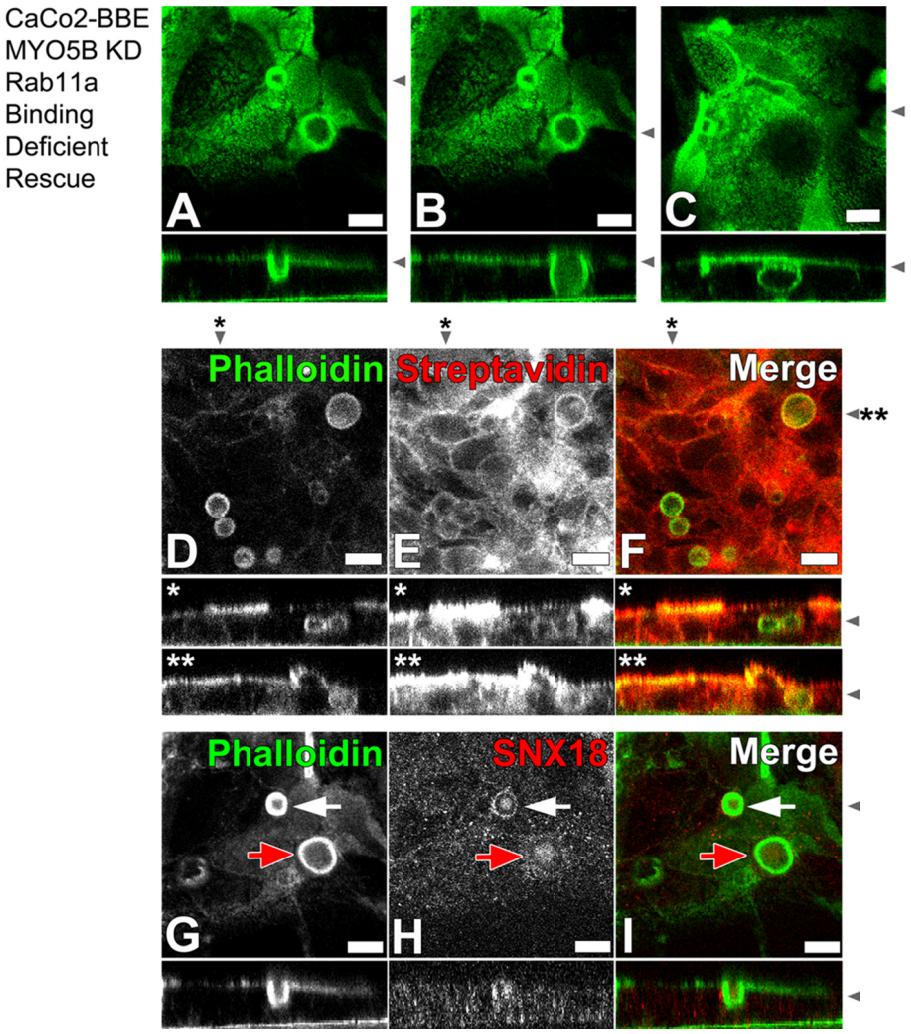

Figure 25. Microvillus inclusions in CaCo2-BBE cells arise from internalization of the apical surface.
In all panels, X-Y confocal images of MYO5B-YE/QR expressing MYO5B-KD cells are shown above Z-axis reconstructions. (A-C) CaCo2-BBE cells were stained with phalloidin (green). A and B use corresponding X-Y and different Z-axis reconstructions from the same field of view. The Z-axis reconstruction in (A) shows the development of an apical invagination, whereas (B) shows a nearly completed microvillus inclusion. (C) Shows a separate field of view where the Z-axis reconstruction demonstrates a completely internalized microvillus inclusion. (D-F) The apical surface of CaCo2-BBE cells were biotinylated and fixed after 24 hours. These cells were then stained with phalloidin (green) and fluorescent-streptavidin (red). "*" indicates the position for the first Z-axis reconstruction directly below the X-Y confocal image. "**" indicates the position for the second Z-axis reconstruction directly below the first Z-axis reconstruction. Fluorescent-streptavidin was observed in microvillus inclusions inside the cells. (G-I) CaCo2-BBE cells from A and B double labeled with both phalloidin and SNX18 showed SNX18 localization at the bottom of a forming microvillus inclusion (white arrow), while more mature microvillus inclusions showed dispersal of SNX18 (red arrow). Scale bars in all panels are 10μm.

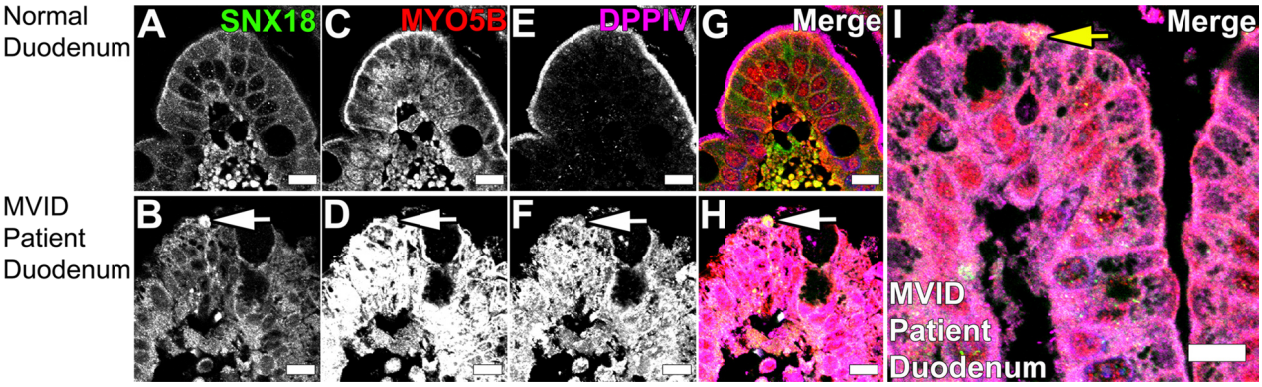

Figure 26. Immunostaining of MVID patient duodenum shows early microvillus inclusions labeled with SNX18, MYO5B, and DPPIV.
(A) Normal duodenum section stained for SNX18 showed sub-apical and lateral localization of SNX18. (B) Staining of MVID patient duodenum for SNX18 showed localization of SNX18 to early microvillus inclusion (white arrow). (C) Normal duodenum stained for MYO5B showed sub-apical localization of MYO5B. (D) Staining of a MVID patient duodenum for MYO5B showed dispersal from the sub-apical region and accumulation and increase of MYO5B staining throughout the cytoplasm and localization of MYO5B to an early microvillus inclusion (white arrow). (E) Normal duodenum stained for DPPIV showed apical localization of DPPIV. (F) Staining of MVID patient duodenum for DPPIV showed localization of DPPIV to an early microvillus inclusion (white arrow). (G-H) Merged images of normal duodenum and MVID patient samples stained with SNX18, MYO5B, and DPPIV from A-F. (I) Merged image of MVID patient duodenum showed an early microvillus inclusion formation (yellow arrow) staining for SNX18, MYO5B and DPPIV. Scale bars in all panels are 10μm.

Discussion

In this chapter, we developed a cellular model of MVID using shRNA to stably knockdown MYO5B and then re-expressed wild type MYO5B and MYO5B mutants in CaCo2-BBE cells. Using this model we demonstrated that loss of MYO5B caused a decrease in apical microvilli and dispersal of Rab8a and Rab11a from the sub-apical surface. Rab8a and Rab11 family members act on recycling endosomes and are involved in the establishment of a variety of specialized apical processes that depend on apical trafficking. Rab8a and Rab11a interactions with MYO5B are required for proper establishment of apical polarity in MDCK cells, and phosphorylation of the Rab11 effector Rab11-FIP2 by Par1b (also known as MARK2) also regulates the formation of polarity and the appropriate assembly of junctional proteins (Roland, Bryant et al. 2011; Lapierre, Avant et al. 2012). Other studies have suggested that Rab8a and Rab11a are involved in the assembly and maintenance of apical primary cilia in kidney cells (Kaplan, Molla-Herman et al. 2010; Knodler, Feng et al. 2010; Lim, Chua et al. 2011). However, enterocytes do not form primary cilia above the transition zone, and, in contrast, the mechanisms behind microvilli formation have not been well characterized. This study supports the concept that MYO5B functions as a dynamic tether for both Rab8a and Rab11a and normally maintains these proteins at their appropriate sub-apical membrane localization. The present investigation has also shown that uncoupling of MYO5B from Rab8a promotes loss of microvilli, since a MYO5B mutant that can bind Rab8a, but not Rab11a, re-established microvilli in CaCo2-BBE MYO5B-KD cells. However, the Rab8a-binding mutant of MYO5B also induced microvillus inclusions. Thus, formation of microvillus inclusions resulted from a loss of interactions between

Rab11a and MYO5B. Similar to expression of MYO5B-YE/QR, re-expression of MYO5B-P660L, the Navajo mutation, led to the formation of microvillus inclusions and exacerbation of the MYO5B-KD phenotype. Thus, MYO5B in concert with Rab8a and Rab11a regulates the polarity of intestinal epithelial cells, and uncoupling of these Rabs from MYO5B causes gross changes in cellular polarity and mucosal integrity in patients with MVID. These results when paired with previous work demonstrate that MYO5B interacts with Rab8a and Rab11a to regulate enterocyte polarity, apical trafficking, and microvilli growth. Both Rab8a and Rab11a bind to MYO5B directly on recycling vesicles (Roland, Bryant et al. 2011). Rab11a also regulates actin dynamics in a MYO5B-dependent manner, and we have now implicated Rab11a in the recycling of apical brush border contents from macropinosomes (Holubcova, Howard et al. 2013). Rab8a also plays a role in apical recycling and trafficking. Cdc42 associates with both Rab8a and Rab11a positive vesicles, and is also activated via Rab8a through Tuba to facilitate regulation of cellular polarity and actin polymerization (Bryant, Datta et al. 2010). All of these processes aid in the formation and maintenance of microvilli (Figure 27).

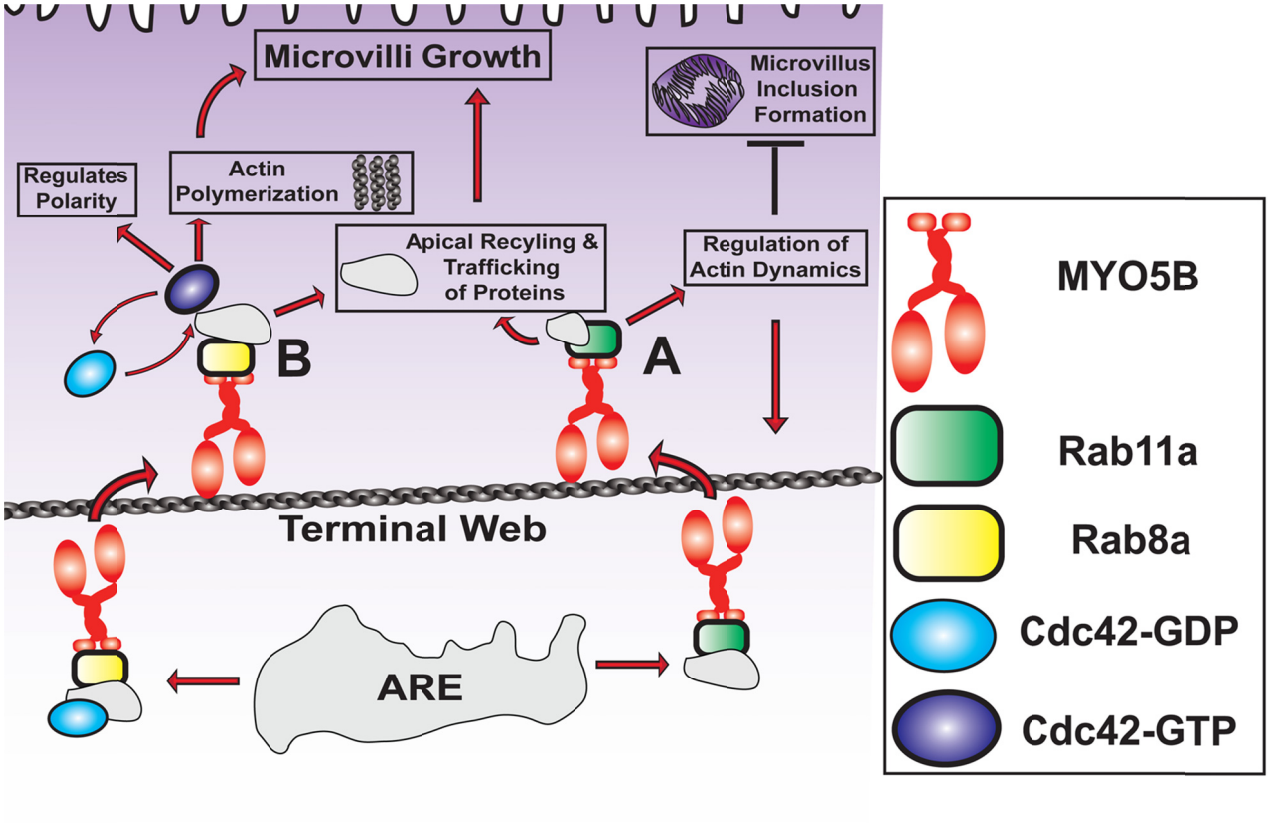

Figure 27. MYO5B interacts with Rab8a and Rab11a to regulate enterocyte polarity, apical trafficking, and microvilli growth.
The gradient shown attempts to illustrate in white (microtubule rich region) and purple (actin rich region). Both Rab8a and Rab11a bind to MYO5B directly on the ARE. (A) Rab11a regulates actin dynamics in a MYO5B-dependent manner, and has been shown to facilitate apical trafficking and recycling. We have demonstrated in this study that Rab11a is needed to halt microvillus inclusion formation, via actin dependent macropinocytosis. (B) Rab8a plays a role in apical recycling and trafficking, and has also been shown to activate Cdc42 via Tuba, which regulates cellular polarity, and facilitates actin polymerization. All of these together aid in microvilli growth.

The pathognomonic characteristic of MVID is the presence of intracellular microvillus inclusions, although they are observed in only 10% of MVID patient enterocytes, mainly at the villus tips. Interestingly, knockdown of MYO5B expression in CaCo2-BBE cells did not induce microvillus inclusions. A previous investigation reported that transient knockdown of MYO5B using siRNA in CaCo2 cells caused an increase in microvillus inclusions (Ruemmele, Muller et al. 2010). Recently, another group has found structures reminiscent of microvillus inclusions with stable knockdown of MYO5B in parental CaCo2 cells (Thoeni, Vogel et al. 2013). The differences observed in our studies likely accrue from our use of the highly polarized CaCo2-BBE cell line. Parental CaCo2 cell lines obtained from ATCC often show variable polarity. Nevertheless, re-expression of either MYO5B-YE/QR or MYO5B-P660L in CaCo2-BBE MYO5B-KD cells induced microvillus inclusions, which formed from internalization of segments of the apical membrane. Whether apical membrane macropinocytosis is a normal cellular process in polarized intestinal epithelial cells remains unclear, but colchicine treatment causes microvillar inclusions to form in normal rat small intestine (Achler, Filmer et al. 1989). In CaCo2 cells, colchicine or nocodazole treatment can also elicit microvillus inclusion formation (Gilbert and Rodriguez-Boulan 1991). Thus, the disruption of normal microtubule-dependent trafficking may cause microvillus inclusions to form. Since the normal apical recycling process is dependent on Rab11a and microtubule-dependent pathways, the microvillus inclusions may reflect the effects of mutant MYO5B molecules on the process of recycling. Thus, the non-functional MYO5B mutants may not cause the formation of microvillus inclusions, but rather induce the phenotype by the inability of

the cell to recycle internalized apical membrane through the Rab11a-dependent recycling system.

Currently, it is not understood why MVID mutations lead to an enterocyte-specific effect as opposed to more global effects, since other highly polarized epithelial tissues appear grossly unaffected by this disease. In addition to the chronic unremitting diarrhea, MVID patients can also develop extra-intestinal liver abnormalities, but it remains uncertain whether liver complications accrue from long-term TPN administration or the disease. In MVID patients, kidney function generally appears normal, but they do have an increased rate of kidney stone development (Halac, Lacaille et al. 2011). In vertebrates, there are three isoforms of myosin V: MYO5A, MYO5B, and MYO5C (Rodriguez and Cheney 2002). All three of these isoforms can interact with Rab10 and Rab8a, but only MYO5A and MYO5B can bind to Rab11 family members (Roland, Lapierre et al. 2009). One possible explanation for the severity of the intestinal phenotype in MVID patients is that MYO5A may compensate for the loss of MYO5B in other polarized cell types, and that low levels of MYO5A in enterocytes make enterocytes more vulnerable to loss or mutation of MYO5B (Roland, Lapierre et al. 2009). To address this possibility, we have attempted to rescue the MYO5B-KD of CaCo2-BBE cells with mCherry-MYO5A-WT, but re-expression of MYO5A was unable to rescue the MYO5B-KD phenotype in CaCo2-BBE cells (data not shown). It may be more likely that the mechanisms for establishing apical microvillar specializations differ in different polarized epithelial cells. Increasing evidence suggests that important parts of the trafficking machinery in one cell type might serve another function in others (Weisz and Rodriguez-Boulan 2009). Furthermore, it should be noted that even if

mutant MYO5B were affecting primary cilia function in kidney cells, few MVID patients have reached the age where polycystic disease from ciliopathy would be detected.

The question remains why infants with MVID manifest such prominent secretory diarrhea. Loss of apical microvilli would be predicted to yield an absorptive diarrhea, and loss of intestinal villi in other intestinal diseases, such as celiac disease, usually occurs without secretory diarrhea (Guarino, Lo Vecchio et al. 2012). The results presented here in both Navajo MVID patient samples and in CaCo2-BBE cells indicate that loss of functional MYO5B causes not only a deficit in microvilli, but also a global loss in polarity, which leads to alterations in both intercellular junctions and ion transport pathways necessary for adaptation through transcellular pumps and channels. The results of these changes lead to a mucosa with decrements in absorptive pathways and a leaky epithelium at the villus tips. This scenario would account for the observed secretory diarrhea. Finally, it is important to note that we observed in the Navajo MVID patient duodenal biopsies that normal ezrin-containing brush borders were often present on the enterocytes in the proximal villus. Similar results have recently been reported in sporadic cases of MVID (Thoeni, Vogel et al. 2013). The loss of apical brush border and formation of microvillus inclusions occurred in cells at the villus tips. Thus, it seems likely that the enterocyte microvilli can be formed initially and that stabilization of initial cell polarity may represent a future target for therapy in MVID infants.

Methods

Cell lines, real-time PCR analysis, lentivirus-mediated MYO5B knockdown, and rescue

Human colonic epithelial CaCo2-BBE and human embryonic kidney 293 (HEK) cell lines were grown in DMEM. The mouse melanoma BF16 cells were grown in RPMI (Cellgro). All cell media was supplemented with L-glutamine (Cellgro), nonessential amino acids (Cellgro), penicillin/streptomycin (Cellgro), 10% fetal bovine serum (FBS; Hyclone), and glucose for RPMI. Cell culture dishes and Transwell filters were purchased from (Costar). For CaCo2-BBE cells, 200,000 cells were plated and grown on 12-well Transwell filters for 15 days in culture unless otherwise stated, and media was changed daily through the culture duration.

Two lentiviral shRNA vectors targeting MYO5B (Open Biosystems V3LHS_323980 and V3LHS_323981) and a control shRNA (Open Biosystems RHS4346) were used for transduction of Caco2-BBE cells. The CaCo2-BBE cells were transduced with lentiviral media produced in HEK cells and selected using puromycin (Cellgro). Rescue of CaCo2-BBE MYO5B-KD was performed using vectors that were synthesized from optimized MYO5B sequences (Geneart) resistant to silencing by the above shRNAs, cloned into mCherry-C2 at the N-terminus, and selected using both puromycin (shRNA vector) and G418 (mCherry vector) selection.

RNA was isolated from CaCo2-BBE control and MYO5B-KD cell lines using TRIzol reagent (Invitrogen) according to the manufacturer's instructions and treated using RQ1 RNase-free DNase (Promega). cDNA was synthesized using a High

Capacity cDNA Reverse Transcriptase Kit (Applied Biosystems) with both oligo-dT and random hexamer primers as described previously by Lapierre, et al. 2012 (Lapierre, Avant et al. 2012). Real-time PCR was performed using a StepOnePlus real-time PCR system with Express SYBR Green ER Supermix (Applied Biosystems) and the following primer pairs:

MYO5B-Forward 5'-CAGCAAGAAAGTCCAGGCGG-3'

MYO5B-Reverse 5'-CCACGGTTTCCTCAGCTCA-3'

GAPDH-Forward 5'-AGATCCCTCCAAAATCAAGTGG-3'

GAPDH-Reverse 5'-GGCAGAGATGATGACCCTTTT- 3'

The above primers were validated for efficiency and melting temperature, and the results were analyzed by the comparative CT method.

Human tissue preparation

MVID patient samples were obtained via endoscopic biopsy for four of the samples we utilized, and via resection for one sample for a total of five MVID patient samples. All tissue samples were obtained through protocols approved by the Phoenix Children's Hospital IRB. All biopsy and resection samples were washed in PBS and fixed in 10% formalin. Samples were stored in 70% ethanol, embedded, and sectioned for immunostaining.

Western blot

The CaCo2-BBE MYO5B-KD and CaCo2-BBE control cell lines were plated on 6-well Transwell filters for 15 days, washed in PBS, and lysed in RIPA buffer (50 mM Tris-HCl, pH 7.4, 150 mM NaCl, 1% NP-40, 0.5% sodium deoxycholate, 0.1% SDS) for 10 minutes at 4°C. The lysates were sonicated for 25 seconds and centrifuged at 16,000 × g for 10 minutes. The protein concentration was determined by bicinchoninic acid (BCA) method using the Pierce BCA protein assay reagent (Pierce) as described previously by Krishnan, et al. 2013 (Krishnan, Lapierre et al. 2013). A 20 µg total protein amount was suspended in 1× SDS Sample buffer, heated for 10 minutes at 70°C, resolved on a 6 to 12% SDS–PAGE gel, and transferred to Protran Nitrocellulose Transfer Membrane (Whatman). The blots were blocked in 5% DMP/TBS-T (5% dry milk powder in Tris-buffered saline, 0.01% Tween-20). The blots were incubated for 1 hour at room temperature or overnight at 4°C in primary antibody diluted in 1% DMP/TBS-T. The blots were washed five times for 10 minutes at room temperature in TBS-T (0.1% Tween-20) and incubated for 1 hour at room temperature with horseradish peroxidase–conjugated secondary antibodies (Jackson ImmunoResearch) and washed five times for 10 minutes at room temperature with TBS-T (0.1% Tween-20), followed by one wash with TBS. Specific tagging was identified by chemiluminescence reagent (Pierce), and detected using BioMax ML film (Kodak). Western blot quantitation was performed using scanned tiffs placed into Image Studio (LI-COR Biosciences) to determine the signal. Using Excel the normalized signal was determined relative to α-Tubulin or β-actin. Significance was determined using the Mann-Whitney one-tailed test,

and these measurements were graphed using Prism-GraphPad. All of these experiments were performed in triplicate for each protein of interest.

Confocal immunofluorescence and SIM

The CaCo2-BBE MYO5B-KD and CaCo2-BBE control cell lines were plated on 12-well Transwell filters and cultured for 15 days. Cells were washed with PBS and fixed. For tight and adherens junction staining, cells were fixed with 100% methanol for 5 minutes at −20°C. For all other staining, the cells were fixed in 4% paraformaldehyde (PFA) for 15 minutes at room temperature. These cells were washed three times with PBS and blocked/extracted for 30 minutes at room temperature in 10% normal donkey serum (Jackson ImmunoResearch) and 0.3% Triton X-100 in PBS. Cells were incubated overnight at 4°C with primary antibodies diluted in 1% normal donkey serum and 0.01% Tween-20 in PBS. Cells were washed three times for 15 minutes at room temperature with 0.01% Tween-20 in PBS (PBS-T). Appropriate secondary antibodies were conjugated for immunofluorescence with Alexa 488, Alexa 568, Alexa 647, Cy3, or Cy5 (1-hour incubation at room temperature). Detailed information on primary antibodies and their dilutions are listed in Table 1. The cells were washed three times in PBS-T and washed once in PBS, and then washed in water and mounted with ProLong Gold plus 4′,6-diamidino-2-phenylindole (DAPI; Invitrogen).

All images were captured with an Olympus FV-1000 confocal microscope (Olympus) using a 60x oil immersion objective with a numerical aperture of 1.42 and using the microscope's software at a 3x optical zoom. The individual images were

converted to tiff files with the FV-1000, and Photoshop (Adobe) or ImageJ was used to create the final figures.

Samples for SIM were prepared as for confocal immunofluorescence (see above). SIM imaging was performed on a DeltaVision OMX microscope (Applied Precision Inc.) using 488 nm, 568 nm, and 642 nm lasers. Reconstruction and alignment of SIM images was performed using softWoRx version 5.0 (Applied Precision Inc.). These corrections were applied back into the acquired images, and Photoshop (Adobe) was used to produce the final images.

Trans-epithelial electrical resistance measurement

The cell lines were plated on 12-well Transwell filters, and media was changed every day. The TEER was measured using a Millicell-ERS (Millipore) for each Transwell filters, the numbers were recorded, and the results are expressed in ohm*cm^2. All of these experiments were done in triplicate for each time point of interest. Significance was determined using the Mann-Whitney one-tailed test, and these measurements were graphed using Prism-GraphPad.

Scanning electron microscopy

CaCo2-BBE cell lines were washed three times with PBS. The cells were fixed with 3% glutaraldehyde in SEM buffer (0.1M sodium phosphate buffer, pH 7.4, 0.1M sucrose) at 4°C overnight. Cells were washed with SEM buffer twice, treated with 1% osmium tetroxide (in SEM buffer) for 1 hour on ice, and washed three times with SEM buffer. The cells were dehydrated with a serial dilution of ethanol (35, 50, 70, 95, and 100%) for 15 min each and incubated with hexamethyldisilazane (HMDS). After the

HMDS treatment, samples were mounted on stubs and coated with gold in a sputter coater, and analyzed using an FEI Quanta 250 SEM (Vanderbilt Cell Imaging Shared Resource, Vanderbilt University).

Immunofluorescence quantitation

All images were captured with an Olympus FV-1000 confocal microscope (Olympus) using a 60x oil immersion objective as detailed above. The Z-stacks were exported as individual images and converted to tiff files using FV-1000 software. These image sequences were opened in ImageJ and the fluorescence mean intensity was determined for each Z-stack (maximum intensity projections), placed in Excel, and means, standard deviation, and standard error were calculated. Significance was determined using the Mann-Whitney one-tailed test, and these measurements were graphed using Prism-GraphPad. All of these experiments were done in triplicate for each selected protein of interest.

Histology and TEM

Normal human and MVID patient duodenum sections were de-paraffinized and were submitted to antigen retrieval in a pressure cooker using the target retrieval solution (Dako North America Inc.). Serum free protein block (Dako North America Inc.) was used for blocking the duodenum, and immunofluorescence staining was performed as stated above for confocal immunofluorescence for all proteins of interest except for Rab8a and Rab11a. Duodenum stained for both Rab8a and Rab11a were placed in serum free block for 8 hours at room temperature or for 48 hours at 4°C. All other

aspects of immunofluorescence staining were performed as stated above. All imaging was performed using the Olympus FV-1000.

TEM samples from MVID patients were prepared and analyzed by the Vanderbilt Cell Imaging Shared Resource, Vanderbilt University.

Transferrin trafficking assay

CaCo2-BBE cells were serum starved for 60 minutes in serum free media at 37°C. Transferrin-Alexa 633 (Molecular Probes®) was added to the basolateral surface for 1 hour at 37°C. The transferrin was chased out with normal media for 60 minutes, and cells were washed 2x in PBS and fixed and prepared for imaging as described above.

Cdc42 activity assay

Cdc42 activity was assayed using the cdc42 activity assay kit (BK034-Cytoskeleton). Cells were plated on 6-well Transwell filters for 15 days as described above for western blot protein isolation. Protein isolation and cdc42 activity was performed as described in the data sheet (BK034-Cytoskeleton).

F-actin pulldown of MYO5B

Actin (0.4mg/mL) was polymerized in actin polymerization buffer (500mM KCl and 20mM MgCl2) and 2mM of ATP and 1mM of DTT were added to the mixture and incubated for 1 hour at room temperature. The polymerized F-actin was stabilized using 6.6μM of phalloidin (Molecular Probes®) and incubated for 20 minutes at room temperature. HEK cells transfected with either 3x-mCitrine-MYO5B-WT-1016x, or 3x-

mCitrine-MYO5B-P660L-1016x were lysed and spun down at 150,000 x g. 1μM of actin was added to the cell lysate supernatant and incubated for 1 hour. The lysates were spun down at 150,000 x g and samples from the supernatant and actin pellet were collected and analyzed by western blot using an affinity-purified chicken anti–myosin Vb antibody (39).

Live cell single molecule total internal reflection fluorescence - fluorescence recovery after photo-bleaching microscopy (TIRF-FRAP)

MYO5B-WT-1016x and MYO5B-P660L-1016x were tagged with three tandem copies of mCitrine (3x-mCitrine) and verified by sequencing. BF16 cells expressing 3x-mCitrine-MYO5B-WT-1016x or 3x-mCitrine-MYO5B-P660L-1016x were plated sparsely in glass bottom imaging dishes. Cells were gently washed 2x in PBS and placed in CO_2-independent media (Gibco®) for imaging experiments. TIRF-FRAP and TIRF microscopy was performed on a Nikon TiE inverted light microscope equipped with a Nikon TIRF illuminator, a 100×/1.49 numerical aperture TIRF objective (used in combination with a 1.5× optivar), and a Hamamatsu ImagEM-CCD camera. Rectified pixel size was 75nm/pixel. Fluorescence was excited using a 50-milliwatt 491-nm diode laser working between 20-30% of full power. Single particle events appeared as bright diffraction restricted spots on the surface of the cell. Cells expressing exceedingly high levels of each construct were chosen for analysis to improve the signal/noise ratio of single molecule detection; image stacks consisting of 500 frames (30s) were captured at 16.667frames/s and subjected to contrast enhancement using ImageJ as similarly described by Mazerik, et al. 2012 (Mazerik and Tyska 2012). Using ImageJ fluorescence maximum intensity for each movie was measured, placed in Excel,

normalized to one, and graphed as a percentage. All of these experiments were done in triplicate for each construct.

Microvillus Inclusion Scoring

Microvillus inclusions in the cell lines presented in this study were measured by assembling 3D-reconstructions of Z-stacks from 8 randomly chosen fields of view of each cell line stained with DPPIV, ezrin, or phalloidin. The absolute number of microvillus inclusions in each 3D-reconstruction was counted. Significance was determined using the Mann-Whitney one-tailed test, and these measurements were graphed using Prism-GraphPad.

Biotin Labeling and Cell surface Biotinylation

For the biotin labeling, CaCo2-BBE cell lines on Transwell filters were washed three times with PBS containing 0.1mM $CaCl_2$ and 1.0mM $MgCl_2$ (PBS-CM) on ice. Biotin working solution (0.5mg/mL in PBS-CM from a 200mg/mL stock dissolved in anhydrous DMSO) was added to the apical side of the filters for 20 minutes at 4°C. The biotin was quenched with five washes of PBS-CM containing 0.2% BSA and 100mM glycine at 4°C. The cells were incubated for 24 hours at 37°C. CaCo2-BBE cells were fixed with PFA as described above. Streptavidin 647 (Molecular Probes®) and Phalloidin 405 (PromoKine) were added in PBS-T. The cells were washed three times in PBS-T and washed once in PBS, and washed in water and mounted with ProLong Gold (Invitrogen).

For cell surface biotinylation assays, CaCo2-BBE cell lines on Transwell filters were washed as specified above, and biotin (0.5mg/mL in PBS-CM from a 200mg/mL

stock dissolved in anhydrous DMSO) was added to the apical or basolateral side of the filters for 20 minutes at 4°C. This process was subsequently repeated for an additional 20 minutes at 4°C. The biotin was quenched with five washes of PBS-CM containing 0.2% BSA and 100mM glycine, and washed two times with PBS-CM at 4°C. The Transwell filters were cut out of the Transwell inserts and placed in Eppendorf tubes containing 800µL of lysis buffer (50mM Hepes (pH 7.5), 150mM NaCl, 1% Triton X-100, 1mM EDTA, 10% glycerol, 10mM sodium pyrophosphate, 2mM sodium orthovanadate, 10mM sodium fluoride, 1mM PMSF, 5µg/mL leupeptin, 5µg/mL pepstatin, and 10µg/mL aprotinin added fresh) (Singh, Bogatcheva et al. 2013). The tubes were gently rotated for 1 hour at 4 °C, filters were removed from the tubes, and lysates were processed for biotinylated protein isolation on streptavidin beads: Protein concentration was determined as described above, and 800µg total protein was re-suspended in isolation dilution buffer (200mM Hepes (pH 7.5), 600mM NaCl, 40% glycerol, and 0.4% Triton X-100) brought up to 700µL with mammalian protease inhibitors (Sigma). 50µL of the Total Protein was obtained and dissociated in 1× SDS Sample buffer and heated for 10 minutes at 70°C. Streptavidin agarose beads (Novagen 69203) were added to the above lysates, and incubated overnight at 4 °C while gently rotating. The samples were centrifuged at 1600 x g for 3 minutes, and 50µL of the Flow Through was obtained and dissociated in 1× SDS Sample buffer and heated for 10 minutes at 70°C. The beads were washed three times with 500µL of the isolation dilution buffer, and centrifuged at 1600 x g for 3 minutes each time. The beads were re-suspended 1× SDS Sample buffer, heated for 10 minutes at 70°C, resolved on a 10% SDS–PAGE gel, and western blots were performed for DPPIV and E-cadherin, as described above. Band densities

were quantified using digitally scanned tiffs placed into Image Studio (LI-COR Biosciences). Using Excel the percentage of total protein in the unbound and streptavidin-bound pools was determined by adding the relative unbound pools to the streptavidin-bound protein pools. Reported values represent the mean ± S.E.M. of three or more independent experiments unless otherwise indicated.

Methods of Statistical Analysis

Reported values represent the mean ± S.E.M. of three or more independent experiments unless otherwise indicated. Statistical significance for all experiments was determined using a Mann-Whitney one-tailed test with significance at $p \leq 0.05$ using Prism-GraphPad.

Study Approval

The studies in these investigations utilized archival paraffin tissue duodenal specimens from normal children and Navajo MVID patients. All procedures and studies were performed according to protocols approved by Institutional Review Boards at both Phoenix Children's Hospital and Vanderbilt University School of Medicine. IRB approval of informed consent was obtained from all families of living subjects prior to research and IRB approved decedent research on tissue blocks from patients who had expired.

Table 1. Antibodies

ND=Not determined

Antibody	CaCo2-IF Antibody Dilution	Human Tissue - IF Antibody Dilution	Western Blot Antibody Dilution
Active cdc42 ewEast #26905	1:100	ND	ND
aPKC (PKC ζ) Santa Cruz #sc-216	1:200	1:200	ND
BSEP (SPGP) Kamiya Biomedical Company #PC-064	ND	1:200	ND
CD10 Abcam #ab47721-100	1:100	1:100	ND
CD71 Invitrogen #13-6800	1:200	1:200	ND
CDC42 Cell signaling # 2462	1:200	1:200	1:250
Claudin-1 Invitrogen #51-9000	1:200	1:200	1:2000
Claudin-2 Invitrogen #51-6100	1:100	ND	1:1000

Claudin-4 Invitrogen #532-9400	1:100	1:200	1:1000
DPPIV abcam #ab129060	ND	ND	1:1000
DPPIV R&D systems #1180-SE	1:100	1:200	1:500
Ds-Red Clontech #632496	ND	ND	1:2000
E-Cadherin BD # 610181	1:300	ND	1:5000
E-Cadherin Cell Signaling #3195S	ND	ND	1:1000
Ezrin Cell Signaling #3145	1:200	1:200	1:5000
H/K-ATPase (mouse) Gift from the Smolka laboratory	ND	1:200	ND
LAMP2a Abcam #ab18528	1:200	ND	ND
MRP2 (M2III-6) Enzo Life Sciences	ND	1:200	ND

#ALX-801-016-C250			
MYO5B (VU410-Chicken) Produced by the Goldenring Laboratory	1:200	1:200	1:1000
Na/K-ATPase Milipore #05-369	1:50	1:50	1:1000
NHE3 (rabbit) Gift from the Ghishan Laboratory	1:400	1:200	ND
p120 BD Transduction Lab # 610133	1:200	1:200	1:2000
p120 (6H11 & FlαSH) Gift from the Reynolds Laboratory	ND	ND	1:1000
Phospho-ERM Cell Signaling #3149	1:200	1:200	ND
Rab11a (8H10-Mouse) Produced by the Goldenring Laboratory	1:200	1:200	ND

Rab11a (VU57-Rabbit) Produced by the Goldenring Laboratory	1:200	1:200	1:2500
Rab11b (VU76-Rabbit) Produced by the Goldenring Laboratory	ND	1:200	ND
Rab8a-AP (Rabbit) Produced by the Goldenring Laboratory	1:200	1:200	1:1000
SGLT1 Abcam #ab14685	ND	1:200	ND
SNX18 Sigma Prestige #HPA037800	1:200	1:200	ND
Syntaxin 3 Abcam #ab4113	1:200	1:200	ND
Syntaxin 4 Santa Cruz #sc-14455	ND	1:200	ND
VDAC-1 Abcam #ab15895	ND	ND	1:1000

Villin-1 Cell signaling # 2369	1:100	1:100	1:5000
ZO-1 Invitrogen #61-7300	1:200	1:200	1:1000
α-Tubulin Cell Signaling #2144	1:200	1:200	1:5000
β-Actin Sigma-Aldrich #A5316	ND	1:200	1:2000
β-Catenin Cell Signaling #9562	1:200	1:200	ND

Acknowledgments

This work was supported by the NIH grant RO1 DK70856 to J.R.G and RAC Awards to M.S. from Phoenix Children's Hospital for initial support of this project. Confocal and structured illumination fluorescence microscopy as well as TEM and SEM imaging was performed through the use of the VUMC Cell Imaging Shared Resource and histological sectioning was performed by Translational Pathology Shared Resource, both supported by National Institute of Health (NIH) Grants CA68485, DK20593, DK58404 and HD15052. Fluorescence slide imaging was performed on an Ariol SL-50 digitizing scanner in the VUMC Digital Histology Shared Resource.

We thank Cathy Caldwell for help with cell culture, Kenya Avant-Mitchell for help with western blots, Z. Bradshaw and Y. Tu for help with actin pull-downs of MYO5B constructs, J. Higginbotham for assistance with CaCo2-BBE cell sorting, J. Mazerik for help with TIRF imaging, R. Nambiar and J. Williams for help with SEM and TEM imaging, A. Reynolds and N. Markham for p120 antibody, F. Ghishan for NHE3 antibodies, I. Macara and R. Guyer for aPKC antibody, and the Vanderbilt University School of Medicine Medical Scientist Training Program for continued support. We thank G. Silber, K. Ingebo, and D. Ursea for the outstanding care that they have provided over the years for the Navajo MVID patients. We thank all of the families of our Navajo patients, who consented to allow archived tissue samples from their children to be utilized in this study.

CHAPTER III

Rab11a loss disrupts polarity, mistrafficks apical proteins, and produces short microvilli in enterocytes

Adapted From: Knowles, B. C., S. Yu, et al. (2014). “Rab11a loss disrupts polarity, mistrafficks apical proteins, and produces short microvilli in enterocytes.” Manuscript in progress. Journal of Cell Science.

Introduction

A large body of research over the past 25 years has transformed the predicted function of Rab small GTPases (Rabs) from mediators of vesicle fusion to universal regulators that coordinate the trafficking of vesicles to specific destinations (Stenmark 2009). Rabs are the largest group in the small GTPase family, and like all small GTPases cycle through GTP bound and GDP bound states that represent their active and inactive states, respectively (Schwartz, Cao et al. 2007). Cycling through activity states allows cells to finely tune Rab trafficking decisions. The conversion of GTP to GDP in Rabs is driven by their intrinsic GTPase activity and GTPase activating proteins (GAPs), which allows GAPs to act as inhibitory regulators of Rabs (Delprato, Merithew et al. 2004). GDP release from Rabs is facilitated by guanine exchange factors (GEFs), which activate Rabs. Since, intracellular GTP is present in much higher concentrations than GDP; GTP is actively bound to Rabs after GDP release. GDP dissociation inhibitors (GDIs) can inhibit the activation of Rabs, and dually functions along with Rab escort proteins (REPs) to guide Rabs to their appropriate vesicles (Matsui, Kikuchi et al.

1990). Although the mechanism behind the regulation of each step that leads to vesicle targeting of Rabs is not fully understood, it is clear that tight control of this process is important for proper cellular regulation (Ullrich, Horiuchi et al. 1994).

Rabs localize trafficking machinery to specific vesicles, which ultimately determines the interactions of that vesicle as it navigates various trafficking pathways. Rab8a, Rab11a, Rab11b, and Rab25 act on the apical recycling endosome (ARE), which is involved in the establishment of specialized apical processes specifically microvilli. Uncoupling of MYO5B from Rab11a can lead to microvillus inclusion formation and immature brush border in intestinal enterocytes (Knowles, Roland et al. 2014).

Once Rabs have been targeted to their appropriate vesicle they regulate key steps in vesicle trafficking including: vesicle formation, vesicle movement, and membrane fusion (Grosshans, Ortiz et al. 2006; Soldati and Schliwa 2006; Schwartz, Cao et al. 2007). Fusion of vesicles and vesicle fusion to the plasma membrane is facilitated by SNAREs. SNAREs from both the targeted vesicle and the acceptor vesicle form the core of the SNARE complex and dictate the specificity of membrane fusion. The SNARE core complex components must be targeted to the membranes by trafficking machinery, and failure to target these proteins disrupts vesicular trafficking in polarized cells (Reales, Sharma et al. 2011). In parietal cells, fusion of tubulovesicles to the apical surface is mediated by STX3, VAMP2, and SNAP25 core SNARE complex as stated in chapter one (Calhoun, Lapierre et al. 1998; Karvar, Yao et al. 2002). Notably, expression of mutant STX3, without targeting sequence, disrupts the apical delivery of proteins in MDCK cells (Sharma, Low et al. 2006). Recently, mutations in *STX3* and

STXBP2 (Munc18-2) have been implicated as the causative agents for Atypical forms of Microvillus Inclusion Disease (MVID), and in patient enterocytes polarity is disrupted and apical microvilli are loss (Muller, Hess et al. 2008; Stepensky, Bartram et al. 2013; Wiegerinck, Janecke et al. 2014).

We have hypothesized that Rab11a plays a crucial role in apical trafficking and membrane recycling required for maintenance of microvilli in polarized enterocytes. In this study, we report that Rab11a regulates apical intestinal enterocyte polarity. Utilizing duodenum samples from Rab11a intestinal specific conditional knockout mice ($Rab11a^{fl/fl}$;villin-cre^{+}) and stable Rab11a knock down in CaCo2-BBE cells, we demonstrate that Rab11a loss results in a decrease in microvilli length, presentation of microvilli along the lateral membranes, mistrafficking of apically trafficked proteins, expansion of the lysosomal compartment, and mislocalization of both Rab8a and Rab11b. Most notably, $Rab11a^{fl/fl}$;villin-cre^{+} mice duodenum and CaCo2-BBE Rab11a-KD cells displayed cytoplasmic mislocalization of STX3, which is required for apical vesicle fusion. These results indicate that Rab11a is a critical regulator of apical trafficking in polarized enterocytes.

Results

Disruption of polarity in the apical compartments is observed in Rab11a$^{fl/fl}$;villin-cre^{+} duodenum samples and Rab11a-KD CaCo2-BBE cells

To examine the role of Rab11a in the establishment of brush borders in enterocytes, we developed Rab11a$^{fl/fl}$;villin-cre^{+} (Rab11a$^{\Delta IEC}$) mice, which display intestinal epithelial cell (IEC) specific loss of Rab11a (Yu, Nie et al. 2014). Our initial work with these mice demonstrated that Rab11a loss in enterocytes elicits mistrafficking of Toll-like Receptor 9 (TLR9). Previous work published by our laboratory has demonstrated that MYO5B coupled Rab11a-dependent trafficking is required for proper apical trafficking and brush border establishment in enterocytes (Knowles, Roland et al. 2014). In wild type duodenal sections, MYO5B immunostaining was concentrated sub-apically in enterocytes below the brush border, and microvilli stained positively for ezrin (Figure 28A). In contrast, the Rab11a$^{\Delta IEC}$ duodenum displayed redistribution of MYO5B, but ezrin staining showed no perturbation of apical ezrin localization in the enterocytes of this tissue (Figure 28A). Interestingly, ezrin also appeared to localize along the basolateral membrane in the Rab11a$^{\Delta IEC}$ duodenum. Upon closer examination using SEM and TEM, microvilli in Rab11a$^{\Delta IEC}$ duodenum were short, and microvilli were observed projecting from the lateral membranes in some enterocytes (Figure 28B). Similar to ezrin, Villin-1 was redistributed from its normal apical localization to the cytoplasm and basolateral membrane (Figure 28C). Interestingly, alkaline phosphatase in the Rab11a$^{\Delta IEC}$ duodenum was mislocalized to the cytoplasm and the enterocytes had increased lysosome associated Lamp2a staining (Figure 28C). Apical NHE3

staining was decreased in the Rab11a$^{\Delta IEC}$ duodenum, with NHE3 also present on lateral membranes (Figure 28C).

We also compared the ultrastructure of both Rab8a knockout (KO) mice and in the Rab11a$^{\Delta IEC}$ mouse duodenum by transmission and scanning electron microscopy. As previously reported, microvillar growth was markedly perturbed in Rab8a-KO mice microvilli when compared to the microvilli of the Rab11a$^{\Delta IEC}$ mice (Figure 29) (Sato, Mushiake et al. 2007).

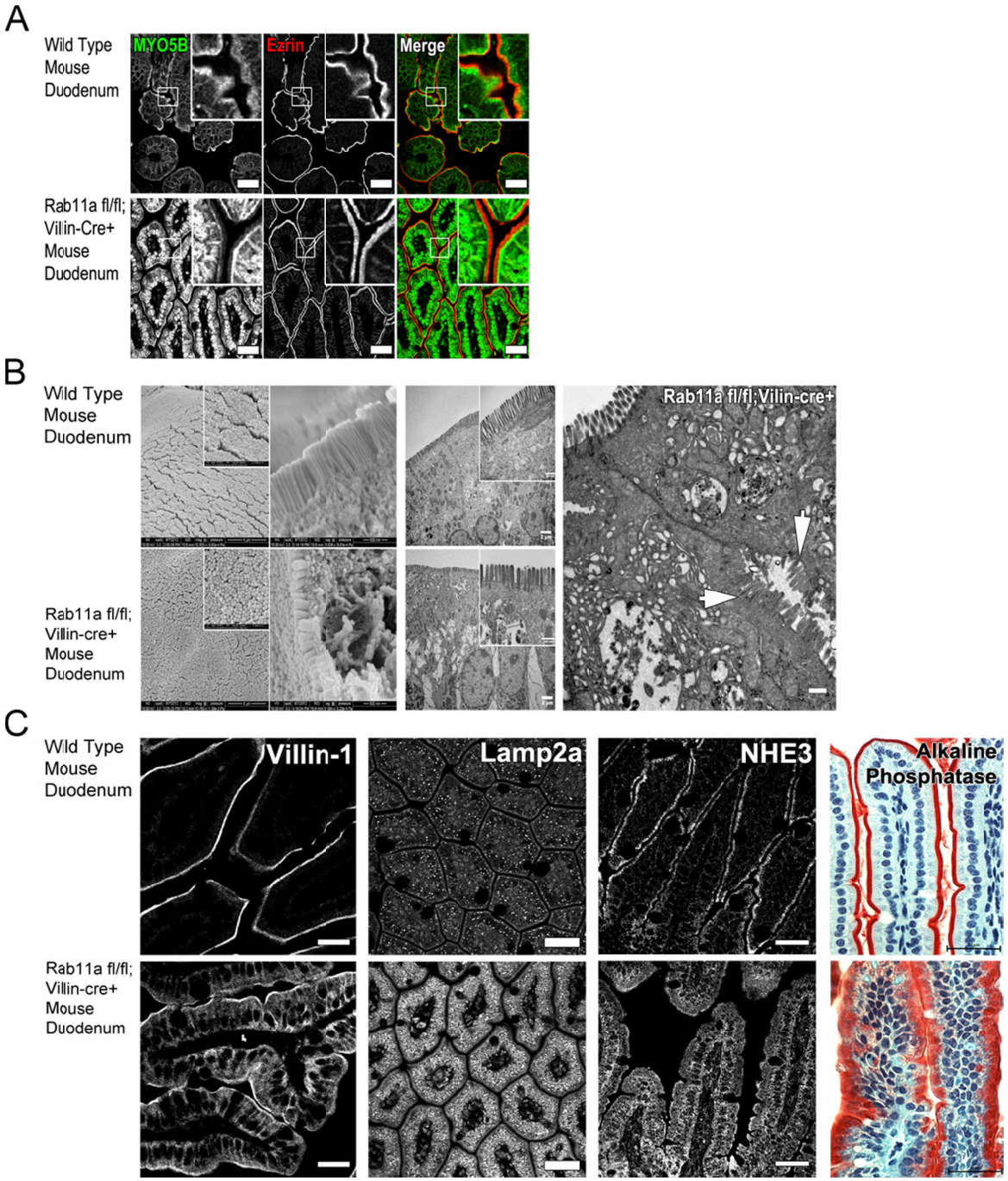

Figure 28. Rab11a loss in the enterocytes of mice causes cytoplasmic redistribution of apical proteins, loss of microvilli, and lateral microvillus inclusions.
(A) Rab11a$^{\Delta IEC}$ mice duodenum display rearrangement of MYO5B and normal distribution of ezrin. Scale bars are 30 μm. (B) SEM and TEM of Rab11a$^{\Delta IEC}$ mice duodenum display short microvilli, large vesicles, and lateral microvillus inclusions. Left: Scale bars are as indicated. (C) Rab11a$^{\Delta IEC}$ mice duodenum has redistribution of villin-1, NHE3, cytoplasmic alkaline phosphatase, and increased Lamp2a staining. Scale bars are 30 μm.

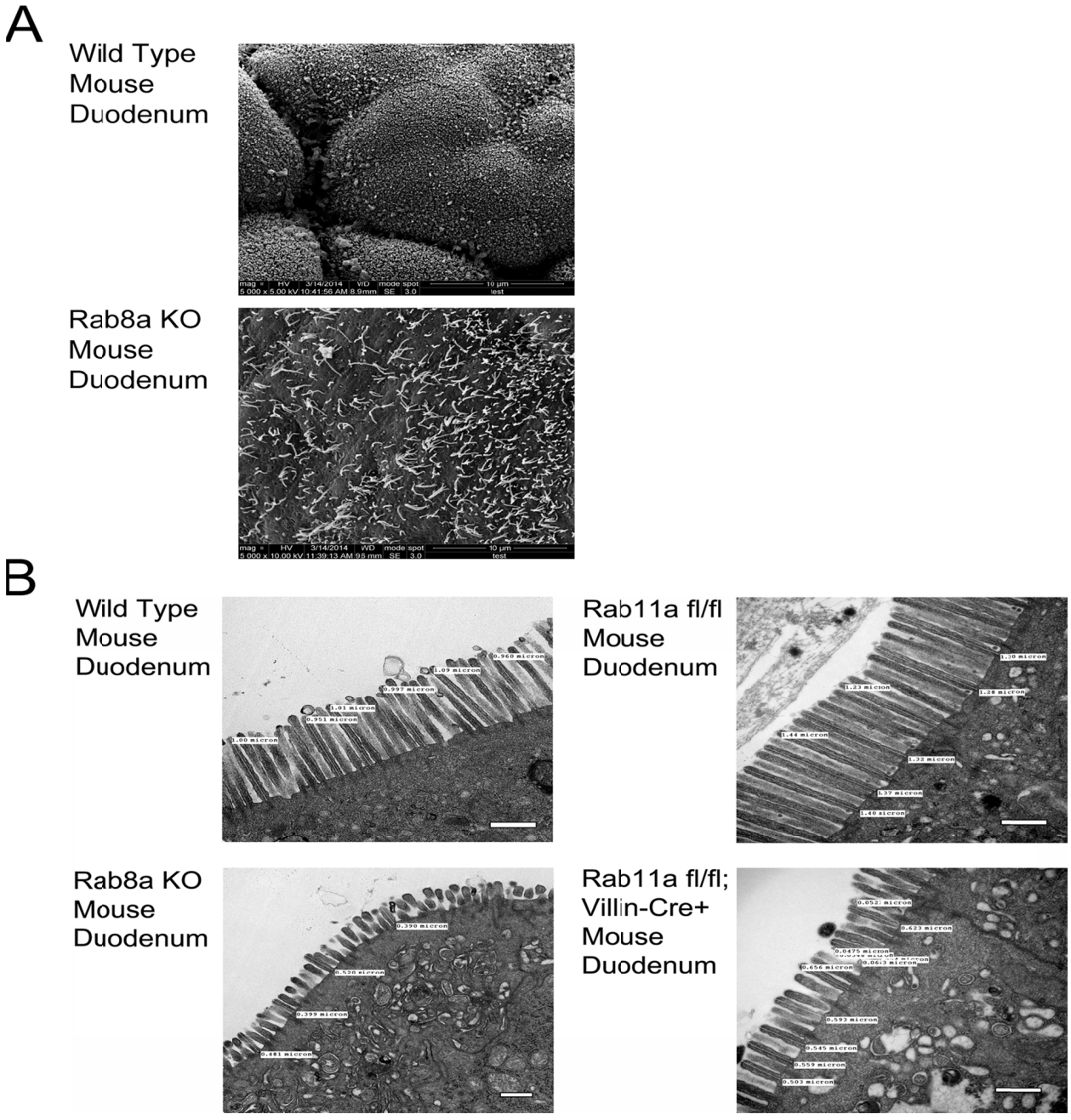

Figure 29. SEM and TEM of Rab8a knockout mice display loss of microvilli.
(A) SEM of Rab8a knockout mice duodenum display sparse brush border. Scale bars are 10 μm. (B) Both Rab8a knockout and Rab11a$^{\Delta IEC}$ mice duodenum display shortened microvilli, but Rab8a knockout mice microvilli from the duodenum are shorter than Rab11a$^{\Delta IEC}$ mice microvilli. Scale bars are 2 μm.

We also produced stable knock down of both Rab8a and Rab11a in CaCo2-BBE cells to examine if loss of these Rabs produced similar phenotypes in a cellular model. The CaCo2-BBE sub-clone cell line from the CaCo2 parental cell line was used, because when grown on permeable Transwell filters these cells form extensive microvilli (Peterson and Mooseker 1992). For this study, lentiviral shRNA vectors targeting Rab8a, Rab11a, and a control shRNA were used for transduction of CaCo2-BBE cells. Both Rab8a and Rab11a mRNA and protein were reduced by greater than 50% when compared to the control cells, and we rescued these cell lines with lentiviral vectors for mCherry fusions of mouse Rab8a and Rab11a (data not shown).

We examined the microvilli of CaCo2-BBE control, Rab11a-KD, and Rab8a-KD cells by immunofluorescence, SEM, and TEM. In control cells, both ezrin and phalloidin were distributed beneath the apical surface, and SEM and TEM displayed a normal arrangement of mature brush border microvilli (Figure 30A). In Rab11a-KD cells, as in the Rab11a$^{\Delta IEC}$ mice both ezrin and phalloidin staining appeared to be distributed normally, but in addition displayed F-actin and ezrin-enriched lateral microvilli. By SEM and TEM Rab11a loss in CaCo2-BBE cells caused the formation of immature microvilli and lateral microvilli (Figure 30A and B). In Rab8a-KD cells, ezrin and phalloidin were distributed on both the apical and basolateral surface of cells, and these cells appeared to loose contact inhibition and pile on top of each other (Figure 30A). Utilizing both SEM and TEM in these cells, we observed that Rab8a-KD caused the formation of severely immature microvilli (Figure 30A). Thus, both Rab8a and Rab11a appear to be essential for normal apical polarity in enterocytes, and loss of Rab11a produces lateral lumens on the basolateral surface of enterocytes.

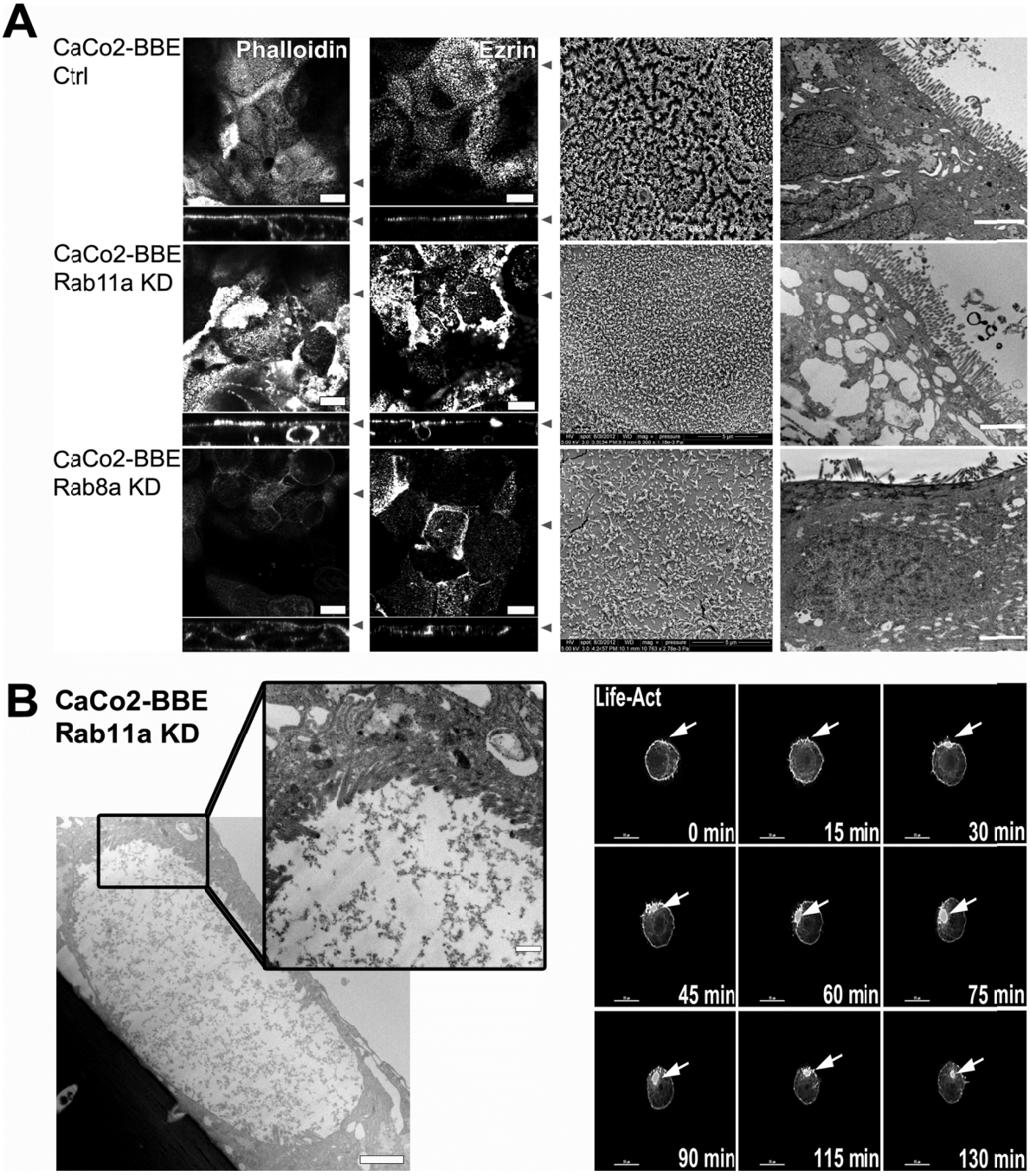

Figure 30. Rab8a-KD and Rab11a-KD in CaCo2-BBE cells recapitulates the phenotype of Rab8a and Rab11a loss in the intestines of mice.
(A) Rab8a-KD and Rab11a-KD causes loss of microvilli in enterocytes by immunofluorescence, SEM, and TEM. Loss of Rab8a produces more immature microvilli than loss of Rab11a, but Rab11a-KD produces microvillus inclusions. (B) Left: TEM of enlarged lateral microvilli containing spaces in CaCo2-BBE Rab11a-KD cell. Right: Time series of CaCo2-BBE Rab11a-KD cells transfected with Life-Act (actin stain) shows the internal accumulation of an actin positive vesicle. Scale bars are as indicated.

The integrity of the basolateral compartment is maintained in Rab11a$^{\Delta IEC}$ enterocytes and Rab11a-KD CaCo2-BBE cells

We next examined the effects of reducing Rab11a on components of the basolateral compartment. To assess the integrity of the basolateral compartment, we immunostained Rab11a$^{\Delta IEC}$ mice duodenum tissue samples for E-cadherin. Rab11a loss did not appear to affect E-cadherin staining in the duodenum as it was distributed along the basolateral surface as observed in control tissues (Figure 31A). We also immunostained Rab11a$^{\Delta IEC}$ duodenum tissue samples for p120 and Na/K-ATPase, and they both were distributed along the basolateral compartment as observed in the control (data not shown). To further assess the integrity of the basolateral surface in the absence of Rab11a, we immunostained CaCo2-BBE cells for claudin-1, β-catenin, and E-cadherin. In control cells, claudin-1 and β-catenin were distributed along the basolateral surface, and E-cadherin was positioned at the junctions (Figure 31B). In the Rab8a-KD cells, claudin-1 appeared to be maintained at its basolateral position, but β-catenin is shifted to cytoplasm. Interestingly, E-cadherin accumulated throughout the cells apical and basolateral membranes, but also accumulated sub-apically (Figure 31B). In Rab11a-KD cells, claudin-1 and β-catenin were distributed along the basolateral surface, but E-cadherin was redistributed to both the apical and basolateral surfaces, as observed previously in CaCo2-BBE MYO5B-KD cells (Figure 31B) (Knowles, Roland et al. 2014). Thus, in CaCo2-BBE Rab11a-KD cells the basolateral integrity was maintained, but E-cadherin appeared to be mistrafficked to the apical surface.

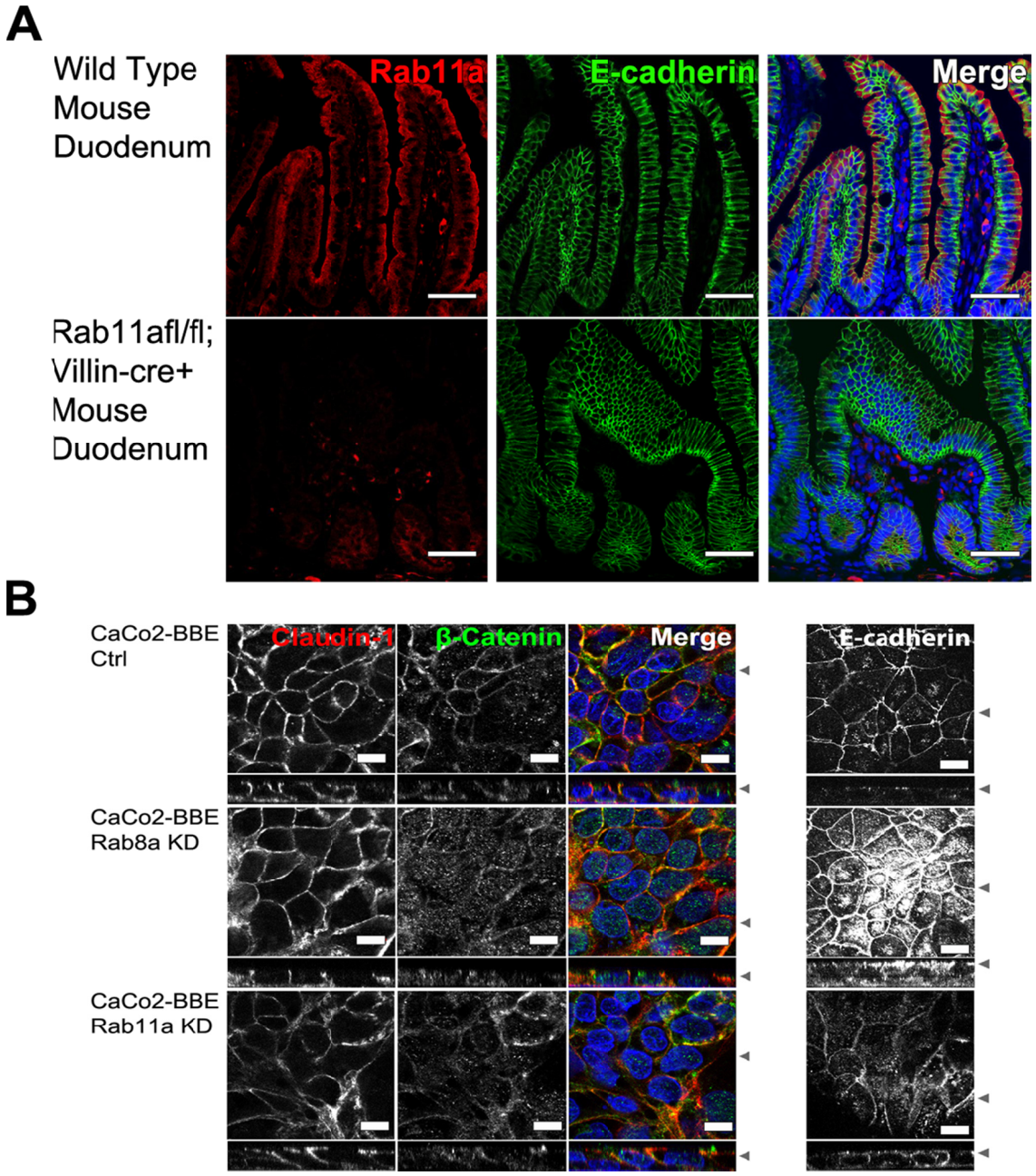

Figure 31. Rab11a loss does not cause loss of basolateral integrity in enterocytes.
(A) In Rab11a$^{\Delta IEC}$ mice duodenum, E-cadherin (green) is maintained in the basolateral compartment of enterocytes, but the cells do appear to lose some contact inhibition. Scale bars are 20 μm. (B) In control CaCo2-BBE cells, claudin-1 (red) and β-catenin (green) are distributed along the basolateral surface, while E-cadherin is positioned in a junctional localization. In Rab8a-KD cells, claudin-1 is maintained at its basolateral position, but both β-catenin and E-cadherin are shifted to cytoplasmic localizations. In Rab11a-KD cells, claudin-1 and β-catenin are distributed along the basolateral surface. While, E-cadherin is redistributed to both the apical and basolateral surfaces. Scale bars are 10 μm.

Loss of Rab11a causes mislocalization of Rab8a and Rab11b

Previous work done in MDCK cells demonstrated that loss of Rab11a caused concomitant increase in Rab8a to compensate for Rab11a loss, and Rab11a through rabin8 (Rab8a GEF) activates Rab8a (Bryant, Datta et al. 2010). In the previous section, we observed that E-cadherin basolateral localization was unaffected by Rab11a loss. To analyze other Rabs that could compensate for Rab11a loss, we immunostained Rab11a$^{\Delta IEC}$ mice duodenum sections for Rab8a and Rab11b. Both Rab8a and Rab11b were distributed sub-apically in control samples (Figure 32A). In the Rab11a$^{\Delta IEC}$ mice samples, Rab8a was dispersed throughout the cytoplasm (Figure 32A). Moreover, in these samples, Rab11b was dispersed throughout the cytoplasm away from its normal distribution and accumulated with increased fluorescence intensity throughout the mucosa (Figure 32A). We also immunostained the CaCo2-BBE cell lines for Rab8a. In control cells, Rab8a was concentrated in lateral sub-apical vesicular complexes (Figure 32B). In Rab8a-KD cells, Rab8a was lost from the cells. In Rab11a-KD cells, Rab8a was increased and dispersed throughout the cytoplasm away from its normal lateral sub-apical distribution (Figure 32B). These findings demonstrate that loss of Rab11a leads to a disordered distribution of Rab8a and Rab11b both *in vitro* and in Rab11a$^{\Delta IEC}$ mice samples, and suggest that these changes might reflect an attempt by cells to compensate for Rab11a loss.

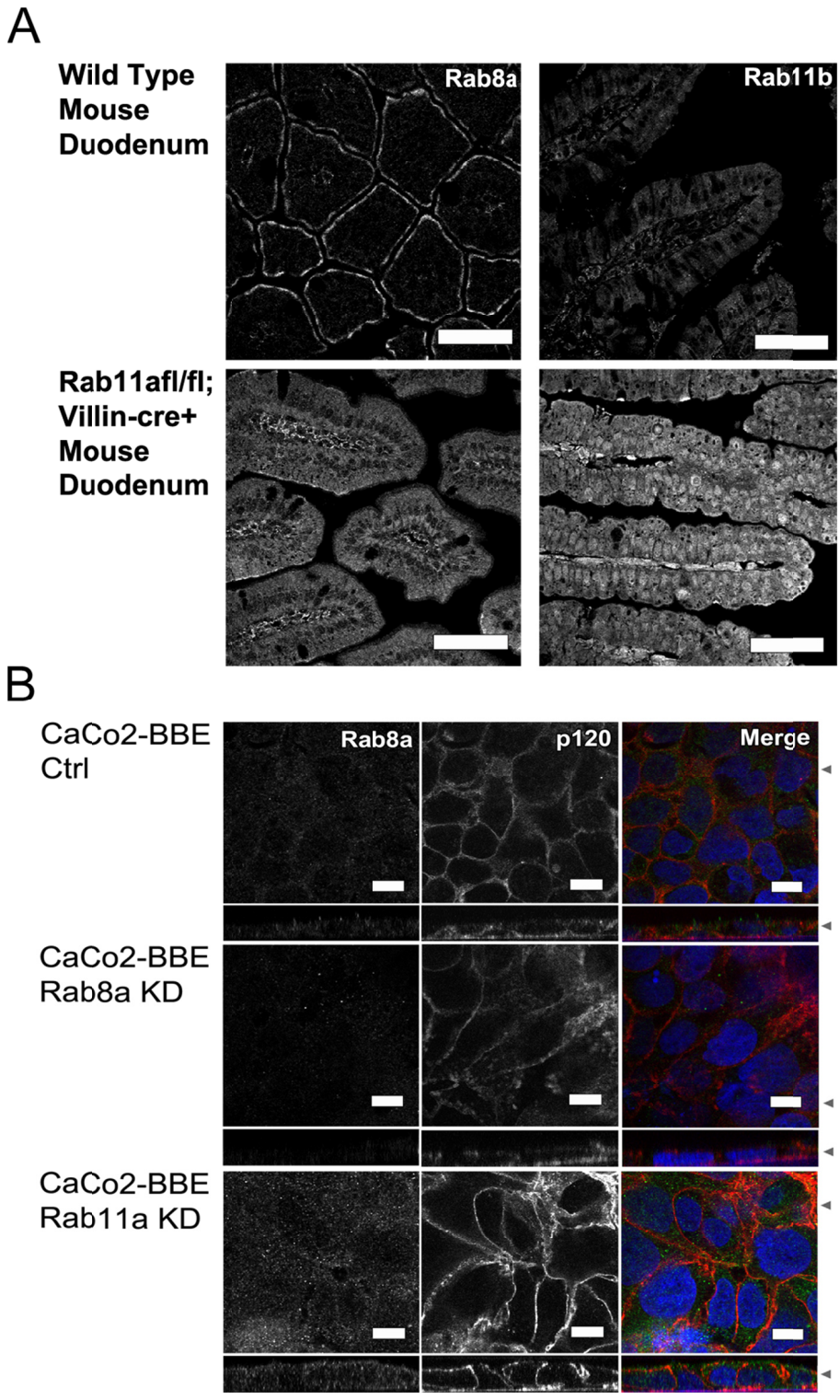

Figure 32. Rab11a loss causes redistribution of Rab8a in enterocytes.
(A) Rab11a$^{\Delta IEC}$ mice duodenum display redistribution of both Rab8a and Rab11b from their normal subapical localization to reorganized cytoplasmic localizations. Scale bars are 50 μm. (B) In CaCo2-BBE cells, Rab11a loss causes redistribution of Rab8a from its normal sub-apical lateral localization to the cytoplasm. Scale bars are 10 μm.

Rab11a loss or mutation in MYO5B causes cytoplasmic redistribution of STX3

Rab11a has recently been implicated, through aPKC (atypical protein kinase C) and Mst4 (mammalian STE20-like protein kinase 4), in promoting the phosphorylation of ezrin, which is required for proper microvilli formation (Dhekne, Hsiao et al. 2014). To examine the status of phosphorylated ezrin and known ezrin kinases, we immunostained Rab11a$^{\Delta IEC}$ mice duodenum for Mst4, aPKC, and phosphorylated ERM proteins. In control samples, Mst4 was distributed throughout the cytoplasm of enterocytes with a distinct sub-apical pool (Figure 33). In Rab11a$^{\Delta IEC}$ samples, Mst4 sub-apical pool is lost (Figure 33). aPKC was distributed along the apical surface in both the control and Rab11a$^{\Delta IEC}$ samples (Figure 33). Interestingly, the distribution of phosphorylated ERM proteins is the same in both the control and Rab11a$^{\Delta IEC}$ samples (Figure 33). Thus, alterations in microvillar structure in Rab11a$^{\Delta IEC}$ samples mice do not correlate with changes in ezrin phosphorylation.

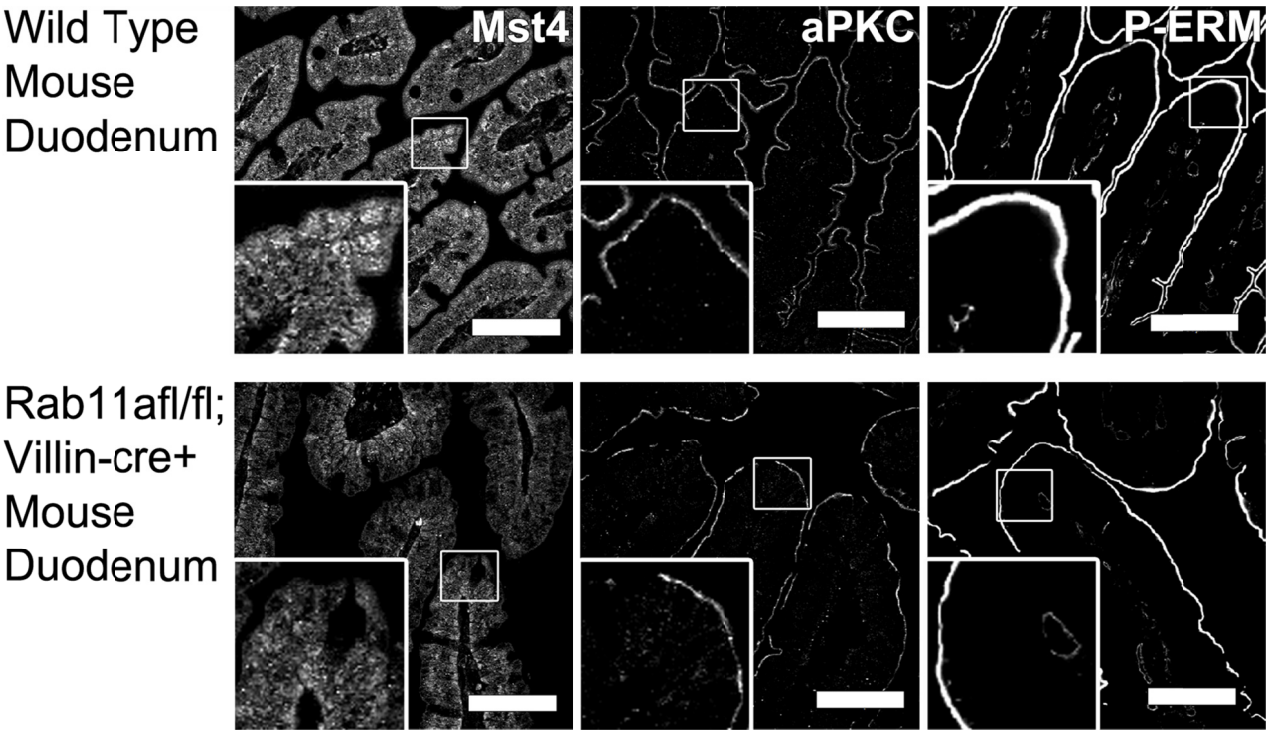

Figure 33. Rab11a$^{\Delta IEC}$ mice duodenum samples display normal localization of aPKC and phosphorylated ERM proteins (P-ERM).
Mst4 is normally localized to the cytoplasm with distinct sub-apical populations, but in Rab11a$^{\Delta IEC}$ duodenum samples the sub-apical populations is lost. aPKC and phosphorylated ERM proteins are localized to the apical surface in both wild type and Rab11a$^{\Delta IEC}$ duodenum samples. Scale bars are 50 μm.

Since, altered ezrin phosphorylation could not account for the shortened microvilli in Rab11a$^{\Delta IEC}$ duodenum samples. We investigated other possible causes of this phenotype. We evaluated whether Rab11a loss might affect apical vesicle fusion in Rab11a$^{\Delta IEC}$ duodenum samples. To investigate this possibility we immunostained the Rab11a$^{\Delta IEC}$ duodenum samples for STX3 (an apical SNARE) and STX4 (a basolateral SNARE protein). In control samples, STX3 was present along the apical surface of enterocytes (Figure 34A). In contrast, STX3 was localized to both the apical surface and to small vesicular puncta below the apical surface in Rab11a$^{\Delta IEC}$ duodenum samples (Figure 34A). Of note, STX3 localized normally at the bottom of the villi in Rab11a$^{\Delta IEC}$ duodenum samples, and mislocalization manifested at the villus tips (Figure 34A). In control samples, STX4 was distributed throughout the cytoplasm in small punctate vesicles as well as in distinct lateral membrane staining (Figure 34A). Similar STX4 staining was observed in Rab11a$^{\Delta IEC}$ duodenum samples (Figure 34A). We also immunostained our CaCo2-BBE cell lines for STX3. In Rab8a-KD cells, STX3 accumulated sub-apically as in control samples (Figure 34B). However, in Rab11a-KD cells STX3 was redistributed from the apical surface to cytoplasmic vesicles and to lateral membrane microvillar spaces (Figure 34B). To further investigate this phenotype, we immunostained MVID patient duodenum samples with mutations in MYO5B for STX3. In these samples, STX3 was distributed away from the apical surface to punctate vesicles below the apical surface (Figure 34C). Thus, loss of Rab11a might impair apical trafficking of proteins and cause apical deficits in proteins that are important for microvilli elongation, because Rab11a and MYO5B are required for trafficking STX3 to its apical position to facilitate final vesicle fusion.

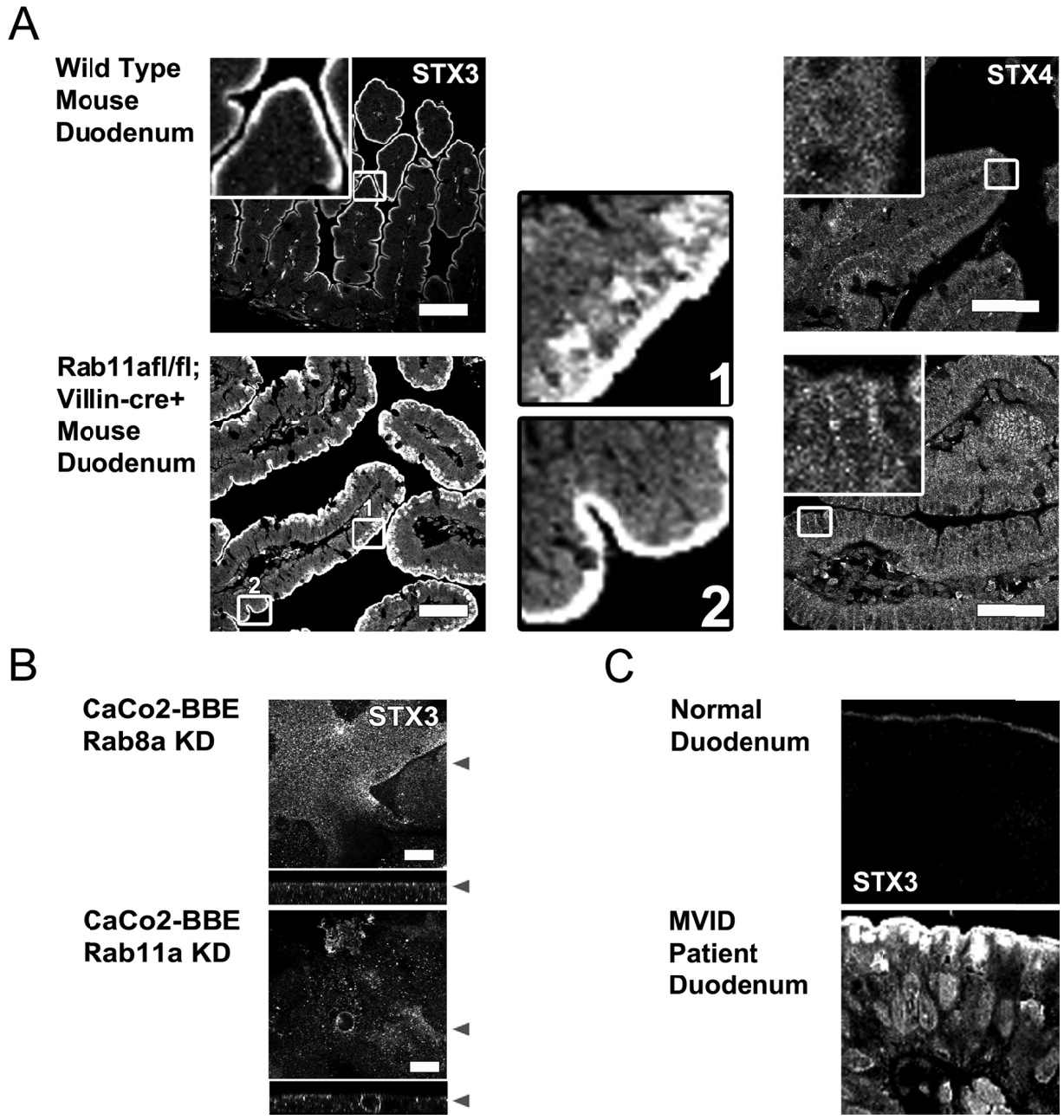

Figure 34. Rab11a is required for the apical localization of STX3 in enterocytes. (A) Left: In wild type mice duodenum, STX3 is localized to the apical surface. In Rab11a$^{\Delta IEC}$ mice duodenum, STX3 is reorganized away from the apical surface in punctate vesicles. Insets indicated by numbers **1** (top) and 2 (bottom) display stark redistribution of STX3 at the top of villi with normal distribution at the bottom of the villi. Right: In both wild type and Rab11a$^{\Delta IEC}$ mice duodenum STX4 is localized to intracellular vesicles. Scale bars are 50 μm. (B) In Rab8a-KD cells, STX3 is localized on the apical surface. In Rab11a-KD cells, STX3 is redistributed away from the apical surface into the cytoplasm and microvillus inclusions. Scale bars are 10 μm. (D) In MVID patient samples, STX3 is relocalized from the apical surface to small punctate vesicles beneath the apical surface.

Discussion

Knocking down Rab11a in MDCK cells disrupts the formation of the apical surface (Bryant, Datta et al. 2010). In this study, we demonstrate Rab11a maintains normal apical polarity in enterocytes. In Rab11a$^{\Delta IEC}$ duodenum samples and CaCo2-BBE Rab11a-KD cells, apically trafficked proteins are mistrafficked, microvilli length is reduced, and lateral microvillus inclusions are formed. In these enterocytes, we also observed expansion of lysosomal compartments, and redistribution of Rab8a and Rab11b. In both Rab11a$^{\Delta IEC}$ duodenum samples and CaCo2-BBE Rab11a-KD cells STX3 is mislocalized to the cytoplasm. STX3 acts as a general SNARE for the apical surface, and is required for final vesicle fusion to the plasma membrane. Interestingly, mutations in *STX3* causes Atypical forms of MVID, and in patient enterocytes polarity is disrupted, microvilli length is reduced, and lateral microvilli are formed (Muller, Hess et al. 2008; Stepensky, Bartram et al. 2013; Wiegerinck, Janecke et al. 2014). Notably, mutation of MYO5B also appears to mistraffic STX3 to small punctate vesicles away from the apical surface in MVID patient samples. This phenotype is similar to the Rab11a$^{\Delta IEC}$ duodenum samples, and suggests that both Rab11a facilitates trafficking of STX3 to the apical surface.

Trafficking of MST4 and aPKC to the apical surface of enterocytes is dependent on MYO5B coupled Rab11a-dependent trafficking, both of which facilitate ezrin phosphorylation that stimulates microvilli growth (Dhekne, Hsiao et al. 2014). Unexpectedly, in Rab11a$^{\Delta IEC}$ duodenum the apical trafficking of aPKC is not affected and Mst4 trafficking to the apical surface is only moderately influenced. Consequently, phosphorylation of ezrin appears to be unaffected in Rab11a$^{\Delta IEC}$ duodenum. This is not

surprising since both Rab8a and Rab11b are reorganized and upregulated in this tissue, and may be able to compensate for some portions of Rab11a function. Indeed, E-cadherin localization appears to be compensated in Rab11a$^{\Delta IEC}$ duodenum, however in Rab11a-KD CaCo2-BBE cells E-cadherin is mistrafficked to the apical surface.

Rab11a in enterocytes appears to be integral to the formation of the normal apical surface. In chapter two, we demonstrated that MYO5B works in concert with both Rab8a and Rab11a to maintain both apical and basolateral polarity (Knowles, Roland et al. 2014). Independently, Rab11a appears to maintain normal apical polarization, but parts of normal Rab11a function may be compensated for in Rab11a$^{\Delta IEC}$ duodenum samples. Similarly, parts of normal Rab8a function can be compensated for by Rab8b, and only with dual knock out of both Rab8a and Rab8b genes can the complete phenotype be appreciated (Sato, Iwano et al. 2014). Note, Rab8b does not interact with MYO5B (Roland, Lapierre et al. 2009). Microvilli development in enterocytes requires apical trafficking to establish and maintain these structures. Rab8a and Rab8b are essential for the initial establishment of microvilli, while Rab11a may play a key role in microvilli elongation through apical trafficking.

Methods

Mice

The conditional Rab11a floxed allele mice were derived from homologous recombination in embryonic stem cells as described previously by Yu et al, 2014 in press at EMBO (Yu, Nie et al. 2014). The Rab8a knockout mice used for the study have also been described previously by Sakamori et al, 2012 (Sakamori, Das et al. 2012). Data for mouse experiments was obtained from 4 individual mice for each genotype group. All experiments were performed using littermates unless stated otherwise.

Cell lines

Human colonic epithelial CaCo2-BBE and human embryonic kidney 293 (HEK) cell lines were grown in DMEM as detailed in chapter two. For CaCo2-BBE cells, 200,000 cells were plated and grown on 12-well Transwell filters for 15 days in culture unless otherwise stated, and media was changed daily through the culture duration as detailed in chapter two.

Lentiviral shRNA vectors targeting Rab8a and Rab11a (Open Biosystems V3LHS_359728 and V3LHS_377860) and a control shRNA (Open Biosystems) were used for transduction of Caco2-BBE cells. The CaCo2-BBE cells were transduced with lentiviral media produced in HEK cells and selected using puromycin (Cellgro). Rescue of CaCo2-BBE Rab8a-KD and Rab11a-KD was performed using vectors that were synthesized from mouse Rab8a and Rab11a sequences resistant to silencing by the above shRNAs, cloned into pCDH lentiviral vectors, and selected using puromycin as described similarly in chapter two.

RNA was isolated from CaCo2-BBE control, Rab8a-KD, and Rab11a-KD cell lines using TRIzol reagent (Invitrogen) according to the manufacturer's instructions and treated using RQ1 RNase-free DNase (Promega). cDNA was synthesized using a High Capacity cDNA Reverse Transcriptase Kit (Applied Biosystems) with both oligo-dT and random hexamer primers as described previously by Lapierre, et al. 2012 (Lapierre, Avant et al. 2012). Real-time PCR was performed using a StepOnePlus real-time PCR system with Express SYBR Green ER Supermix (Applied Biosystems) and the following primer pairs:

Rab8a-Forward 5'- ACCGGCTGTGTCCCATATCT-3'

Rab8a-Reverse 5'- GACGCCTTCAACTCCACTTT-3'

Rab11a-Forward 5'- TTCGCGTCTGTCTGACATTT-3'

Rab11a-Reverse 5'- TTGAAACTTCGGCCCTAGAC-3'

GAPDH-Forward 5'-AGATCCCTCCAAAATCAAGTGG-3'

GAPDH-Reverse 5'-GGCAGAGATGATGACCCTTTT- 3'

The above primers were validated for efficiency and melting temperature, and the results were analyzed by the comparative CT method as described previously in chapter two.

Tissue preparation

All tissue samples were obtained through protocols approved by the Rutgers University IRB. All mouse duodenum sections from dissections were washed in PBS

and fixed in 4% Paraformaldehyde or 2% Paroformaldehyde/2% Glutaraldehyde in 0.1M sodium cacodylate pH7.4. For immunofluorescence, samples were stored in 70% ethanol, embedded, and sectioned for further staining with proper antibodies.

Confocal immunofluorescence

The CaCo2-BBE control, Rab8a-KD, and Rab11a-KD cell lines were plated on 12-well Transwell filters and cultured for 15 days. Cells were prepared for immunofluorescence as described in chapter two. All images were captured with an Olympus FV-1000 confocal microscope (Olympus) using a 60x oil immersion objective with a numerical aperture of 1.42 and using the microscope's software at a 3x optical zoom. The individual images were converted to tiff files with the FV-1000, and Photoshop (Adobe) was used to create the final figures.

Histology, SEM, and TEM

Mouse duodenum sections were de-paraffinized and were submitted to antigen retrieval in a pressure cooker using the target retrieval solution as described previously in chapter two (Dako North America Inc.). Samples were then prepared for immunofluorescence as previously described. All imaging was performed using the Olympus FV-1000. CaCo2-BBE cell lines and mouse tissue were prepared as described in chapter two for SEM. Samples were mounted on stubs and coated with gold in a sputter coater, and analyzed using an FEI Quanta 250 SEM (Vanderbilt Cell Imaging Shared Resource, Vanderbilt University). TEM samples from MVID patients were prepared and analyzed by the Vanderbilt Cell Imaging Shared Resource, Vanderbilt University.

CHAPTER IV

Alterations in polarity occur throughout the gastrointestinal tract in Microvillus Inclusion Disease

Adapted From: Knowles, B. C., M. G. Martin et al. (2014). “Alterations in polarity occur throughout the gastrointestinal tract in Microvillus Inclusion Disease.” Manuscript in progress. The Journal of Pathology.

Introduction

Children with Microvillus Inclusion Disease (MVID) present with unremitting neonatal diarrhea and have generalized villus blunting, loss of polarity and microvilli, and pathognomonic intracellular microvillus inclusions in enterocytes of the small intestine (Davidson, Cutz et al. 1978). Previous investigations have identified inactivating mutations in myosin-Vb (MYO5B) as the causative agent for this disease, and recent investigations have identified syntaxin-3 (STX3) mutations as the cause of a milder “Atypical” form of MVID (Erickson, Larson-Thome et al. 2008; Muller, Hess et al. 2008; Wiegerinck, Janecke et al. 2014). MVID research since 1978 has justly focused on the enterocytes of the small intestine. Consequently, other highly polarized gastrointestinal tissues have not been examined in detail in spite of the prominent role of the apical recycling system in establishing polarity and promoting proper function in these tissue types including the stomach, liver, and the large intestine (Wakabayashi, Dutt et al. 2005; Forte and Zhu 2010; Sakamori, Das et al. 2012; Melendez, Liu et al. 2013; Knowles, Roland et al. 2014).

In gastric parietal cells, regulated apical recycling is the primary pathway for movement of H/K-ATPase-containing tubulovesicles to the apical surface, and these cells have the highest endogenous level of Rab11a of all polarized epithelial cells (Forte, Limlomwongse et al. 1969; Forte, Limlomwongse et al. 1969; Goldenring, Soroka et al. 1994). The parietal cells main function is to pump protons (H^+) into the lumen of the stomach using H/K-ATPase at the apical plasma membrane (Forte, Ganser et al. 1974). This function requires transitioning between two apical structural arrangements; resting and stimulated. In the resting state, the apical surface is elaborated into apical invaginations comprising the intracellular canaliculi, which represent an expanded apical plasma membrane supported by F-actin bundled with ezrin (Rosenfeld, McAllister et al. 1981; Yao, Thibodeau et al. 1993; Ammar, Nguyen et al. 2001; Zhou, Zhu et al. 2005). Underneath the apical surface of the intracellular canaliculi, Rab11a-containing tubulovesicles harbor a resting pool of H/K-ATPase (Black, Forte et al. 1981; Goldenring, Soroka et al. 1994; Matsukawa, Nakayama et al. 2003). Upon stimulation, H/K-ATPase-containing vesicles migrate and fuse into the apical canaliculi. Structural changes to form the stimulated configuration trigger phosphorylation of ezrin, and result in the formation of multiple microvillar extensions from on the canalicular surface, which increased the apical availability of H/K-ATPase (Forte, Machen et al. 1977; Duman, Tyagarajan et al. 1999; Matsukawa, Nakayama et al. 2003).

Similarly, both the liver and colon are highly polarized tissues that depend on apical vesicle trafficking for their normal function. Hepatocytes polarize into two distinct surfaces; one surface opens into bile canaliculi with sparse microvilli (apical), while the

second surface faces sinusoidal capillaries (basolateral) (Treyer and Musch 2013). MYO5B-coupled Rab11a-dependent trafficking is required by apical ATP-binding-cassette (ABC) transporters to establish the apical surface in hepatocytes, and expression of dominant negative mutations in either Rab11a or MYO5B caused aberrant trafficking of ABC transporters, BSEP and MRP2 (Wakabayashi, Dutt et al. 2005). Interestingly, in enterocytes MYO5B interaction with Rab8a promotes the initiation of microvilli growth, and MYO5B interaction with Rab11a is required for apical recycling of membranes internalized through apical macropinocytosis and also facilitates the maintenance of microvilli in enterocytes (Knowles, Roland et al. 2014). MYO5B has also been implicated in the recruitment to the apical surface of MST4 and aPKC, which are responsible for the phosphorylation of ezrin in enterocytes (Dhekne, Hsiao et al. 2014). As a result, Rab8a and Rab11a-dependent apical trafficking coupled to MYO5B facilitate proper trafficking in both hepatocytes and enterocytes (Sato, Mushiake et al. 2007; Knowles, Roland et al. 2014).

In the Navajo population, MVID has an incidence of 1 case per 12,000 live births, with a homozygous *MYO5B-P660L* (1979C>T p.Pro660Leu, exon 16) mutation inherited in an autosomal recessive pattern, responsible for all cases (Pohl, Shub et al. 1999; Erickson, Larson-Thome et al. 2008). In this report, we examined tissue samples from a 7-year-old Navajo male with MVID, diagnosed at 3 days of age, who underwent a multi-organ transplant at 11 months of age because of end stage liver failure. Based on studies done on this patient and two other MVID patients with similar presentations, we report that MYO5B appears to regulate global gastrointestinal tract polarity. The Navajo MVID patient's stomach parietal cells showed altered intracellular canalicular

localization, alterations in the distribution of MYO5B and its associated Rabs (Rab8a and Rab11a), and disruption of apical and basolateral markers specifically ezrin, Na/K-ATPase, and p120-catenin (p120). As expected, the enterocytes of the large intestine in three separate MVID samples displayed similar deficits to those previously observed in the enterocytes of the small intestine in chapter two including: loss of apical villin-1 and alterations in the distribution of MYO5B. However, pathognomonic microvillus inclusions were not observed in enterocytes of the large intestine. Hepatocytes in these patients also appeared to display accumulation of MYO5B, redistribution of Rab8a and Rab11a, and aberrant trafficking MRP2 and BSEP. The pancreas of the Navajo MVID patient also displayed fragmentation of Islets of Langerhans with accumulation of insulin-staining cells throughout the pancreas. These novel findings suggest that the effects of MYO5B mutations in MVID patients are not tissue specific. Rather alterations in polarity are observed across many epithelial tissue types.

Materials and Methods

Tissue preparation

Our primary patient was transplanted, because of end stage liver disease. The transplant included segmental transplant of the liver (left lobe), stomach, pancreas, small intestine, and colon with an arterial interposition graft. The patient is now receiving immunosuppressive therapy with tacrolimus and tolerating both oral and enteral feedings. The family gave consent, under an IRB approved protocol, to allow for evaluation of tissue samples from the native organs that were removed at the time of the transplant. Other MVID patient samples were obtained via tissue resection for two liver samples and two colon samples. All tissue samples were obtained through protocols approved by the Phoenix Children's Hospital IRB and Mattel Children's Hospital. All biopsy and resection samples were prepared as detailed in chapter two.

Histology

Normal human and MVID patient sections were de-paraffinized and were submitted to antigen retrieval as detailed in chapter two. Serum free protein block (Dako North America Inc.) was used for blocking tissue, and primary incubation was performed as detailed in chapter two. Appropriate secondary antibodies were conjugated for immunofluorescence with Alexa 488, Alexa 568, Alexa 647, Cy3, or Cy5 (1.5-hour incubation at room temperature). Detailed information on primary antibodies and their dilutions are listed in Table 1. Images were captured with an Olympus FV-1000 confocal microscope (Olympus) using a 60x oil immersion objective with a numerical aperture of

1.42. The individual images were converted to tiff files with the FV-1000, and Photoshop (Adobe) was used to create the final figures.

Samples for structured illumination microscopy (SIM) were prepared as for confocal immunofluorescence (see above). SIM imaging was performed on a DeltaVision OMX microscope (Applied Precision Inc.) using 488 nm, 568 nm, and 642 nm lasers. Reconstruction and alignment of SIM images was performed using softWoRx version 5.0 (GE/Applied Precision Inc.). These corrections were applied back into the acquired images, and Adobe Photoshop was used to produce the final images as detailed in chapter two.

Study Approval

The studies in these investigations utilized archival paraffin tissue specimens from normal children, Navajo MVID patients, and non-Navajo MVID patients. All procedures and studies were performed according to protocols approved by Institutional Review Boards at both Phoenix Children's Hospital, Mattel Children's Hospital, and Vanderbilt University School of Medicine. IRB approval of informed consent was obtained from all families of living subjects prior to research and IRB approved decedent research on tissue blocks from patients who had expired.

Results

Inactivating Mutation of MYO5B causes loss of polarity in parietal cells

Previous work has demonstrated that parietal cells depend on regulated Rab11a-dependent trafficking of H/K-ATPase containing tubulovesicle pools to the apical surface to pump H^+ into the lumen of the stomach (Duman, Tyagarajan et al. 1999). H/K-ATPase-containing tubulovesicles from parietal cells contain a wide array of apical trafficking proteins including: Rab11a, VAMP2, and STX3 (Lapierre, Avant et al. 2007; Forte and Zhu 2010). However, the role of MYO5B on these vesicles remains unclear. Since, MYO5B interacts directly with Rab11a to facilitate vesicle trafficking in other cell types, we reasoned that mutations in MYO5B might affect parietal cell function, because of their high levels of Rab11a (Goldenring, Soroka et al. 1994; Duman, Tyagarajan et al. 1999; Roland, Bryant et al. 2011). To examine the effects of the Navajo MYO5B mutation (*MYO5B-P660L*) on parietal cells in MVID patients, we immunostained stomach biopsy samples from a Navajo MVID patient for H/K-ATPase and ezrin. In normal stomach sections, ezrin and H/K-ATPase immunostaining was concentrated in the apical canalicular region of parietal cells (Figure 35A). In contrast, MVID patient samples showed a marked redistribution of ezrin to the cytoplasm, and concentration of H/K-ATPase to more compressed membrane structures (Figure 35A). Structured illumination microscopy (SIM) of the MVID patient samples revealed aberrant intracellular localization of H/K-ATPase (Figure 35B). Notably, the localization of pepsinogen in chief cells appeared to be unaffected in MVID patient stomach sections (data not shown).

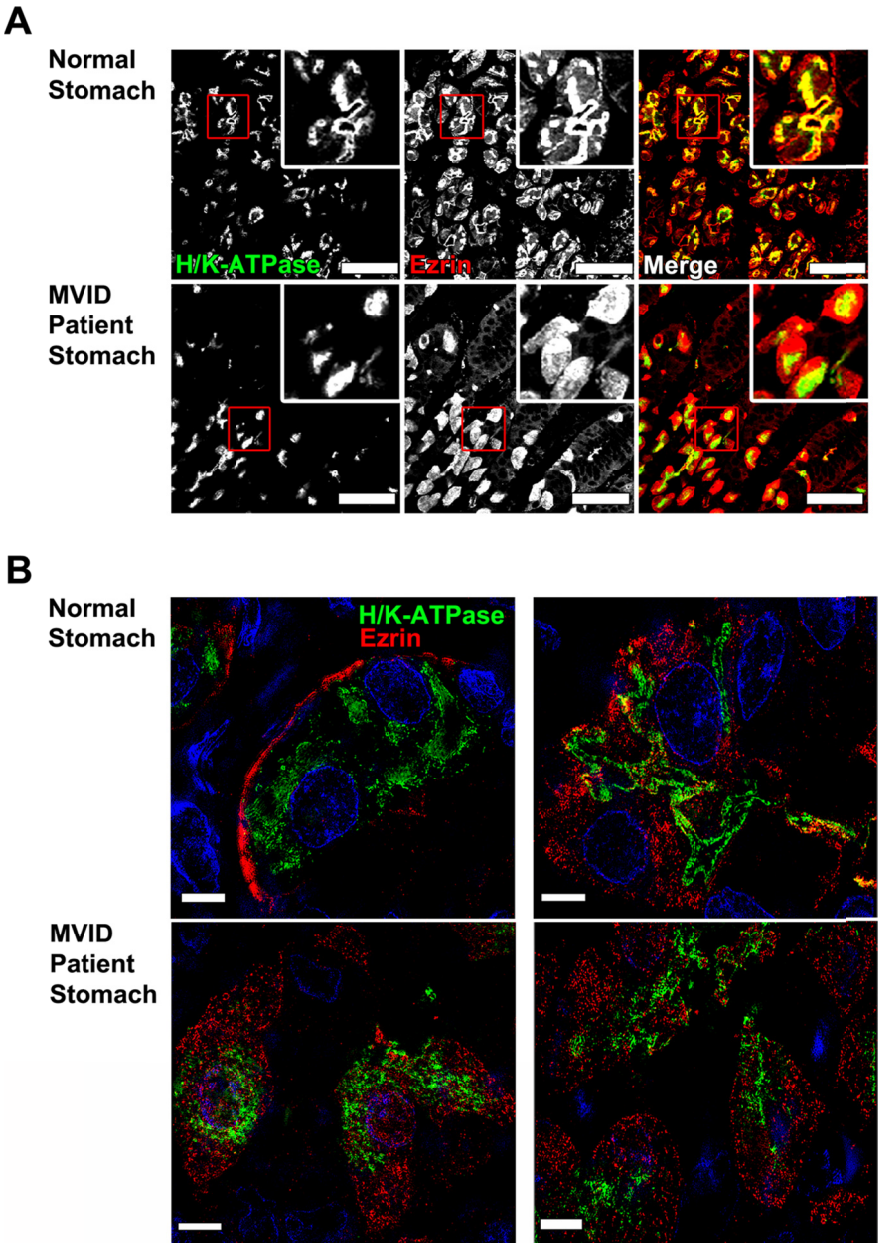

Figure 35. Immunostaining of Navajo MVID patient stomach samples reveal that mutation of MYO5B cause loss of normal apical canalicular surfaces in parietal cells.

(A) Top: Normal stomach immunostaining for H/K-ATPase (green) and ezrin (red) showed canalicular localization of both ezrin and H/K-ATPase in parietal cells. Bottom: MVID patient stomach immunostaining for H/K-ATPase and ezrin showed aberrant cytoplasmic redistribution of both markers in parietal cells. (B) Top: SIM imaging of H/K-ATPase and ezrin in normal parietal cells. Left: Parietal cells with normal resting pool of H/K-ATPase. Right: Parietal cells with normal H/K-ATPase distributed to canalicular surface. Bottom: SIM imaging of the MVID patient samples revealed an aberrant accumulation of intracellular H/K-ATPase. Contrast enhancement of SIM images were adjusted separately. Scale bars in A are 50μm in the panels and B are 5μm.

Ezrin switches between inactive (bound to itself between amino and carboxyl-termini) and active (unfolded) conformations, which in enterocytes are mainly facilitated by aPKC and Mst4-dependent phosphorylation of threonine 567 (T567). Recently studies have suggested that both aPKC and Mst4 are positioned at their apical location via Rab11a-dependent and MYO5B-coupled trafficking (Zhu, Zhou et al. 2007; Dhekne, Hsiao et al. 2014). To examine the effects of MYO5B-P660L on the distribution of its Rab effectors in parietal cells, we immunostained Navajo MVID patient stomach biopsy samples for MYO5B, Rab8a, and Rab11a. In normal stomach sections, H/K-ATPase and Rab11a immunostaining appear to overlap in tubulovesicles (Figure 36A). In contrast, in MVID patient samples immunostaining of H/K-ATPase was distributed throughout the cytoplasm (Figure 36A). In normal stomach sections, MYO5B was distributed along the apical intracellular canaliculus and basolateral membranes. But MYO5B was decreased and redistributed to cytoplasmic locations in the MVID patient samples (Figure 36B). In normal stomach sections, Rab8a was distributed intracellularly along the basolateral membrane in parietal cells, but Rab8a was redistributed along both apical and basolateral membranes in the MVID patient's parietal cells (Figure 36C). Interestingly, phosphorylated ERM (Ezrin, Radixin, Moesin) proteins appear to be decreased in MVID patient stomach sections when compared to normal stomach sections (Figure 36C). Thus, MYO5B appears to be essential for H/K-ATPase canalicular delivery to the apical surface and might play a role in regulating ezrin phosphorylation in parietal cells.

Normal function of parietal cells is dependent upon the establishment of electrochemical gradients and contact with neighboring cells. To evaluate the integrity of

these systems in the basolateral compartment of the MVID patient stomach samples, we immunostained the stomach sections for p120 and Na/K-ATPase. In normal stomach sections, Na/K-ATPase and p120-catenin (p120) immunostaining was localized to the basolateral surface of parietal cells (Figure 36C). In contrast, MVID patient samples showed an increase and cytoplasmic redistribution of both Na/K-ATPase and p120, but generally maintained their basolateral distribution (Figure 36C). These findings confirmed that mutation of MYO5B in the Navajo MVID patients' stomach can cause disruption of normal polarity in parietal cells.

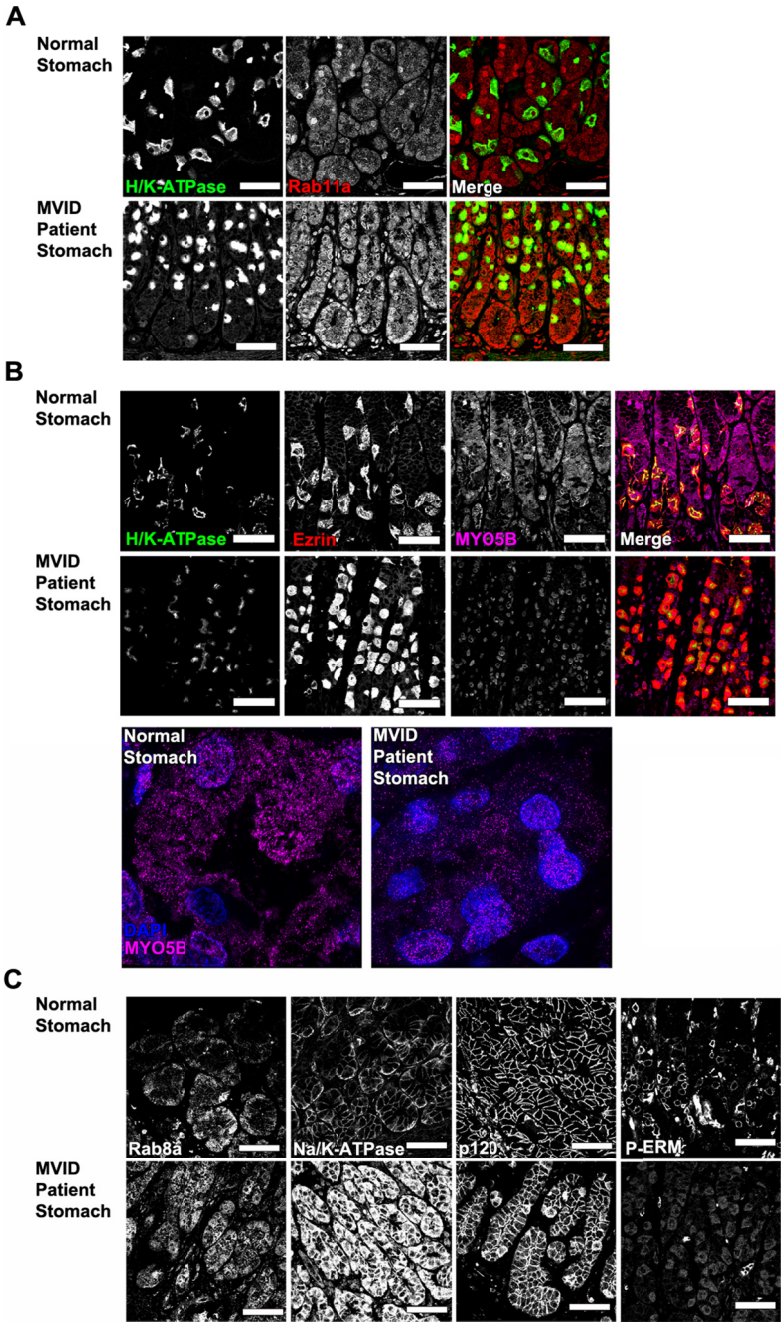

Figure 36. Immunostaining of Navajo MVID patient stomach samples demonstrated that MYO5B mutation leads to redistribution of Rab8a and Rab11a. (A) MVID patient stomach parietal cells showed aberrant cytoplasmic redistribution of Rab11a. (B) MVID patient stomach parietal cells showed redistribution of MYO5B from both the apical and basolateral surfaces to the nuclear envelope. Contrast enhancement of SIM images in lower panels were adjusted separately. (C) In MVID patient samples, Rab8a, Na/K-ATPase, and p120 maintain normal basolateral localization, but have increased cytoplasmic localization. Phosphorylated ERM proteins appear to be markedly decreased in in the MVID patient samples. Scale bars are 50μm in all panels.

Mutation of MYO5B causes loss of apical polarity in the enterocytes of the large intestine

MVID disrupts normal apical and basolateral polarity in the enterocytes of the small intestine (Knowles, Roland et al. 2014). The enterocytes of the large intestine function to absorb water after initial digestion in the small intestine, but in the context of MVID the large intestine has not been studied extensively. To examine the effects of mutations in MYO5B on the large intestine, we immunostained MVID patient colon samples for MYO5B, villin-1, p120, E-cadherin, and claundin-2 (CLDN2). In control colon samples, villin-1 was localized to the apical surface and MYO5B was localized sub-apically. In MVID patient colon samples, apical villin-1 was reduced and along with MYO5B these proteins were redistributed throughout the cytoplasm (Figure 37A). Interestingly, phosphorylated ERM was reduced in MVID patient samples, and both Rab8a and Rab11a were redistributed to the cytoplasm (data not shown). In both the control and MVID patient colon samples, p120, E-cadherin, and CLDN2 were all normally localized along the basolateral surface (Figure 37B). Thus, MYO5B mutations in colonocytes may affect apical distribution of proteins, but the basolateral compartment remains intact.

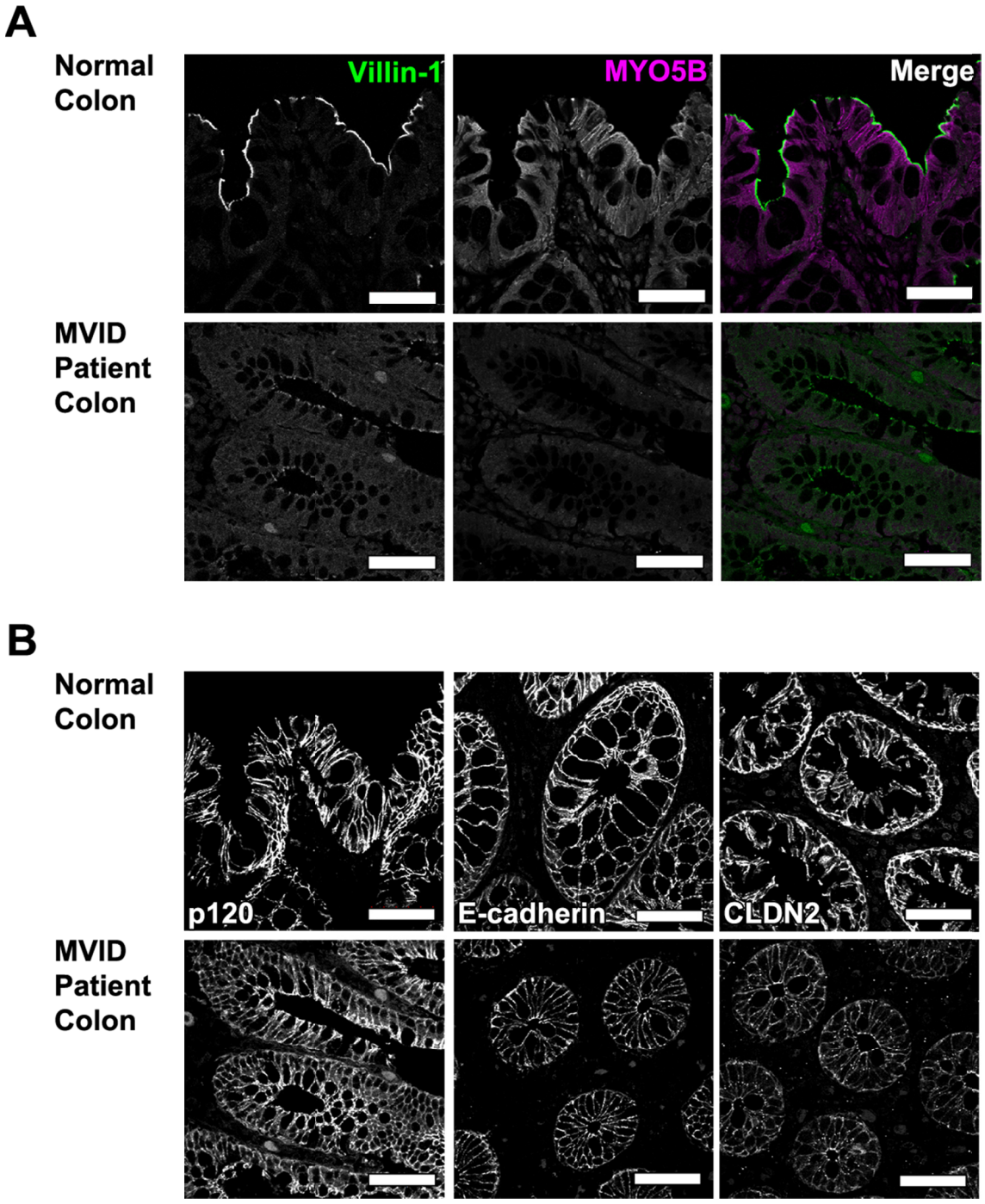

Figure 37. The integrity of the basolateral compartment is maintained in MVID colonocytes, and the apical surface is disrupted.
(A) Normal colon immunostaining for villin-1 (green) and MYO5B (magenta) showed apical distribution of villin-1 and sub-apical distribution of MYO5B. Equivalent staining in MVID patient colon samples, showed some loss of apical villin-1 and cytoplasmic redistribution of MYO5B. (B) In both control and MVID patient colonocytes, p120, E-cadherin, and CLDN2 maintains normal basolateral distribution. Scale bars are 50μm in all panels.

MYO5B mutation leads to redistribution of BSEP and MRP2 in MVID patient liver samples

To investigate the effects of MYO5B mutations on vesicle trafficking in the liver, we immunostained patient samples for the ATP-binding cassette transporters BSEP (Bile Salt Export Pump) and MRP2 (Multidrug Resistance-associated Protein 2). A previous investigation noted that in MVID patient liver samples, proper trafficking of BSEP was disrupted, but MRP2 appeared to be unaffected (Girard, Lacaille et al. 2013). Whether MVID patient MYO5B mutation affect hepatic biliary function and cause cholestasis or if cholestasis is caused by long term total parenteral nutrition (TPN) treatment has yet to be established definitively. To determine the effects of MYO5B mutation on MVID patient samples we immunostained MVID liver samples for ezrin, MYO5B, and phosphorylated ERM. In normal liver sections, ezrin, MYO5B, and phosphorylated ERM proteins lined the bile canalicular surface (Figure 38A). In MVID patient liver sections, ezrin was relocated to large intracellular punctate structures, while MYO5B and phosphorylated ERM proteins were mislocalized intracellularly (Figure 38A). In normal liver sections, E-cadherin and p120 connect neighboring hepatocytes, but in MVID patient sections both E-cadherin and p120 were distributed throughout the cytoplasm (Figure 38B). In normal liver sections, both MRP2 and BSEP line sinusoidal surfaces, but in MVID patient sections both MRP2 and BSEP were distributed throughout the cytoplasm of hepatocytes (Figure 38C). It should, be noted that all patient samples were from MVID patients on total parenteral nutrition (TPN) therapy, which is known to disrupt normal liver function. As a result, although MYO5B mutations appear to disrupt hepatocyte function, the effects could be partially due to TPN therapy.

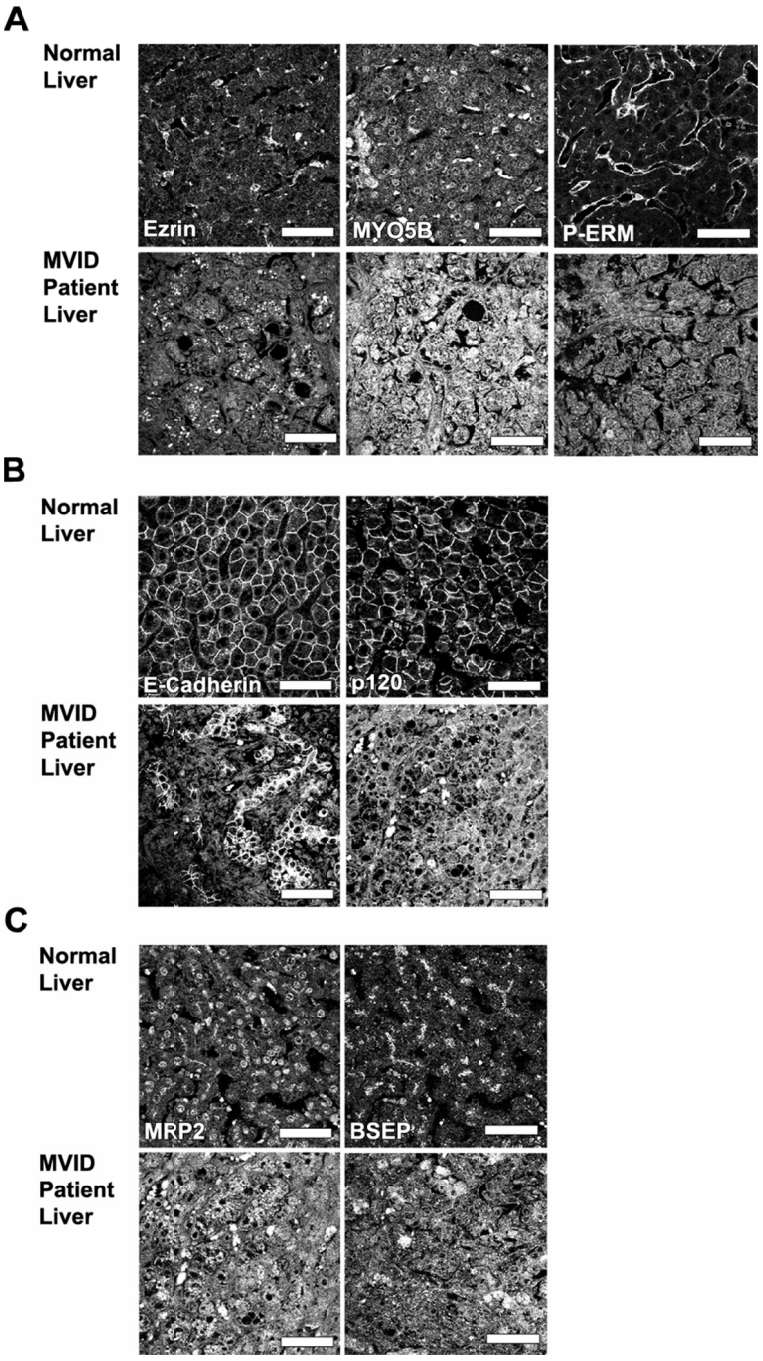

Figure 38. Immunostaining of MVID patient liver tissue samples shows redistribution of normal canalicular and sinusoidal surface proteins.
(A) Ezrin, MYO5B, and phosphorylated ERM proteins are redistributed from normal the bile canalicular surface to intracellular puncta in MVID patient samples. Contrast enhancement in panels were adjusted separately (B) Both p120 and E-cadherin in control sections connect neighboring hepatocytes, but in MVID patient sections they are redistributed to the cytoplasm. (C) MRP2 and BSEP are normally distributed along sinusoidal surfaces, but in MVID patient sections they are redistributed to intracellular vesicles. Scale bars are 50μm in all panels.

Functional MYO5B is required for proper morphology of the endocrine pancreas

In muscle cells after insulin-stimulation, translocation of GLUT4-positive vesicles to the plasma membrane is facilitated by MYO5B coupled to Rab8a-dependent trafficking (Ishikura and Klip 2008). Interestingly, disruption of this pathway should lead to Type II Diabetes, and recently one 10 year old Navajo MVID patient was reported to have an abnormal form of Type II diabetes (Oatman, Djedjos et al. 2013). We evaluated beta cells in an MVID patient's pancreas using immunohistochemistry for insulin. In normal pancreas sections, insulin staining was positive in beta cells of the Islets of Langerhans (Figure 39). In MVID patient pancreas sections, insulin staining demonstrated the presence of fragmented small collections of islet cells throughout the pancreas, but acinar cell mass was generally maintained (Figure 39).

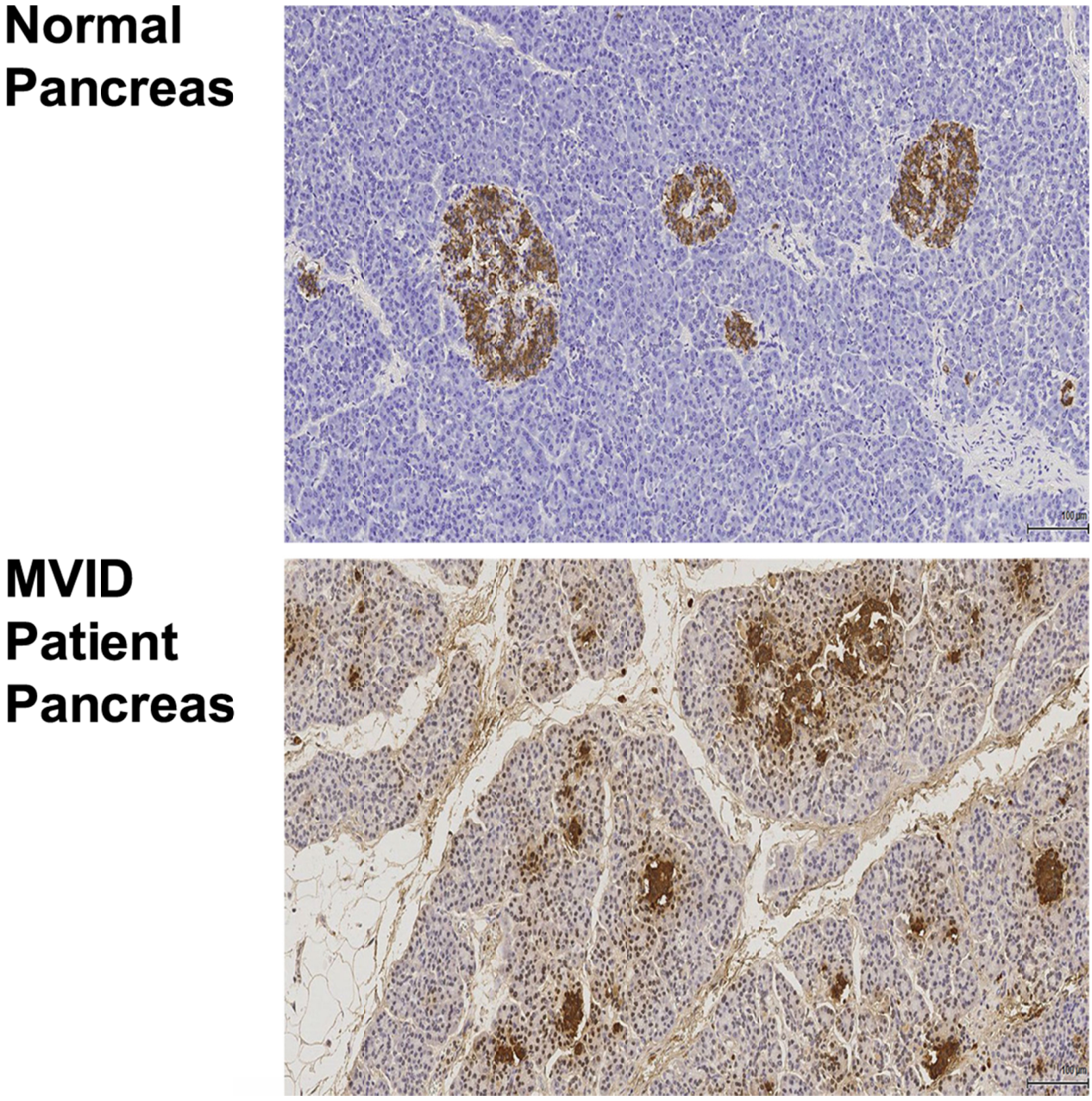

Figure 39. Immunohistochemical diaminobenzidine (DAB) staining of pancreas demonstrates accumulation of insulin staining in MVID patient samples.
(Above) Insulin stains beta cells specifically in normal sections. (Below) In MVID patient samples, small collection of insulin-staining cells are observed throughout the pancreas. Scale bars are 100μm in both panels.

Discussion

Previous studies in MVID have focused on the impact of inactivating mutations in MYO5B on the polarity, morphology, and function of enterocytes of the small intestine (Knowles, Roland et al. 2014). In this study, we evaluated the effects of mutations in MYO5B on the integrity of other organs in the gastrointestinal tract. We found that mutation of MYO5B has profound effects on polarity in the stomach, liver, and colon. In the Navajo MVID patient gastric parietal cells, H/K-ATPase was abnormally located intracellularly and did not associate with intracellular canaliculi. In stomach samples, Na/K-ATPase was redistributed to the cytoplasm, and phosphorylated ERM proteins were drastically decreased. The apical recycling endosome (ARE) acts as the central decision point for both the biosynthetic and endocytic pathways as they traffic and recycle proteins and lipids to and from the plasma membrane. Through its interactions with Rab8a and Rab11a, MYO5B plays a crucial role in apical recycling on the ARE, and leads to the polarization of cells into apical and basolateral domains (Bryant and Mostov 2008; Knowles, Roland et al. 2014). Thus, it is not surprising that mutation of MYO5B would lead to loss of polarity in stomach parietal cells, because these cells have the highest endogenous levels of Rab11a, which interacts directly with MYO5B and was mistrafficked to the nuclear envelope in MVID patient parietal cells. Recently, MYO5B and Rab11a have been linked to ezrin phosphorylation in enterocytes, and we found a decrease in phosphorylated ERM member proteins in MVID patient stomach sections (Dhekne, Hsiao et al. 2014). Currently, it is not understood if phosphorylation of ezrin results in or is a consequence of the stimulated morphology in parietal cells.

Interestingly, MYO5B loss in enterocytes causes a reduction in apical ezrin (Knowles, Roland et al. 2014).

In the three MVID patient colon samples studied in this report, colonocytes showed loss of microvillar markers, alterations in the distribution of MYO5B, and dispersal of Rab8a and Rab11a, but interestingly no changes in claudin-2, E-cadherin, and p120. Large cystic spaces were often detected, but microvillus inclusions were not detected in enterocytes of the large intestine. The principle disease manifestation of MVID is chronic unremitting secretory diarrhea. We have recently suggested that the pathophysiology of MVID is likely due to loss of polarity that results from uncoupling of MYO5B from Rab8a and Rab11a (Knowles, Roland et al. 2014). Loss of apical polarity in the enterocytes of the colon likely contributes to the clinical MVID phenotype, since the colon is unable to compensate for excess fluid secreted into the lumen of the small intestine.

In the three liver samples examined in this report, hepatocytes contained intracellular punctate ezrin, and displayed aberrant intracellular localization of both MRP2 and BSEP. Our findings contrast with earlier published work which demonstrated mistrafficking of BSEP, but MRP2 was not affected. These discrepancies might be due to combination of patients with different stages of end stage liver disease and the divergent immunohistochemical approaches utilized to asses these proteins. In previously published work, pre-transplant MVID patient livers displayed fibrosis and abnormal bile canalicular surfaces (Girard, Lacaille et al. 2013). However, it is not known if these changes were due to TPN therapy or resulted from mutations in MYO5B. Increasing evidence suggests that MYO5B plays essential roles in normal liver function,

but more sophisticated model systems will be required to discern these functions away from the consequences of current MVID therapy.

In this chapter, we have observed the consequences of mutations in MYO5B in highly polarized organs. Indeed, MYO5B appears to be essential for the proper function of epithelial cells that have been observed in this chapter. Notably, MVID patient pancreas also displayed abnormal beta cell distribution in small or fragmented Islets of Langerhans. In contrast, exocrine pancreas as well as the zymogen-secreting chief cells of the stomach did not show significant alterations. It is not clear how alterations in polarity in the epithelia outside the small intestine will affect long-term quality of life in patients with MVID. Certainly sequelae in the small intestine and liver will be abrogated in patients after combined liver-small intestine transplant. Hypochlorhydria in the stomach is not likely to have significant clinical impact in these patients. Nevertheless, our studies suggest that the loss of functional MYO5B will likely have manifestations in multiple organs and one may expect that alterations in trafficking may also be manifested in the brain, heart, lungs, and kidneys of MVID patients.

Acknowledgements

This work was supported by the NIH grant RO1 DK70856 to J.R.G and RAC Awards to M.S. from Phoenix Children's Hospital for initial support of this project. Confocal and structured illumination fluorescence microscopy imaging was performed through the use of the VUMC Cell Imaging Shared Resource and histological sectioning was performed by Translational Pathology Shared Resource, both supported by National Institute of Health (NIH) Grants CA68485, DK20593, DK58404 and HD15052. Fluorescence slide imaging was performed on an Ariol SL-50 digitizing scanner in the VUMC Digital Histology Shared Resource.

We thank I. Macara and R. Guyer for aPKC antibody, and the Vanderbilt University School of Medicine Medical Scientist Training Program for continued support.

CHAPTER V

Conclusions and future directions

Conclusions

Adapted From: Knowles, B. C., M. J. Tyska, and J. R. Goldenring. (2014). “Apical vesicle trafficking takes center stage in neonatal enteropathies.” Editorial. Gastroenterology.

Typical MVID

Alterations in intestinal polarity have been revealed to be associated with intestinal diarrheal states, and might have profound effects on diseases throughout the gastrointestinal tract. Microvillus Inclusion disease (MVID) was believed to be an intestinal specific disease that was initially characterized in 1978 in 5 infants experiencing chronic, unremitting, secretory diarrhea (Davidson, Cutz et al. 1978). Studies of initial patient biopsy samples from the small intestine revealed profound villus atrophy, crypt hypoplasia, absence of microvilli, malabsorption of glucose, and defective sodium transport. In these MVID patients feeding was discontinued and total parenteral nutrition (TPN) was started, but secretory diarrhea persisted. Later investigations revealed that the pathognomonic microvillus inclusions were observed in 10% of enterocytes, and these inclusions contained apical enterocyte proteins such as sucrase isomaltase, alkaline phosphatase, and sodium hydrogen exchanger 3 (Ameen and Salas 2000). Moreover, membrane proteins that normally traffic to the apical domain were mislocalized to a sub-apical compartment, while sodium potassium ATPase (Na/K-

ATPase) basolateral localization was unaffected in the biopsy samples (Cutz, Rhoads et al. 1989; Ameen and Salas 2000; Reinshagen, Naim et al. 2002). The causative agent of this disease remained obscure until 2007 when Sato et al. demonstrated that Rab8a knockout mice display phenotypic similarities to MVID, suggesting that defects in trafficking to the apical domain may underpin this disease (Sato, Mushiake et al. 2007). However, no mutations in Rab8a were identified in humans. Concurrently, it was demonstrated that MYO5B regulates intracellular trafficking and endocytic recycling by localizing with specific Rab small GTPases (Rab8a, Rab10, and Rab11) in sub-apical vesicles (Roland, Kenworthy et al. 2007). These two studies taken together culminated in 2008 with reports from Europe and the United States that mutations in the *Myosin Vb* (*MYO5B)* gene cause MVID (Erickson, Larson-Thome et al. 2008; Muller, Hess et al. 2008). However, in the original report from Europe, there was one MVID patient without any *MYO5B* mutation. Since then 41 published mutations in the *MYO5B* gene have been identified in MVID patients (van der Velde, Dhekne et al. 2013). Recently, Wiegerinck, et al. identified patients with mutations in syntaxin-3 (STX3) that also gave rise to an MVID-like disease phenotype (Wiegerinck, Janecke et al. 2014).

Atypical MVID

The brief report by Wiegerinck, et al. describes two cases involving toddlers who present with watery diarrhea and severe metabolic acidosis (Wiegerinck, Janecke et al. 2014). Interestingly, both of these children developed increased tolerance for enteral feeding, but still required partial TPN and sodium-bicarbonate supplementation. Biopsy samples from these “Atypical” MVID patients, revealed accumulation of PAS-positive vesicles sub-apically, microvillus inclusions, and lateral lumens with microvilli via

histology and transmission electron microscopy. Whole exome sequencing revealed that mutations in STX3, rather than MYO5B, were the underlying cause of “Atypical” MVID in these cases. Stable expression of mutant STX3 in CaCo2 cells and organoid cultures derived from crypts of one patient recapitulated the “Atypical” MVID phenotype. Most interestingly, the clinical signs and treatment used for these two patients differ significantly from MVID, and support the classification of these patients into a distinct but related class of enteropathy (Figure 40A).

New Insights into the Pathophysiology of MVID

Wiegerinck, et al. have provided novel insights into the pathophysiology of neonatal enteropathies by supporting the likely role for aberrations in apical trafficking. Both Rab8a and Rab11a bind to MYO5B directly on recycling vesicles, and MYO5B most likely functions as a dynamic tether for both Rab8a and Rab11a and normally maintains these proteins at their appropriate sub-apical membrane location (Roland, Bryant et al. 2011; Knowles, Roland et al. 2014). MYO5B interaction with Rab8a promotes the initiation of microvilli growth, and MYO5B interaction with Rab11a is required for apical recycling of membranes internalized through apical macropinocytosis and also facilitates the maintenance of microvilli (Knowles, Roland et al. 2014). Thus, MYO5B in concert with Rab8a and Rab11a regulates the polarity of intestinal epithelial cells, and uncoupling of these Rabs from MYO5B causes gross changes in cellular polarity and mucosal integrity in patients with MVID. These results together with previous work demonstrated that MYO5B interacts with Rab8a and Rab11a to regulate enterocyte polarity, apical trafficking, and microvilli growth.

Rab11a regulates actin dynamics, apical trafficking, and recycles the apical brush border contents from macropinosomes in a MYO5B-dependent manner (Holubcova, Howard et al. 2013; Knowles, Roland et al. 2014). Cdc42 also associates with both Rab8a and Rab11a positive vesicles, and is activated via Rab8a through Tuba, a Cdc42 GEF, to facilitate regulation of cellular polarity and actin polymerization (Bryant, Datta et al. 2010). Rab11a positive vesicles utilize STX3, an apically targeted t-SNARE, to facilitate vesicle fusion of apically trafficked proteins to the plasma membrane (Carmosino, Valenti et al. 2010). The process of vesicular fusion to the plasma membrane is likely the last step in Rab11a-dependent apical trafficking in enterocytes. In chapter three we demonstrated that loss of Rab11a or mutation of MYO5B caused cytoplasmic relocalization of STX3, and Rab11a is involved in STX3 localization. Interestingly, patients with mutations in the STX3 binding protein *STXBP2/Munc18-2*, after treatment of their primary disease, have persistent chronic diarrhea, loss of microvilli, and histological findings consistent with the “Atypical” MVID described in the present report (Stepensky, Bartram et al. 2013). All of these processes in concert aid in the formation and maintenance of apical surface and microvilli (Figure 1B). Currently, it is not clear how STX3 mutations affect the full range of apical trafficking events and epithelial polarity. Further studies will be required to compare the deficits present in STX3 mutants compared with MYO5B mutants and how MYO5B mutations may impact STX3 function in typical MVID patients.

A

MVID type	Disease onset	Mutation	Diarrhea type	Enteral feeding	Microvillus inclusions
Typical	Early or late	Myosin Vb	Secretory	Intolerance	Present in 10% of enterocytes
Atypical	Variable	Syntaxin 3 STXBP2/Munc18-2	Variable	Partial tolerance	Present in some enterocytes but lateral lumens with micovilli observed

B

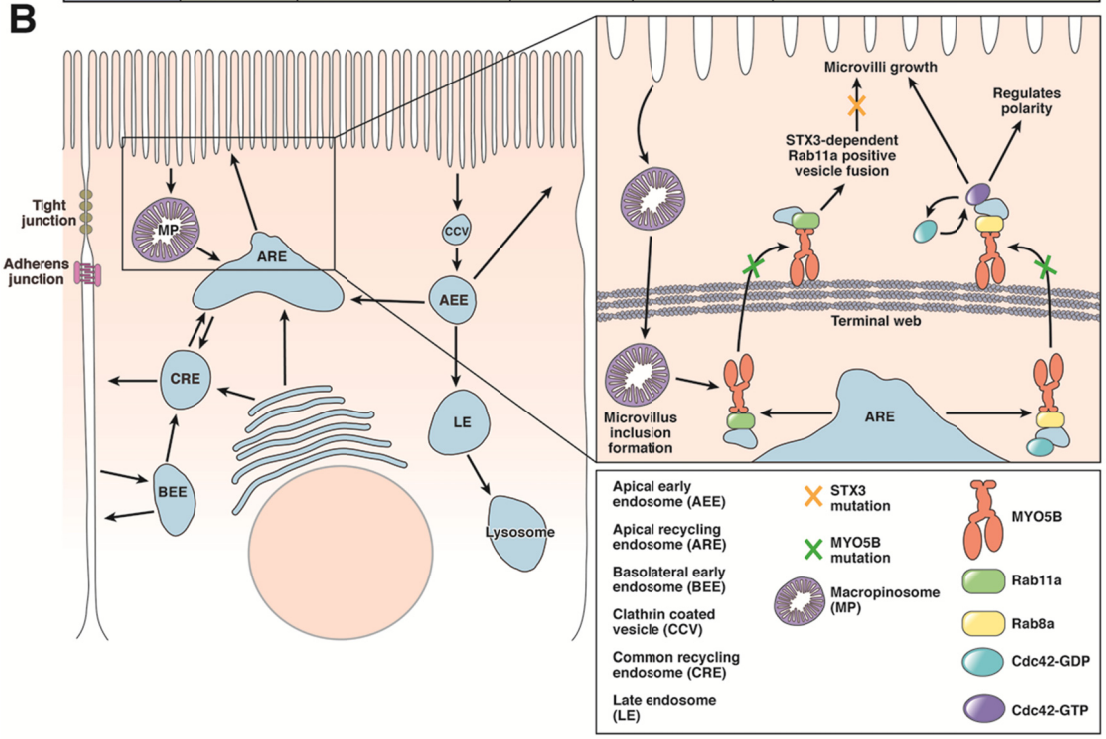

Figure 40. Loss of STX3 inhibits MYO5B-dependent Rab11a-positive vesicle fusion to the apical plasma membrane and causes atypical microvillus inclusion disease (MVID).

(A) Reclassification of MVID into typical and atypical MVID based on disease onset, gene mutation, diarrhea type, feeding tolerance, and microvillus inclusion presentation. (B) Left: Normal enterocyte with proper vesicle trafficking of cargo. Right: Magnified image of ARE and its predicted interaction with macropinosomes. Both Rab8a and Rab11a bind to MYO5B directly on the ARE. Mutations in MYO5B that cause MVID obstruct MYO5B motor function, and prevent all subsequent apical trafficking via MYO5B-dependent pathways. Rab8a facilitates MYO5B-dependent apical trafficking and recycling, and has also been shown to activate Cdc42 via Tuba, which regulates cellular polarity, and facilitates actin polymerization. Rab11a facilitates apical trafficking and recycling via MYO5B-dependent pathways. Rab11a also normally regulates actin dynamics in a MYO5B-dependent manner, and is required to recycle microvilli after macropinocytosis. This recycling prevents microvillus inclusion formation after macropinocytosis of the microvilli. STX3 is required for final Rab11a positive vesicle fusion to the apical surface and mutations in STX3 disrupt the normal function of this pathway. All of these pathways together aid in microvilli growth and the maintenance of apical polarity.

Why toddlers with “atypical” MVID have a milder phenotype when compared with “typical” MVID patients has not been definitively determined, but it appears most likely due to the association of STX3 with Rab11a-positive recycling vesicles. Since STX3 does not participate in Rab8a-positive vesicle fusion, Rab8a-dependent apical trafficking may not be affected by mutations in STX3, and as result only a partial MVID phenotype was observed in these patients with STX3 mutations. STX3 is localized specifically to the apical surface of epithelial cells, which is similar to the localization of MYO5B, and this localization likely accounts for the lack of initial extra-intestinal manifestation of this disease (ter Beest, Chapin et al. 2005; Lapierre, Avant et al. 2007). However, the epithelial cells of the stomach, colon, liver, and kidney are highly polarized, and depend on the fusion of Rab11a-positive vesicles to the plasma membrane for the secretion of acid, maintenance of apical polarity, trafficking of transporters, and establishment of primary cilia. As a result, mutations in *STX3* could lead to achlorhydria, disrupt apical surface of the colon, cause cholestasis, and/or polycystic kidney disease. Similarly in typical MVID patients with mutations in *MYO5B*, extra-intestinal manifestations of MVID have been studied in chapter four. However, MVID patients do not live long enough for the consequences of these changes to manifest due to the complications of the current therapies, without intestinal transplant.

Pharmacological treatment for MVID has not advanced significantly since 1978. This disease is still treated initially with total parenteral nutrition (TPN) and ultimately with dual small intestine and liver transplant (Oliva, Perman et al. 1994). Notably, in chapter two we laid the framework for possible MVID treatment by illustrating that the primary disease manifestation occurs at the tips of villi in the small intestine. Hence, if

tip enterocytes could be compelled to adapt a lower villus phenotype rather than the villus tip characteristics; the enterocytes may be stabilized and the unremitting diarrhea could be ameliorated. This therapy, however, could only serve as a bridge to eventual dual bowel and liver transplant, since incomplete differentiation could present with several deleterious effects over time. Notably, through the use of widely available whole exome sequencing our ability to detect mutations in patients that present with intractable diarrhea or diarrhea has drastically improved, and more mutations in apical trafficking components will likely be found to be responsible for diarrheal states. We anticipate that exome sequencing of patients who present with severe unexplained neonatal diarrhea will likely become the standard of care. Optimistically, within the next decade not only will these diseases be diagnosed properly, but as organoid transplantation and genome editing (CRISPR, ZFN, GEEN etc.) technologies become more feasible therapeutic options, repair of mutations in *MYO5B*, *STX3*, and other mutations may provide viable treatment alternatives.

Summary

As a whole, the studies I have undertaken in the Goldenring laboratory over the past four years have been integral to uncovering the mechanism behind the pathophysiology of MVID. Although, it had been previously discovered that mutations in MYO5B caused MVID, no studies had determined how or why the disease occurred (Muller, Hess et al. 2008). We were able to recapitulate the MVID phenotype by knocking down MYO5B in CaCo2-BBE cells. By rescuing our CaCo2-BBE MYO5B-KD cell lines with either Rab8a- or Rab11a-selective MYO5B mutants, we were able to separate the activity of MYO5B coupled Rab8a-dependent trafficking from Rab11a-

dependent trafficking. Rab8a-dependent trafficking appears to be involved in the initiation of microvilli, while Rab11a-dependent trafficking seems to be required for apical trafficking and microvilli elongation. Utilizing a similar approach, we knocked down Rab11a in CaCo2-BBE cells, and, with our collaborator Dr. Nan Gao, examined the small intestine of Rab11a$^{fl/fl}$;villin-cre^{+} mice. In both cases, loss of Rab11a appeared to decrease microvillar length in enterocytes, and concomitantly disrupted normal STX3 trafficking. Also, contrary to MVID dogma, we discovered that mutation of MYO5B appears to disrupt polarity throughout the entire gastrointestinal tract. Thus, this body of work has made great strides in furthering our understanding of general intestinal polarity, and the consequences of modifications to the fundamental trafficking machinery involved in maintaining intestinal polarity.

Future directions

Examining the effects of loss of MYO5B in MYO5B knockout mice

Introduction

In chapter two, we learned that loss of MYO5B can recapitulate some aspects of the MVID phenotype. In order to test whether this could be recapitulated *in vivo*, we obtained ES cell lines from the Knockout Mouse Project (KOMP) consortium, and, in collaboration with the Vanderbilt ES cell core facility, the ES cells were injected into albino C57BL/6 mice and produced chimeric founders. We then produced $MYO5B^{+/-}$ heterozygous mice and crossed these mice to obtain a germline knockout mouse. The direct $MYO5B^{-/-}$ knockout did not appear to be lethal, but the mouse was abnormally small and was sacrificed at 3 weeks. Initial examination did not show any distinct changes in the small intestine of this mouse. Unfortunately, we have been unable to produce another $MYO5B^{-/-}$ mouse, and as a result we bred heterozygous $MYO5B^{+/-}$ mice to FLP-expressing mice to delete the terminating cassette. We have begun breeding $MYO5B^{fl/fl}$ mice to villin-$creERT2^{+}$ for targeted deletion in enterocytes, and we have obtained $MYO5B^{fl/+}$;villin-$creERT2^{+}$ mice that are currently being bred to produce homozygous mice.

Research Design and Methods

We will evaluate the impact of conditional intestinal MYO5B loss in mice small intestines compared to littermates after tamoxifen induction by staining for polarity markers detailed in chapter two. Intestine and kidney tissue samples should be collected from neonates, newly weaned mice, and adult mice. The tissues will then be

examined for alterations in microvillar proteins, primary cilia (kidney tissue), junctional proteins, and apical-basolateral proteins. Samples will then be examined by SEM and TEM for structural alterations. Next, we will breed our mice to H/K-ATPase-CreERT2 mice, which will allow targeted inducible deletion of genes in gastric parietal cells, and we will examine the stomach tissue as described for the stomach in chapter four. In addition, we will utilize Dr. Karp's adenovirus cre system for liver-specific loss of MYO5B, and we will examine this tissue as described for the liver in chapter four.

Conditional intestinal MYO5B loss should mimic the phenotypic characteristics of MVID, which should allow us to assess the full scope of pathology associated with MYO5B-deficient enterocytes. In addition, the MYO5B$^{fl/fl}$ mice can be utilized to produce other targeted organ-specific knockouts. In the future, we will also evaluate the effects of MYO5B deletion in other key organs such as the kidney, lung, heart, and the brain using specific targeted cre recombinase mice. Ultimately, these mice could be used to investigate pharmacotherapy aimed at stabilizing the villus tips of the small intestine that is the primary source of the disease in MVID patients.

Potential Problems and Alternative Approaches

We have produced one germline MYO5B knockout mouse that did not appear to mimic the MVID phenotype as predicted. In chapter two, we reported that expression of MYO5B mutant in CaCo2-BBE MYO5B-KD cells exacerbated loss of polarity in these cells. If the MYO5B$^{fl/fl}$;villin-cre^{+} mice fail to mimic the MVID phenotype, a proven alternative for targeted inhibition of MYO5B action is the expression of MYO5B tail constructs that can act as dominant negative MYO5B. Thus, we could create a

transgenic mouse utilizing MYO5B tail or MYO5B-P660L constructs with floxed-stop that would allow the mutant MYO5B to be expressed following tamoxifen induction. These mice could then be bred with villin-cre mice foe intestine-specific MYO5B mutants, which should mimic the MVID phenotype.

Loss or mutation of MYO5B in kidney cells causes morphological changes to primary cilia

Introduction

In chapter four, we learned that mutations in MYO5B do not lead to an enterocyte specific phenotype contrary to the current MVID dogma. To examine the effects of the MYO5B reduction on polarity and apical trafficking in kidney cells we utilized a similar approach to what was undertaken in chapter two. For this study, lentiviral shRNA vectors targeting canine MYO5B and a scrambled control shRNA were utilized for transduction of MDCK cells (Roland, Bryant et al. 2011). We knocked down endogenous MYO5B MDCK cells, and then re-expressed MYO5B-P660L and MYO5B mutants with preferential binding for Rab8a, Rab10, or Rab11a. Morphologically in MYO5B-KD MDCK cell lines, primary cilia formation was disrupted. This is not surprising since primary cilia require normal Rab8a and Rab11a trafficking to form properly. We also performed correlative studies in MVID patient kidney samples and found similar disruption of primary cilia formation in these samples. Thus, if the MVID patients lived to adulthood they could develop other non-gastrointestinal tract related pathologies resembling Polycystic Kidney Disease or other ciliopathies because Rab8a and Rab11a are mislocalized (Knodler, Feng et al. 2010).

Research Design and Methods

The MDCK cells were transduced with lentiviral media produced in 293T cells and then selected in media containing puromycin. By quantitative PCR MYO5B mRNA expression was reduced by 50% compared with the scrambled control (data not shown). In a collaboration with the Mostov laboratory we have also created the following MDCK cell lines: mCherry-MYO5B-WT, mCherry-MYO5BΔD-WT (lacking Rab10 binding capacity), mCherry-MYO5BΔD-YE/QR (lacking Rab11a binding capacity), mCherry-MYO5BΔD-QL/YC (lacking Rab8a binding capacity), and mCherry-MYO5B-P660L (Navajo MVID mutation) (Roland, Bryant et al. 2011). Our preliminary data showed that MYO5B reduction in MDCK cells does not lead to a loss of apical microvilli or dispersion of Rab11a and Rab8a as we observed in the CaCo2-BBE MYO5B-KD cells. However, it does cause morphological changes in primary cilia in both the MDCK MYO5B-KD cells and MVID patient kidney tissue (Figure 41). These results suggest that some of the roles of MYO5B in these cells can be compensated. The mechanism behind this compensation and why only some trafficking processes are altered still remains to be elucidated.

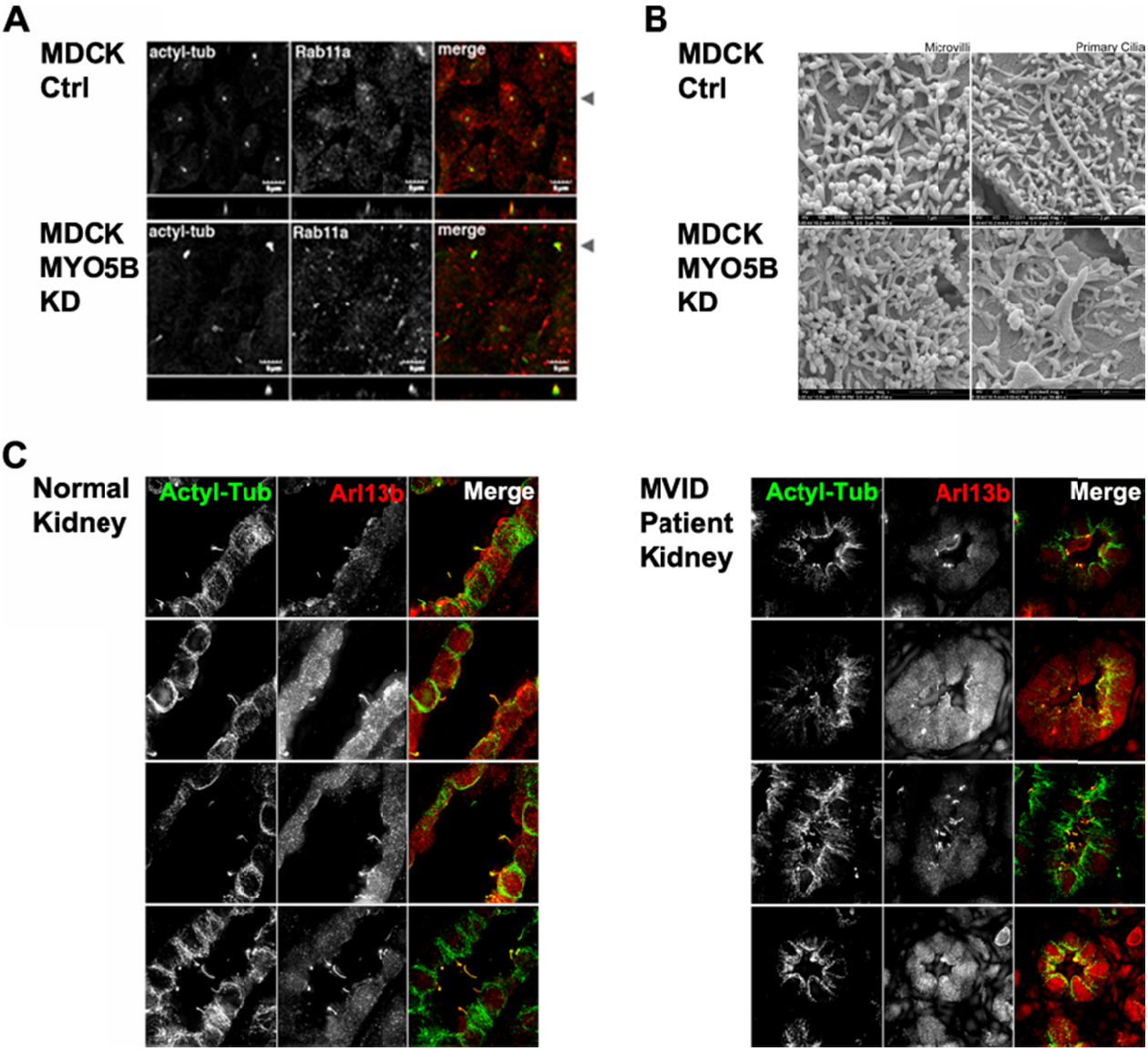

Figure 41. Loss or mutation of MYO5B causes deformation of primary cilia.
(A) MDCK cells co-stained with Rab11a (red) and acetylated tubulin (green). Top: Primary cilia in the control cells are long and thin. Bottom: Primary cilia in the MYO5B KD cells are thick and misshaped, and Rab11a is not dispersed. Image was generated by Dr. Lapierre. (B) SEM of apical surface of MDCK cell lines. Left: Microvilli in both the control and MYO5B KD cell lines are not disrupted. Right: Primary cilia in the MYO5B-KD cell line is thickened and has and abnormal shape. (C) SIM imaging of normal (left) and MVID (right) patient kidney tissue samples. Samples were stained for acetylated tubulin (green) and Arl13b (red). MVID patient kidney tissue displays misshaped primary cilia. Contrast enhancements of SIM images were adjusted separately, and initial images were generated by Dr. Lapierre.

Primary Cilia Characterization

Our preliminary studies in MDCK MYO5B-KD cells revealed misshaped, condensed primary cilia relative to the scramble control cells. This primary cilia formation defect is likely due to aberrant localization of Rab8a and Rab11a. Similar defects are present in MVID patient kidney samples, and over time this defect could lead to a Polycystic Kidney Disease-like phenotype. Disruption of primary cilia formation may also be the underlying cause of diseases that have been associated with MVID such as craniosynostosis, abnormal vertebrae, absent corpus callosum, and hydronephrosis (Salvatore 2007; Gathungu, Pashankar et al. 2008). To evaluate the integrity of the primary cilia and the contribution of the coordinated action of MYO5B with Rab8a and Rab11a, we will examine the cell lines we created to determine which Rab interaction are necessary in kidney cells for proper cilia formation. The cells will be fixed and immunostained for acetylated-tubulin, Arl13b, Rabin8, Rab11a, Rab8a, and F-actin. Cells will be imaged by confocal immunofluorescence microscopy to determine the effects on the primary cilia. We have also obtained gallbladder samples along with our kidney tissue, and we will be able to assess primary cilia alterations in other tissue types using the aforementioned antibodies and techniques, and compare the findings to the MDCK cell lines.

Potential Problems and Alternative Approaches

MVID patients do not generally live to adulthood due to their primary disease, and as a result kidney disease is generally never detected. Also, the patient tissue is limited and paraffin embedded, and we cannot utilize electron microscopy studies to

give us deeper insight the defects associated with MYO5B mutation. To circumvent these problems we can utilize MYO5B$^{fl/fl}$ mice discussed previously to generate MYO5B specific loss in the kidney epithelium. This will allow us to examine the results of MYO5B loss in adult mice to fully understand the complete consequences of deficits in apical trafficking on kidney primary cilia formation.

Determining the role of Myosin Vb in other Enteropathies

Introduction

Apical trafficking and recycling of cargo in polarized epithelial cells is integral to the identity and function of enterocytes, and as a result mutations in key components of this system would likely be evolutionarily unviable. In the general population, however, nonsynonymous SNPs are present in all components of the apical trafficking system (ESP 2014). Some of which should be detrimental, but they do not appear to directly cause known human diseases. This apparent paradox is reconciled in three parts. First, many of these mutations occur in only one of two alleles, and as a result might not cause noticeable symptoms. Second, our understanding of these proteins is based on studies utilizing expression of dominant negative constructs, which although powerful is an error prone approach to gage protein function. Finally, subtle changes are not easily detected by our current methods of detecting shifts in trafficking. The consequences of these subtle mutations in apical recycling in the human population are hard to predict, but studies done in the past decade have begun to shed light on the extreme end of this continuum. Homozygous or dominant negative mutations in *MYO5B*, *STX3*, and *STXBP2/Munc18-2* have been revealed as the causative agents for both Typical and

Atypical MVID. As a result a cascade of mutations in apical polarity proteins could circumvent systemic redundancy, and lead to relapsing and remitting intractable diarrhea.

Celiac disease is an autoimmune disorder that mainly affects the small intestine, and occurs in genetically predisposed individuals of all ages. Symptoms may include pain and distress in the digestive tract, fatigue, and diarrhea or constipation. Pathologically, after gliadin exposure the immune system cross reacts with the tissue of the small intestine triggering inflammation that in turn causes villus blunting and loss of microvilli, leading to malabsorption and diarrhea. In the United States, it is estimated that between 0.06% to 0.95% of the population has celiac disease, with European populations having a much higher prevalence of the disease (Rewers 2005).

Since the morphological characteristics in MVID overlap with those seen with celiac disease (villus blunting and diarrhea) we have hypothesized that mutations in *MYO5B*, *STX3*, *STXBP2* or other MYO5B related genes might account for populations of patients with celiac disease who fail to respond to gluten-free diet (10-15% of celiac patients) and/or similar enteropathies (Roshan, Leffler et al. 2011). Indeed we have identified one patient with 3 SNP variants in *MYO5B* sequence who has displayed relapsing and remitting symptoms of MVID for the past 21 years. An analysis of this patient MYO5B mutations suggests that the mutant MYO5B protein is more susceptible to degradation than wild type protein (Figure 42). However, it is unknown if this is the patient only mutation and the cause of this relapsing form of MVID. The paper described in the previous section, suggests that a mutations in the STX3 can cause Atypical MVID (Wiegerinck, Janecke et al. 2014). Therefore, we are now seeking to examine whether

patients with celiac disease who do not improve with gluten-free diets may have mutations in *MYO5B* that potentially destabilize the protein or other apical trafficking and recycling genes. To evaluate this possibility we will utilize both directed, whole exome, and eventually whole genome sequencing of our relapsing and remitting MVID patient and parents, and 7 patients with refractory celiac disease to look for other mutations that could be responsible for this variant form of MVID. Also, we will utilize BioVU to gain exome sequences of patients with celiac disease that responds to gluten free diets as a control, and other patient sequences with diarrhea as the cases to examine nonsynonymous SNPs in *MYO5B* and other MYO5B linked genes. It should be noted, that previous studies have reported discordant results as to the association of another myosin motor myosin-IXB and the development of celiac disease and refractory celiac disease Type II (Monsuur, de Bakker et al. 2005; Hunt, Monsuur et al. 2006). **This study aims to determine if polymorphisms or mutations in *MYO5B* or MYO5B linked genes are associated with refractory celiac disease and other similar enteropathies.**

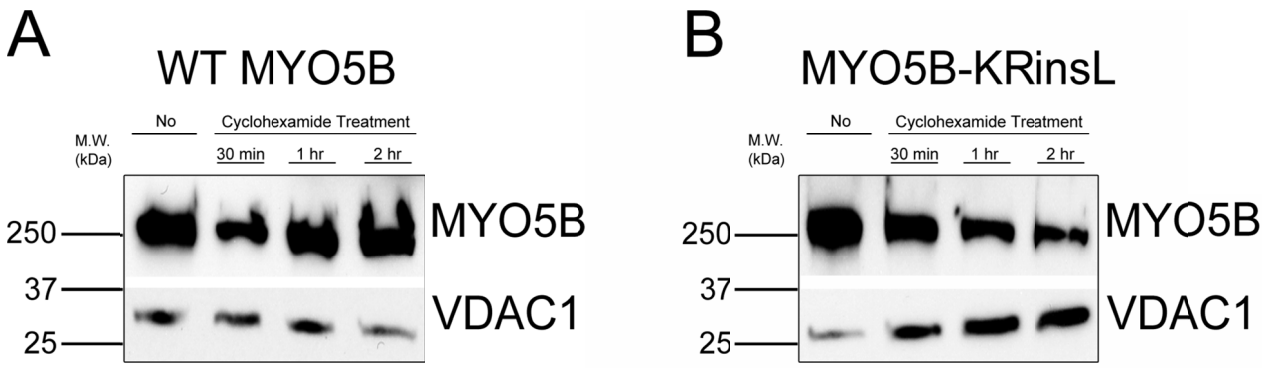

Figure 42. MYO5B-KRinsL appears to be less stable when compared to MYO5B-WT.
(A) MYO5B-WT expressed in HeLa cells does not appear to change significantly after cyclohexamide treatment up to two hours. (B) MYO5B-KRinsL expressed in HeLa cells appears to decrease after cyclohexamide treatment. Western blot generated by Dr. Schafer.

Preliminary Results

To establish the cause of our MVID patient's relapsing remitting phenotype we cloned the three mutations *MYO5B-KRinsL* (p.Lys380Asn, p.Arg989His, and Leu1129ins) that our patient had, as determined by previous collaboration with Dr. Erickson and Dr. Shub, into the synthetic mCherry MYO5B vector, and transfected both wild type and the relapsing remitting MYO5B-KRinsL into HeLa cells. The cells were then treated with cyclohexamide, and protein was collected for western blot analysis. By western blot analysis it was determined the MYO5B-KRinsL was unstable and was degraded faster than wild type (Figure 42). Interestingly, HeLa cells transfected with MYO5B-KRinsL show accumulation of MYO5B in large vesicles reminiscent of lysosomes. Both single and double mutant combinations of all three of our patient's mutations have been created to determine which mutant or combination of mutations is responsible for the instability of MYO5B-KRinsL in enterocytes. This data together with the new data on Atypical MVID, suggests that other gene mutations in both the Rab8a and Rab11a apical trafficking and fusion cascade in enterocytes may play a role in enterocyte polarity and ultimately the principle function of these cells to absorb nutrients (Wiegerinck, Janecke et al. 2014). The consequence of defects in either trafficking cascade appears to cause intractable diarrhea, which may have been incorrectly diagnosed until now.

Research Design and Methods

The presentation of our patient with relapsing and remitting MVID and our initial preliminary studies suggests that contrary to the MVID dogma *MYO5B* mutations can

present clinically as non-lethal and less severe diarrhea. Our preliminary studies suggest that SNPs that destabilize MYO5B may cause diarrhea. Also, a recent publication suggests that other genes involved in the cell surface-recycling pathway may lead to a variant form of MVID (Wiegerinck, Janecke et al. 2014). MVID is one of the most profoundly detrimental infantile diarrheal diseases, and if mutations in *MYO5B* or MYO5B associated genes can not only cause MVID but can also lead to refractory celiac disease or other diarrheal states the implications of this cannot be overstated. Our preliminary studies suggest that SNPs that destabilize *MYO5B* may cause diarrhea. **Our hypothesis is that refractory celiac disease type I is caused by variant SNPs in stability hotspots in *MYO5B*, and might work in conjunction with apical trafficking and fusion cascade gene mutations resulting in a diarrheal state that is triggered by a cellular stress response, which stops the synthesis of new MYO5B protein.** Our production of single and double mutant combinations of all three of our patient's mutations, along with other possible apical trafficking and fusion cascade gene mutations identified by whole exome sequencing, will allow us to test which of these mutations is responsible for destabilization of MYO5B. This will allow us to not only focus on the relevant SNP variants, but will also allow us to functionally test the consequences of our patient's SNPs on enterocytes ability to recover from cellular stress response using our CaCo2-BBE MYO5B-KD cell line. We have chosen to focus on our patient with relapsing and remitting MVID mutations because of the ability to compare findings in the cellular model that we will create with human tissue.

The sequencing part of our study will be done in two phases. Initially, we will sequence *MYO5B* in the 7 refractory celiac disease DNA samples obtained from our

collaborators at the Mayo clinic, and compare the results to NCBI and BioVU reference exome sequences. We will also perform directed exome sequencing utilizing GeneRead DNAseq Custom Panel, and total genome sequencing to look for other SNP variants that could affect the apical recycling pathway. In the second phase, we will utilize BioVU and the Illumina Infinium HumanExome BeadChip. Using the record counter we have determined that 747 patients meet our criteria for inclusion in this study, and these patients have exome sequences in the synthetic derivative. The refractory celiac disease phenotype of these patients will be defined further by a manual review of the patient's de-identified medical record. We will have two control groups in this study. The first will be patients with no history of chronic diarrhea, and the second will be celiac disease patients that are responsive to a gluten-free diet. Using this data we will be able to define the full extent of the association of SNPs in *MYO5B* and MYO5B associated genes with refractory celiac disease using linear regression. To functionally test the consequences of these new SNPs on enterocytes ability to recover from cellular stress response we will utilize knockdown in CaCo2-BBE cell lines, and we will clone these new mutations into mCherry constructs for rescue. Since this is an initial screening protocol, detailed power calculations are not necessary.

Characterization of the Instability Hotspot of MYO5B

Synthetic mCherry-MYO5B-K, mCherry-MYO5B-R, mCherry-MYO5B-insL, mCherry-MYO5B-KR, mCherry-MYO5B-KinsL, and mCherry-MYO5B-RinsL will be transfected into CaCo2-BBE cells. The cells will then be treated with cyclohexamide, and protein will be collected for westerns. By western blot analysis it will be determined which mutation or pair of mutations contributes to the instability of MYO5B protein in

enterocytes. Using the CaCo2-BBE MYO5B KD cells that we have developed previously we will rescue this cell line with mCherry-MYO5B-WT, m-Cherry-MYO5B-KRinsL, mCherry-MYO5B-K, mCherry-MYO5B-R, mCherry-MYO5B-insL, mCherry-MYO5B-KR, mCherry-MYO5B-KinsL, and mCherry-MYO5B-RinsL in order to determine the functional consequences of MYO5B instability. These cells will be grown on Transwell filters for 15 days, and imaged using scanning electron microscopy and confocal microscopy to determine the state of their microvilli and polarity. Finally, these cell lines will be subjected to cellular stress by treating them with IFN-alpha/beta cocktail for 3 days, and then re-imaged initially and 3 days after treatment.

Refractory Celiac Disease Patient Samples Directed and Whole Exome Sequencing

Operating in concert with Vanderbilt University School of Medicine's VAnderbilt Technologies for Advanced Genomics (VANTAGE) initially we will apply directed sequencing using GeneRead DNAseq Custom Panel including: MYO5B, DBN1, EZR, SNAP25, STX3, VAMP2, and VAMP8. The results of which will be analyzed using Vanderbilt Technologies for Advanced Genomics Analysis and Research Design (VANGARD) for quantitative analysis of genomic data generated. This preliminary analysis will be followed by whole exome sequencing utilizing Infinium HumanExome BeadChip Kit. Finally, whole genome sequencing using shotgun sequencing of DNA fragments with standard short-insert paired-end libraries. As with the previous experiment, we will utilize VANGARD for quantitative analysis.

Analysis of BioVU samples

Using the record counter in BioVU we have already determined that 747 patients meet our criteria for inclusion in this study, have exome sequences in the synthetic derivative, and samples available for DNA sequencing (Table 2). We will analyze these patient's SNPs to determine the association between refractory celiac disease and *MYO5B* and MYO5B associated genes. According to previous studies 10% of celiac disease patients have refractory celiac disease, but this might not be representative of the sequenced exome data within the synthetic derivative.

Relapsing and remitting MVID patient appear phenotypically as refractory celiac disease. However, other intestinal malabsorption diseases also present in a very similar manner. Using the record counter in BioVU we have already determined that 195 patients with unspecified intestinal malabsorption ICD-9 code (579.9), 5 patients with tropical sprue ICD-9 code (579.1), and 110 patients with other specified intestinal malabsorption ICD-9 code (579.8) have exome sequences in the synthetic derivative, and we can analyze these patient's SNPs to determine the association between these intestinal malabsorption diseases and *MYO5B* and MYO5B associated genes.

Functional Characterization of Novel Mutations in MYO5B in BioVU Patient Samples

Using knockdowns in CaCo2-BBE cells we will rescue these cell lines with novel synthetic *MYO5B* and MYO5B associated mutations found in patient samples to determine the functional consequences of MYO5B mutations in concert with novel nonsynonymous SNPs on the stability of enterocyte polarity and function. These cells will then be characterized as described previously for the instability hotspot of MYO5B.

Table 2. BioVU Sample Criteria

Exclude Where:	Include Where:
Contains ICD code in group 042-Human immunodeficiency virus (HIV) disease	Genotyping for Illumina Infinium HumanExome BeadChip
Age Between 45 and 64	Contains ICD code 579-Intestinal malabsorption ~~ 2 or more
Age Greater Than or Equal To 65	Contains ICD code 579.0-Celiac disease ~~ 2 or more
Contains ICD code in group 129-Intestinal parasitism, unspecified	Contains ICD code 579.8-Other specified intestinal malabsorption ~~ 2 or more
Contains ICD code in group 004-Shigellosis	Contains ICD code 579.9-Unspecified intestinal malabsorption ~~ 2 or more
Contains ICD code in group 001-Cholera	Contains ICD code 787.91-Diarrhea ~~ 3 or more
Contains ICD code in group 005-Other food poisoning (bacterial)	

Potential Problems and Alternative Approaches

Our primary analysis of the functional consequences of hotspot mutation in MYO5B will focus on the behavior of cells on permeable filters, because this method has been well-established for looking at CaCo2 cell polarity. However, our lab has previously described that cells grown on filters can overcome some trafficking and polarity deficits. 3-D cultures using gels made of collagen can overcome this shortcoming, and our lab has recently obtained considerable experience in the analysis of epithelial cells in 3-D culture. We can therefore also analyze many of the same standards of polarity and apical trafficking in 3-D cultures of CaCo2 cells, which can form polarized cysts and tubular structures.

Mutation of MYO5B is responsible for MVID, but no direct link between MYO5B and refractory celiac disease has been made. Our previous studies have demonstrated that Rab8a and Rab11a lie upstream of MYO5B in the enterocyte polarity cascade, and as a result the refractory celiac disease mutation may be present in these genes. If the sequences of MYO5B in refractory celiac disease and other malabsorption disease patients do not reveal mutation within the instability hotspot of MYO5B these genes should be the next sequencing target. These genes are highly conserved in humans, and are subjected to little variants. This is due to the short sequences that they have, and because mutation of these genes have detrimental effects across many cell types. A mutation in these genes that changes the function is not likely, but could result in a diarrheal phenotype as observed in the Rab8a knockout mouse.

One of the principal limitations of exome sequencing is only being able to identify those variants found in the coding region of genes which affect protein function. However, for our purposes since we only wish to interrogate mutations that would lead to protein malfunction analyzing data obtained from exome sequencing is ideal.

Knockdown of key polarity proteins in CaCo2-BBE cells might not be viable, and cells might not be able to overcome loss of polarity to stabilize on Transwell filters. However, our lab has recently begun to utilize Ls174T-W4 cells that polarize as single cells on plastic with doxycycline stimulation. This system could be used to evaluate the knockdowns without polarizing on Transwell filters for 15 days.

REFERENCES

Achler, C., D. Filmer, et al. (1989). "Role of microtubules in polarized delivery of apical membrane proteins to the brush border of the intestinal epithelium." The Journal of cell biology **109**(1): 179-189.

Ameen, N. A. and P. J. Salas (2000). "Microvillus inclusion disease: a genetic defect affecting apical membrane protein traffic in intestinal epithelium." Traffic **1**(1): 76-83.

Ammar, D. A., P. N. Nguyen, et al. (2001). "Functionally distinct pools of actin in secretory cells." American journal of physiology. Cell physiology **281**(2): C407-417.

Arpin, M. C., T.; Louvard, D. (1999). Cross-talk between Apical and Basolateral Domains of Epithelial Cells Regulates Microvillus Assembly. Epithelial Morphogenesis in Development and Disease. W. B. Birchmeier, Carmen. Amsterdam, Harwood Academic**:** 95-116.

Atwood, S. X., C. Chabu, et al. (2007). "Cdc42 acts downstream of Bazooka to regulate neuroblast polarity through Par-6 aPKC." Journal of cell science **120**(Pt 18): 3200-3206.

Babbey, C. M., R. L. Bacallao, et al. (2010). "Rab10 associates with primary cilia and the exocyst complex in renal epithelial cells." American journal of physiology. Renal physiology **299**(3): F495-506.

Baetz, N. W. and J. R. Goldenring (2013). "Rab11-family interacting proteins define spatially and temporally distinct regions within the dynamic Rab11a-dependent recycling system." Molecular biology of the cell **24**(5): 643-658.

Band, A. M. and E. Kuismanen (2005). "Localization of plasma membrane t-SNAREs syntaxin 2 and 3 in intracellular compartments." BMC Cell Biology **6**(1): 26.

Black, J. A., T. M. Forte, et al. (1981). "Inhibition of HCl secretion and the effects on ultrastructure and electrical resistance in isolated piglet gastric mucosa." Gastroenterology **81**(3): 509-519.

Bonifacino, J. S. (2014). "Adaptor proteins involved in polarized sorting." The Journal of cell biology **204**(1): 7-17.

Bonifacino, J. S. and L. M. Traub (2003). "Signals for sorting of transmembrane proteins to endosomes and lysosomes." Annual review of biochemistry **72**: 395-447.

Brock, S. C., J. R. Goldenring, et al. (2003). "Apical recycling systems regulate directional budding of respiratory syncytial virus from polarized epithelial cells." Proc Natl Acad Sci U S A **100**(25): 15143-15148.

Bryant, D. M., A. Datta, et al. (2010). "A molecular network for de novo generation of the apical surface and lumen." Nature cell biology **12**(11): 1035-1045.

Bryant, D. M. and K. E. Mostov (2008). "From cells to organs: building polarized tissue." Nat Rev Mol Cell Biol **9**(11): 887-901.

Cabezas, A., K. Pattni, et al. (2006). "Cloning and subcellular localization of a human phosphatidylinositol 3-phosphate 5-kinase, PIKfyve/Fab1." Gene **371**(1): 34-41.

Cai, D., D. P. McEwen, et al. (2009). "Single molecule imaging reveals differences in microtubule track selection between Kinesin motors." PLoS biology **7**(10): e1000216.

Calhoun, B. C., L. A. Lapierre, et al. (1998). "Rab11a redistributes to apical secretory canaliculus during stimulation of gastric parietal cells." The American journal of physiology **275**(1 Pt 1): C163-170.

Capaldo, C. T. and I. G. Macara (2007). "Depletion of E-cadherin disrupts establishment but not maintenance of cell junctions in Madin-Darby canine kidney epithelial cells." Molecular biology of the cell **18**(1): 189-200.

Carmosino, M., G. Valenti, et al. (2010). "Polarized traffic towards the cell surface: how to find the route." Biology of the cell / under the auspices of the European Cell Biology Organization **102**(2): 75-91.

Casanova, J. E., X. Wang, et al. (1999). "Association of Rab25 and Rab11a with the apical recycling system of polarized Madin-Darby canine kidney cells." Molecular biology of the cell **10**(1): 47-61.

Chang, J., M. R. Chance, et al. (2008). "Proteomic changes during intestinal cell maturation in vivo." Journal of proteomics **71**(5): 530-546.

Chehade, M. S., Scott H (2005). Infantile food protein-induced enterocolitis syndrome. Recent Advances in Paediatrics T. J. David. London, Royal Society of Medicine Press. **22:** 140.

Chen, C. P., M. C. Chiang, et al. (2010). "Microvillus inclusion disease: prenatal ultrasound findings, molecular diagnosis and genetic counseling of congenital diarrhea." Taiwanese journal of obstetrics & gynecology **49**(4): 487-494.

Chiang, M. C., J. F. Hsu, et al. (2013). "Bowel "Dissection" in Microvillus Inclusion Disease." Pediatrics and neonatology: In Press.

Crawley, S. W., D. A. Shifrin, Jr., et al. (2014). "Intestinal brush border assembly driven by protocadherin-based intermicrovillar adhesion." Cell **157**(2): 433-446.

Cresawn, K. O., B. A. Potter, et al. (2007). "Differential involvement of endocytic compartments in the biosynthetic traffic of apical proteins." EMBO J **26**(16): 3737-3748.

Cutz, E., J. M. Rhoads, et al. (1989). "Microvillus inclusion disease: an inherited defect of brush-border assembly and differentiation." N Engl J Med **320**(10): 646-651.

Davidson, G. P., E. Cutz, et al. (1978). "Familial enteropathy: a syndrome of protracted diarrhea from birth, failure to thrive, and hypoplastic villus atrophy." Gastroenterology **75**(5): 783-790.

De La Cruz, E. M., A. L. Wells, et al. (1999). "The kinetic mechanism of myosin V." Proc Natl Acad Sci U S A **96**(24): 13726-13731.

De Matteis, M. A., A. Di Campli, et al. (2007). "Lipid-transfer proteins in membrane trafficking at the Golgi complex." Biochimica et biophysica acta **1771**(6): 761-768.

De Matteis, M. A. and A. Godi (2004). "PI-loting membrane traffic." Nature cell biology **6**(6): 487-492.

Delprato, A., E. Merithew, et al. (2004). "Structure, exchange determinants, and family-wide rab specificity of the tandem helical bundle and Vps9 domains of Rabex-5." Cell **118**(5): 607-617.

Desclozeaux, M., J. Venturato, et al. (2008). "Active Rab11 and functional recycling endosome are required for E-cadherin trafficking and lumen formation during epithelial morphogenesis." American journal of physiology. Cell physiology **295**(2): C545-556.

Dhekne, H. S., N. H. Hsiao, et al. (2014). "Myosin Vb and Rab11a regulate phosphorylation of ezrin in enterocytes." Journal of cell science **127**(Pt 5): 1007-1017.

Dingemans, K. P. (1969). "The relation between cilia and mitoses in the mouse adenohypophysis." The Journal of cell biology **43**(2): 361-367.

Ducharme, N. A., A. J. Ham, et al. (2011). "Rab11-FIP2 influences multiple components of the endosomal system in polarized MDCK cells." Cellular logistics **1**(2): 57-68.

Duman, J. G., K. Tyagarajan, et al. (1999). "Expression of rab11a N124I in gastric parietal cells inhibits stimulatory recruitment of the H+-K+-ATPase." The American journal of physiology **277**(3 Pt 1): C361-372.

Ellis, M. A., B. A. Potter, et al. (2006). "Polarized biosynthetic traffic in renal epithelial cells: sorting, sorting, everywhere." American journal of physiology. Renal physiology **291**(4): F707-713.

Erickson, R. P., K. Larson-Thome, et al. (2008). "Navajo microvillous inclusion disease is due to a mutation in MYO5B." Am J Med Genet A **146A**(24): 3117-3119.

ESP. (2014). "Exome Variant Server NHLBI GO Exome Sequencing Project (ESP)." Retrieved May 15, 2014 accessed, 2014, from http://evs.gs.washington.edu/EVS/.

Fan, S., T. W. Hurd, et al. (2004). "Polarity proteins control ciliogenesis via kinesin motor interactions." Current biology : CB **14**(16): 1451-1461.

Feng, S., A. Knodler, et al. (2012). "A Rab8 guanine nucleotide exchange factor-effector interaction network regulates primary ciliogenesis." The Journal of biological chemistry **287**(19): 15602-15609.

Ferkol, T. W. and M. W. Leigh (2012). "Ciliopathies: the central role of cilia in a spectrum of pediatric disorders." The Journal of pediatrics **160**(3): 366-371.

Ferrary, E., M. Cohen-Tannoudji, et al. (1999). "In vivo, villin is required for Ca(2+)-dependent F-actin disruption in intestinal brush borders." The Journal of cell biology **146**(4): 819-830.

Fielding, A. B., E. Schonteich, et al. (2005). "Rab11-FIP3 and FIP4 interact with Arf6 and the exocyst to control membrane traffic in cytokinesis." The EMBO journal **24**(19): 3389-3399.

Follit, J. A., F. Xu, et al. (2009). "Characterization of mouse IFT complex B." Cell motility and the cytoskeleton **66**(8): 457-468.

Fonte, V. G., R. L. Searls, et al. (1971). "The relationship of cilia with cell division and differentiation." The Journal of cell biology **49**(1): 226-229.

Forte, G. M., L. Limlomwongse, et al. (1969). "The development of intracellular membranes concomitant with the appearance of HCl secretion in oxyntic cells of the metamorphosing bullfrog tadpole." Journal of cell science **4**(3): 709-727.

Forte, J. G., A. L. Ganser, et al. (1974). "The K+-stimulated ATPase system of microsomal membranes from gastric oxyntic cells." Annals of the New York Academy of Sciences **242**(0): 255-267.

Forte, J. G., D. K. Hanzel, et al. (1989). "Pumps and pathways for gastric HCl secretion." Annals of the New York Academy of Sciences **574**: 145-158.

Forte, J. G., L. Limlomwongse, et al. (1969). "Ion transport and the development of hydrogen ion secretion in the stomach of the metamorphosing bullfrog tadpole." The Journal of general physiology **54**(1): 76-95.

Forte, J. G. and L. Zhu (2010). "Apical recycling of the gastric parietal cell H,K-ATPase." Annual review of physiology **72**: 273-296.

Forte, T. M., T. E. Machen, et al. (1977). "Ultrastructural changes in oxyntic cells associated with secretory function: a membrane-recycling hypothesis." Gastroenterology **73**(4 Pt 2): 941-955.

Fukumoto, Y., Y. Shintani, et al. (2008). "The regulatory or phosphorylation domain of p120 catenin controls E-cadherin dynamics at the plasma membrane." Experimental cell research **314**(1): 52-67.

Fuller, S. D. and K. Simons (1986). "Transferrin receptor polarity and recycling accuracy in "tight" and "leaky" strains of Madin-Darby canine kidney cells." The Journal of cell biology **103**(5): 1767-1779.

Furuse, M., M. Hata, et al. (2002). "Claudin-based tight junctions are crucial for the mammalian epidermal barrier: a lesson from claudin-1-deficient mice." The Journal of cell biology **156**(6): 1099-1111.

Garbett, D., D. P. LaLonde, et al. (2010). "The scaffolding protein EBP50 regulates microvillar assembly in a phosphorylation-dependent manner." The Journal of cell biology **191**(2): 397-413.

Gassama-Diagne, A., W. Yu, et al. (2006). "Phosphatidylinositol-3,4,5-trisphosphate regulates the formation of the basolateral plasma membrane in epithelial cells." Nature cell biology **8**(9): 963-970.

Gathungu, G. N., D. S. Pashankar, et al. (2008). "Microvillus inclusion disease associated with coarctation of the aorta and bicuspid aortic valve." J Clin Gastroenterol **42**(4): 400-403.

Gilbert, T. and E. Rodriguez-Boulan (1991). "Induction of vacuolar apical compartments in the Caco-2 intestinal epithelial cell line." Journal of cell science **100 (Pt 3)**: 451-458.

Girard, E., D. Chmiest, et al. (2014). "Rab7 is functionally required for selective cargo sorting at the early endosome." Traffic **15**(3): 309-326.

Girard, M., F. Lacaille, et al. (2013). "MYO5B and BSEP contribute to cholestatic liver disorder in Microvillous Inclusion Disease." Hepatology.

Gloerich, M., J. P. ten Klooster, et al. (2012). "Rap2A links intestinal cell polarity to brush border formation." Nature cell biology **14**(8): 793-801.

Goh, L. K., F. Huang, et al. (2010). "Multiple mechanisms collectively regulate clathrin-mediated endocytosis of the epidermal growth factor receptor." The Journal of cell biology **189**(5): 871-883.

Golachowska, M. R., C. M. Dael, et al. (2011). "Divergent Effects of MYO5B Mutations on Apical Brush Border and Apical Recycling Endosome Organization in Kidney and Intestinal Epithelial Cells of Microvillus Inclusion Disease Patients Presenting with Transient Renal Fanconi Syndrome." Journal of Pediatric Gastroenterology and Nutrition.

Goldenring, J. R. (2013). "A central role for vesicle trafficking in epithelial neoplasia: intracellular highways to carcinogenesis." Nature reviews. Cancer **13**(11): 813-820.

Goldenring, J. R., C. J. Soroka, et al. (1994). "Enrichment of rab11, a small GTP-binding protein, in gastric parietal cells." The American journal of physiology **267**(2 Pt 1): G187-194.

Grant, B. D. and J. G. Donaldson (2009). "Pathways and mechanisms of endocytic recycling." Nature reviews. Molecular cell biology **10**(9): 597-608.

Grigoriev, I., D. Splinter, et al. (2007). "Rab6 regulates transport and targeting of exocytotic carriers." Developmental cell **13**(2): 305-314.

Groisman, G. M., M. Amar, et al. (2002). "CD10: a valuable tool for the light microscopic diagnosis of microvillous inclusion disease (familial microvillous atrophy)." Am J Surg Pathol **26**(7): 902-907.

Grosshans, B. L., D. Ortiz, et al. (2006). "Rabs and their effectors: achieving specificity in membrane traffic." Proceedings of the National Academy of Sciences of the United States of America **103**(32): 11821-11827.

Guarino, A., A. Lo Vecchio, et al. (2012). "Chronic diarrhoea in children." Best practice & research. Clinical gastroenterology **26**(5): 649-661.

Gut, A., F. Kappeler, et al. (1998). "Carbohydrate-mediated Golgi to cell surface transport and apical targeting of membrane proteins." The EMBO journal **17**(7): 1919-1929.

Halac, U., F. Lacaille, et al. (2011). "Microvillous inclusion disease: how to improve the prognosis of a severe congenital enterocyte disorder." J Pediatr Gastroenterol Nutr **52**(4): 460-465.

Hales, C. M., R. Griner, et al. (2001). "Identification and characterization of a family of Rab11-interacting proteins." J Biol Chem **276**(42): 39067-39075.

Heiska, L., K. Alfthan, et al. (1998). "Association of ezrin with intercellular adhesion molecule-1 and -2 (ICAM-1 and ICAM-2). Regulation by phosphatidylinositol 4, 5-bisphosphate." The Journal of biological chemistry **273**(34): 21893-21900.

Hickson, G. R., J. Matheson, et al. (2003). "Arfophilins are dual Arf/Rab 11 binding proteins that regulate recycling endosome distribution and are related to Drosophila nuclear fallout." Molecular biology of the cell **14**(7): 2908-2920.

Hokanson, D. E. and A. P. Bretscher (2012). "EPI64 interacts with Slp1/JFC1 to coordinate Rab8a and Arf6 membrane trafficking." Molecular biology of the cell **23**(4): 701-715.

Holubcova, Z., G. Howard, et al. (2013). "Vesicles modulate an actin network for asymmetric spindle positioning." Nature cell biology **15**(8): 937-947.

Hopkins, C. R. and I. S. Trowbridge (1983). "Internalization and processing of transferrin and the transferrin receptor in human carcinoma A431 cells." The Journal of cell biology **97**(2): 508-521.

Horgan, C. P., S. R. Hanscom, et al. (2010). "Rab11-FIP3 links the Rab11 GTPase and cytoplasmic dynein to mediate transport to the endosomal-recycling compartment." Journal of cell science **123**(Pt 2): 181-191.

Hubbard, A. L., B. Stieger, et al. (1989). "Biogenesis of endogenous plasma membrane proteins in epithelial cells." Annual review of physiology **51**: 755-770.

Hunt, K. A., A. J. Monsuur, et al. (2006). "Lack of association of MYO9B genetic variants with coeliac disease in a British cohort." Gut **55**(7): 969-972.

Ikonen, E. and K. Simons (1998). "Protein and lipid sorting from the trans-Golgi network to the plasma membrane in polarized cells." Seminars in cell & developmental biology **9**(5): 503-509.

Ishikura, S. and A. Klip (2008). "Muscle cells engage Rab8A and myosin Vb in insulin-dependent GLUT4 translocation." Am J Physiol Cell Physiol **295**(4): C1016-1025.

Jayasundar, J. J., J. H. Ju, et al. (2012). "Open conformation of ezrin bound to phosphatidylinositol 4,5-bisphosphate and to F-actin revealed by neutron scattering." The Journal of biological chemistry **287**(44): 37119-37133.

Jin, H., S. R. White, et al. (2010). "The conserved Bardet-Biedl syndrome proteins assemble a coat that traffics membrane proteins to cilia." Cell **141**(7): 1208-1219.

Kajiho, H., K. Sakurai, et al. (2011). "Characterization of RIN3 as a guanine nucleotide exchange factor for the Rab5 subfamily GTPase Rab31." The Journal of biological chemistry **286**(27): 24364-24373.

Kaplan, O. I., A. Molla-Herman, et al. (2010). "The AP-1 clathrin adaptor facilitates cilium formation and functions with RAB-8 in C. elegans ciliary membrane transport." J Cell Sci **123**(Pt 22): 3966-3977.

Karvar, S., X. Yao, et al. (2002). "Localization and function of soluble N-ethylmaleimide-sensitive factor attachment protein-25 and vesicle-associated membrane protein-2 in functioning gastric parietal cells." The Journal of biological chemistry **277**(51): 50030-50035.

Kelly, E. E., C. P. Horgan, et al. (2010). "Class I Rab11-family interacting proteins are binding targets for the Rab14 GTPase." Biology of the cell / under the auspices of the European Cell Biology Organization **102**(1): 51-62.

Kitt, K. N., D. Hernandez-Deviez, et al. (2008). "Rab14 regulates apical targeting in polarized epithelial cells." Traffic **9**(7): 1218-1231.

Knodler, A., S. Feng, et al. (2010). "Coordination of Rab8 and Rab11 in primary ciliogenesis." Proc Natl Acad Sci U S A **107**(14): 6346-6351.

Knowles, B. C., J. T. Roland, et al. (2014). "MYO5B uncoupling from Rab8a and Rab11a elicits microvillus inclusion disease." Journal of Clinical Investigation **In Press**.

Knowles, B. C., J. T. Roland, et al. (2014). "Myosin Vb uncoupling from RAB8A and RAB11A elicits microvillus inclusion disease." The Journal of clinical investigation.

Kodera, N., D. Yamamoto, et al. (2010). "Video imaging of walking myosin V by high-speed atomic force microscopy." Nature **468**(7320): 72-76.

Krishnan, M., L. A. Lapierre, et al. (2013). "Rab25 regulates integrin expression in polarized colonic epithelial cells." Molecular biology of the cell **24**(6): 818-831.

Lakadamyali, M., M. J. Rust, et al. (2006). "Ligands for clathrin-mediated endocytosis are differentially sorted into distinct populations of early endosomes." Cell **124**(5): 997-1009.

Lake, B. D. (1988). "Microvillus inclusion disease: specific diagnostic features shown by alkaline phosphatase histochemistry." Journal of clinical pathology **41**(8): 880-882.

Lanzetti, L., A. Palamidessi, et al. (2004). "Rab5 is a signalling GTPase involved in actin remodelling by receptor tyrosine kinases." Nature **429**(6989): 309-314.

Lapierre, L. A., K. M. Avant, et al. (2007). "Characterization of immunoisolated human gastric parietal cells tubulovesicles: identification of regulators of apical recycling." American journal of physiology. Gastrointestinal and liver physiology **292**(5): G1249-1262.

Lapierre, L. A., K. M. Avant, et al. (2012). "Phosphorylation of Rab11-FIP2 regulates polarity in MDCK cells." Molecular biology of the cell **23**(12): 2302-2318.

Lapierre, L. A., R. Kumar, et al. (2001). "Myosin vb is associated with plasma membrane recycling systems." Molecular biology of the cell **12**(6): 1843-1857.

Lapierre, L. A., R. Kumar, et al. (2001). "Myosin vb is associated with plasma membrane recycling systems." Mol Biol Cell **12**(6): 1843-1857.

Lawe, D. C., A. Chawla, et al. (2002). "Sequential roles for phosphatidylinositol 3-phosphate and Rab5 in tethering and fusion of early endosomes via their interaction with EEA1." The Journal of biological chemistry **277**(10): 8611-8617.

Lehtonen, S., E. Lehtonen, et al. (1999). "Vesicular transport and kidney development." The International journal of developmental biology **43**(5): 425-433.

Leung, S. M., W. G. Ruiz, et al. (2000). "Sorting of membrane and fluid at the apical pole of polarized Madin-Darby canine kidney cells." Molecular biology of the cell **11**(6): 2131-2150.

Lim, Y. S., C. E. Chua, et al. (2011). "Rabs and other small GTPases in ciliary transport." Biol Cell **103**(5): 209-221.

Lock, J. G. and J. L. Stow (2005). "Rab11 in recycling endosomes regulates the sorting and basolateral transport of E-cadherin." Molecular biology of the cell **16**(4): 1744-1755.

Mammoto, A., T. Ohtsuka, et al. (1999). "Rab11BP/Rabphilin-11, a downstream target of rab11 small G protein implicated in vesicle recycling." The Journal of biological chemistry **274**(36): 25517-25524.

Marchelletta, R. R., D. T. Jacobs, et al. (2008). "The class V myosin motor, myosin 5c, localizes to mature secretory vesicles and facilitates exocytosis in lacrimal acini." American journal of physiology. Cell physiology **295**(1): C13-28.

Mari, M., M. V. Bujny, et al. (2008). "SNX1 defines an early endosomal recycling exit for sortilin and mannose 6-phosphate receptors." Traffic **9**(3): 380-393.

Marrs, J. A., C. Andersson-Fisone, et al. (1995). "Plasticity in epithelial cell phenotype: modulation by expression of different cadherin cell adhesion molecules." The Journal of cell biology **129**(2): 507-519.

Martin-Belmonte, F., A. Gassama, et al. (2007). "PTEN-mediated apical segregation of phosphoinositides controls epithelial morphogenesis through Cdc42." Cell **128**(2): 383-397.

Matsui, Y., A. Kikuchi, et al. (1990). "Molecular cloning and characterization of a novel type of regulatory protein (GDI) for smg p25A, a ras p21-like GTP-binding protein." Mol Cell Biol **10**(8): 4116-4122.

Matsukawa, J., K. Nakayama, et al. (2003). "Role of ADP-ribosylation factor 6 (ARF6) in gastric acid secretion." The Journal of biological chemistry **278**(38): 36470-36475.

Matter, K., M. Brauchbar, et al. (1990). "Sorting of endogenous plasma membrane proteins occurs from two sites in cultured human intestinal epithelial cells (Caco-2)." Cell **60**(3): 429-437.

Mazelova, J., L. Astuto-Gribble, et al. (2009). "Ciliary targeting motif VxPx directs assembly of a trafficking module through Arf4." The EMBO journal **28**(3): 183-192.

Mazelova, J., N. Ransom, et al. (2009). "Syntaxin 3 and SNAP-25 pairing, regulated by omega-3 docosahexaenoic acid, controls the delivery of rhodopsin for the biogenesis of cilia-derived sensory organelles, the rod outer segments." Journal of cell science **122**(Pt 12): 2003-2013.

Mazerik, J. N. and M. J. Tyska (2012). "Myosin-1A targets to microvilli using multiple membrane binding motifs in the tail homology 1 (TH1) domain." The Journal of biological chemistry **287**(16): 13104-13115.

Mehta, A. D., R. S. Rock, et al. (1999). "Myosin-V is a processive actin-based motor." Nature **400**(6744): 590-593.

Melendez, J., M. Liu, et al. (2013). "Cdc42 coordinates proliferation, polarity, migration, and differentiation of small intestinal epithelial cells in mice." Gastroenterology **145**(4): 808-819.

Mellman, I. (1996). "Endocytosis and molecular sorting." Annual review of cell and developmental biology **12**: 575-625.

Mills, I. G., A. T. Jones, et al. (1998). "Involvement of the endosomal autoantigen EEA1 in homotypic fusion of early endosomes." Current biology : CB **8**(15): 881-884.

Mishra, R., M. Grzybek, et al. (2010). "Galectin-9 trafficking regulates apical-basal polarity in Madin-Darby canine kidney epithelial cells." Proceedings of the National Academy of Sciences of the United States of America **107**(41): 17633-17638.

Misura, K. M., R. H. Scheller, et al. (2000). "Three-dimensional structure of the neuronal-Sec1-syntaxin 1a complex." Nature **404**(6776): 355-362.

Monsuur, A. J., P. I. de Bakker, et al. (2005). "Myosin IXB variant increases the risk of celiac disease and points toward a primary intestinal barrier defect." Nature genetics **37**(12): 1341-1344.

Mooseker, M. S. (1985). "Organization, chemistry, and assembly of the cytoskeletal apparatus of the intestinal brush border." Annual review of cell biology **1**: 209-241.

Mooseker, M. S. and L. G. Tilney (1975). "Organization of an actin filament-membrane complex. Filament polarity and membrane attachment in the microvilli of intestinal epithelial cells." The Journal of cell biology **67**(3): 725-743.

Muller, T., M. W. Hess, et al. (2008). "MYO5B mutations cause microvillus inclusion disease and disrupt epithelial cell polarity." Nat Genet **40**(10): 1163-1165.

Muller, T., M. W. Hess, et al. (2008). "MYO5B mutations cause microvillus inclusion disease and disrupt epithelial cell polarity." Nature genetics **40**(10): 1163-1165.

Nachury, M. V., A. V. Loktev, et al. (2007). "A core complex of BBS proteins cooperates with the GTPase Rab8 to promote ciliary membrane biogenesis." Cell **129**(6): 1201-1213.

Nachury, M. V., E. S. Seeley, et al. (2010). "Trafficking to the ciliary membrane: how to get across the periciliary diffusion barrier?" Annu Rev Cell Dev Biol **26**: 59-87.

Naslavsky, N., M. Boehm, et al. (2004). "Rabenosyn-5 and EHD1 interact and sequentially regulate protein recycling to the plasma membrane." Molecular biology of the cell **15**(5): 2410-2422.

Nedvetsky, P. I., E. Stefan, et al. (2007). "A Role of myosin Vb and Rab11-FIP2 in the aquaporin-2 shuttle." Traffic **8**(2): 110-123.

Nelson, W. J., R. Wilson, et al. (1992). "Regulation of epithelial cell polarity: a view from the cell surface." Cold Spring Harbor symposia on quantitative biology **57**: 621-630.

Niggli, V., C. Andreoli, et al. (1995). "Identification of a phosphatidylinositol-4,5-bisphosphate-binding domain in the N-terminal region of ezrin." FEBS letters **376**(3): 172-176.

Nokes, R. L., I. C. Fields, et al. (2008). "Rab13 regulates membrane trafficking between TGN and recycling endosomes in polarized epithelial cells." The Journal of cell biology **182**(5): 845-853.

Novick, P. and M. Zerial (1997). "The diversity of Rab proteins in vesicle transport." Curr Opin Cell Biol **9**(4): 496-504.

Oatman, O., C. Djedjos, et al. (2013). "Diabetes in Microvillus Inclusion Disease." Journal of Pediatric Gastroenterology and Nutrition.

Oliva, M. M., J. A. Perman, et al. (1994). "Successful intestinal transplantation for microvillus inclusion disease." Gastroenterology **106**(3): 771-774.

Omori, Y., C. Zhao, et al. (2008). "Elipsa is an early determinant of ciliogenesis that links the IFT particle to membrane-associated small GTPase Rab8." Nature cell biology **10**(4): 437-444.

Overgaard, C. E., K. M. Sanzone, et al. (2009). "Deciliation is associated with dramatic remodeling of epithelial cell junctions and surface domains." Molecular biology of the cell **20**(1): 102-113.

Pandey, K. N. (2010). "Small peptide recognition sequence for intracellular sorting." Current opinion in biotechnology **21**(5): 611-620.

Pastural, E., F. J. Barrat, et al. (1997). "Griscelli disease maps to chromosome 15q21 and is associated with mutations in the myosin-Va gene." Nature genetics **16**(3): 289-292.

Peterson, M. D. and M. S. Mooseker (1992). "Characterization of the enterocyte-like brush border cytoskeleton of the C2BBe clones of the human intestinal cell line, Caco-2." J Cell Sci **102 (Pt 3)**: 581-600.

Pierobon, P., S. Achouri, et al. (2009). "Velocity, processivity, and individual steps of single myosin V molecules in live cells." Biophysical journal **96**(10): 4268-4275.

Pierobon, P., S. Achouri, et al. (2009). "Velocity, processivity, and individual steps of single myosin V molecules in live cells." Biophys J **96**(10): 4268-4275.

Pinson, K. I., L. Dunbar, et al. (1998). "Targeted disruption of the mouse villin gene does not impair the morphogenesis of microvilli." Developmental dynamics : an official publication of the American Association of Anatomists **211**(1): 109-121.

Pocard, T., A. Le Bivic, et al. (2007). "Distinct v-SNAREs regulate direct and indirect apical delivery in polarized epithelial cells." Journal of cell science **120**(Pt 18): 3309-3320.

Pohl, J. F., M. D. Shub, et al. (1999). "A cluster of microvillous inclusion disease in the Navajo population." J Pediatr **134**(1): 103-106.

Provance, D. W., E. Addison, et al. (2008). "Myosin-Vb functions as a dynamic tether for peripheral endocytic compartments during transferrin trafficking." BMC Cell Biology **9**(1): 44.

Qi, M., J. A. Williams, et al. (2013). "Rab11-FIP1C and Rab14 direct plasma membrane sorting and particle incorporation of the HIV-1 envelope glycoprotein complex." PLoS pathogens **9**(4): e1003278.

Qin, Y., W. H. Meisen, et al. (2010). "Tuba, a Cdc42 GEF, is required for polarized spindle orientation during epithelial cyst formation." The Journal of cell biology **189**(4): 661-669.

Rafelski, S. M. and J. A. Theriot (2005). "Bacterial shape and ActA distribution affect initiation of Listeria monocytogenes actin-based motility." Biophysical journal **89**(3): 2146-2158.

Reales, E., N. Sharma, et al. (2011). "Basolateral sorting of syntaxin 4 is dependent on its N-terminal domain and the AP1B clathrin adaptor, and required for the epithelial cell polarity." PLoS One **6**(6): e21181.

Reinshagen, K., H. Y. Naim, et al. (2002). "Autophagocytosis of the apical membrane in microvillus inclusion disease." Gut **51**(4): 514-521.

Rewers, M. (2005). "Epidemiology of celiac disease: what are the prevalence, incidence, and progression of celiac disease?" Gastroenterology **128**(4 Suppl 1): S47-51.

Reynolds, A. B. (2007). "p120-catenin: Past and present." Biochimica et biophysica acta **1773**(1): 2-7.

Rhoads, J. M., R. C. Vogler, et al. (1991). "Microvillus inclusion disease. In vitro jejunal electrolyte transport." Gastroenterology **100**(3): 811-817.

Rickman, C., C. N. Medine, et al. (2007). "Functionally and spatially distinct modes of munc18-syntaxin 1 interaction." The Journal of biological chemistry **282**(16): 12097-12103.

Rief, M., R. S. Rock, et al. (2000). "Myosin-V stepping kinetics: a molecular model for processivity." Proc Natl Acad Sci U S A **97**(17): 9482-9486.

Rodriguez-Boulan, E. and I. G. Macara (2014). "Organization and execution of the epithelial polarity programme." Nature reviews. Molecular cell biology **15**(4): 225-242.

Rodriguez-Boulan, E. and S. K. Powell (1992). "Polarity of epithelial and neuronal cells." Annual review of cell biology **8**: 395-427.

Rodriguez, O. C. and R. E. Cheney (2002). "Human myosin-Vc is a novel class V myosin expressed in epithelial cells." J Cell Sci **115**(Pt 5): 991-1004.

Rojas, R., T. van Vlijmen, et al. (2008). "Regulation of retromer recruitment to endosomes by sequential action of Rab5 and Rab7." The Journal of cell biology **183**(3): 513-526.

Roland, J., A. Kenworthy, et al. (2007). "Myosin Vb Interacts with Rab8a on a tubular network containing EHD1 and EHD3." Mol Biol Cell **18**: 2828 - 2837.

Roland, J. T., D. M. Bryant, et al. (2011). "Rab GTPase-Myo5B complexes control membrane recycling and epithelial polarization." Proc Natl Acad Sci U S A **108**(7): 2789-2794.

Roland, J. T., L. A. Lapierre, et al. (2009). "Alternative splicing in class V myosins determines association with Rab10." J Biol Chem **284**(2): 1213-1223.

Rosenfeld, G. C., E. McAllister, et al. (1981). "Cytochalasin inhibition of isolated rat gastric parietal cell function." Journal of cellular physiology **109**(1): 53-57.

Roshan, B., D. A. Leffler, et al. (2011). "The incidence and clinical spectrum of refractory celiac disease in a north american referral center." The American journal of gastroenterology **106**(5): 923-928.

Ruemmele, F. M., T. Muller, et al. (2010). "Loss-of-function of MYO5B is the main cause of microvillus inclusion disease: 15 novel mutations and a CaCo-2 RNAi cell model." Hum Mutat **31**(5): 544-551.

Sakamori, R., S. Das, et al. (2012). "Cdc42 and Rab8a are critical for intestinal stem cell division, survival, and differentiation in mice." The Journal of clinical investigation **122**(3): 1052-1065.

Salvatore, S. H., B.; Vandenplas, Y (2007). Chronic enteropathy and feeding. Nutrition Support for Infants and Children at Risk. R. J. V. Cooke, Yvan; Wahn, Ulrich. . Basel, Switzerland; New York, Karger**:** 123.

Saotome, I., M. Curto, et al. (2004). "Ezrin is essential for epithelial organization and villus morphogenesis in the developing intestine." Developmental cell **6**(6): 855-864.

Sato, T., T. Iwano, et al. (2014). "Rab8a and Rab8b are essential for several apical transport pathways but insufficient for ciliogenesis." Journal of cell science **127**(Pt 2): 422-431.

Sato, T., S. Mushiake, et al. (2007). "The Rab8 GTPase regulates apical protein localization in intestinal cells." Nature **448**(7151): 366-369.

Sawaguchi, A., F. Aoyama, et al. (2006). "Ultrastructural transformation of gastric parietal cells reverting from the active to the resting state of acid secretion revealed in isolated rat gastric mucosa model processed by high-pressure freezing." Journal of electron microscopy **55**(2): 97-105.

Schafer, J. C., N. W. Baetz, et al. (2014). "Rab11-FIP2 Interaction with MYO5B Regulates Movement of Rab11a-Containing Recycling Vesicles." Traffic **15**(3): 292-308.

Schonteich, E., G. M. Wilson, et al. (2008). "The Rip11/Rab11-FIP5 and kinesin II complex regulates endocytic protein recycling." Journal of cell science **121**(Pt 22): 3824-3833.

Schuck, S., M. J. Gerl, et al. (2007). "Rab10 is involved in basolateral transport in polarized Madin-Darby canine kidney cells." Traffic **8**(1): 47-60.

Schwartz, S. L., C. Cao, et al. (2007). "Rab GTPases at a glance." J Cell Sci **120**(Pt 22): 3905-3910.

Serrador, J. M., M. Vicente-Manzanares, et al. (2002). "A novel serine-rich motif in the intercellular adhesion molecule 3 is critical for its ezrin/radixin/moesin-directed subcellular targeting." The Journal of biological chemistry **277**(12): 10400-10409.

Sfakianos, J., A. Togawa, et al. (2007). "Par3 functions in the biogenesis of the primary cilium in polarized epithelial cells." The Journal of cell biology **179**(6): 1133-1140.

Shapiro, L. and W. I. Weis (2009). "Structure and biochemistry of cadherins and catenins." Cold Spring Harbor perspectives in biology **1**(3): a003053.

Sharma, M., N. Naslavsky, et al. (2008). "A role for EHD4 in the regulation of early endosomal transport." Traffic **9**(6): 995-1018.

Sharma, N., S. H. Low, et al. (2006). "Apical targeting of syntaxin 3 is essential for epithelial cell polarity." The Journal of cell biology **173**(6): 937-948.

Simons, K. and G. van Meer (1988). "Lipid sorting in epithelial cells." Biochemistry **27**(17): 6197-6202.

Singh, B., G. Bogatcheva, et al. (2013). "Transformation of polarized epithelial cells by apical mistrafficking of epiregulin." Proceedings of the National Academy of Sciences of the United States of America **110**(22): 8960-8965.

Soldati, T. and M. Schliwa (2006). "Powering membrane traffic in endocytosis and recycling." Nat Rev Mol Cell Biol **7**(12): 897-908.

Sonnichsen, B., S. De Renzis, et al. (2000). "Distinct membrane domains on endosomes in the recycling pathway visualized by multicolor imaging of Rab4, Rab5, and Rab11." J Cell Biol **149**: 901 - 914.

Stechly, L., W. Morelle, et al. (2009). "Galectin-4-regulated delivery of glycoproteins to the brush border membrane of enterocyte-like cells." Traffic **10**(4): 438-450.

Stenmark, H. (2009). "Rab GTPases as coordinators of vesicle traffic." Nature reviews. Molecular cell biology **10**(8): 513-525.

Stenmark, H., R. Aasland, et al. (2002). "The phosphatidylinositol 3-phosphate-binding FYVE finger." FEBS letters **513**(1): 77-84.

Stenmark, H., R. G. Parton, et al. (1994). "Inhibition of rab5 GTPase activity stimulates membrane fusion in endocytosis." The EMBO journal **13**(6): 1287-1296.

Stepensky, P., J. Bartram, et al. (2013). "Persistent defective membrane trafficking in epithelial cells of patients with familial hemophagocytic lymphohistiocytosis type 5 due to STXBP2/MUNC18-2 mutations." Pediatric blood & cancer **60**(7): 1215-1222.

Strick, D. J. and L. A. Elferink (2005). "Rab15 effector protein: a novel protein for receptor recycling from the endocytic recycling compartment." Molecular biology of the cell **16**(12): 5699-5709.

Szperl, A. M., M. R. Golachowska, et al. (2011). "Functional characterization of mutations in the myosin Vb gene associated with microvillus inclusion disease." J Pediatr Gastroenterol Nutr **52**(3): 307-313.

Takagishi, Y. and Y. Murata (2006). "Myosin Va mutation in rats is an animal model for the human hereditary neurological disease, Griscelli syndrome type 1." Annals of the New York Academy of Sciences **1086**: 66-80.

Takahashi, S., K. Kubo, et al. (2012). "Rab11 regulates exocytosis of recycling vesicles at the plasma membrane." Journal of cell science **125**(Pt 17): 4049-4057.

ten Klooster, J. P., M. Jansen, et al. (2009). "Mst4 and Ezrin induce brush borders downstream of the Lkb1/Strad/Mo25 polarization complex." Developmental cell **16**(4): 551-562.

ter Beest, M. B., S. J. Chapin, et al. (2005). "The role of syntaxins in the specificity of vesicle targeting in polarized epithelial cells." Molecular biology of the cell **16**(12): 5784-5792.

Thoeni, C. E., G. F. Vogel, et al. (2013). "Microvillus inclusion disease: loss of myosin Vb disrupts intracellular traffic and cell polarity." Traffic.

Treyer, A. and A. Musch (2013). "Hepatocyte polarity." Comprehensive Physiology **3**(1): 243-287.

Turunen, O., T. Wahlstrom, et al. (1994). "Ezrin has a COOH-terminal actin-binding site that is conserved in the ezrin protein family." The Journal of cell biology **126**(6): 1445-1453.

Tyska, M. J., A. T. Mackey, et al. (2005). "Myosin-1a is critical for normal brush border structure and composition." Molecular biology of the cell **16**(5): 2443-2457.

Ullrich, O., H. Horiuchi, et al. (1994). "Membrane association of Rab5 mediated by GDP-dissociation inhibitor and accompanied by GDP/GTP exchange." Nature **368**(6467): 157-160.

Ullrich, O., S. Reinsch, et al. (1996). "Rab11 regulates recycling through the pericentriolar recycling endosome." The Journal of cell biology **135**(4): 913-924.

van der Velde, K. J., H. S. Dhekne, et al. (2013). "An Overview and Online Registry of Microvillus Inclusion Disease Patients and their MYO5B Mutations." Human mutation.

Van Itallie, C. M. and J. M. Anderson (2006). "Claudins and epithelial paracellular transport." Annual review of physiology **68**: 403-429.

Vandrangi, P., D. D. Lo, et al. (2013). "Electrostatic properties of confluent Caco-2 cell layer correlates to their microvilli growth and determines underlying transcellular flow." Biotechnology and bioengineering **110**(10): 2742-2748.

Varthakavi, V., R. Smith, et al. (2006). "The pericentriolar recycling endosome plays a key role in Vpu-mediated enhancement of HIV-1 particle release." Traffic **7**: 298 - 307.

Vega-Salas, D. E., P. J. Salas, et al. (1988). "Exocytosis of vacuolar apical compartment (VAC): a cell-cell contact controlled mechanism for the establishment of the apical plasma membrane domain in epithelial cells." The Journal of cell biology **107**(5): 1717-1728.

Velvarska, H. and D. Niessing (2013). "Structural insights into the globular tails of the human type v myosins Myo5a, Myo5b, And Myo5c." PLoS One **8**(12): e82065.

Verhage, M., A. S. Maia, et al. (2000). "Synaptic assembly of the brain in the absence of neurotransmitter secretion." Science **287**(5454): 864-869.

Wakabayashi, Y., P. Dutt, et al. (2005). "Rab11a and myosin Vb are required for bile canalicular formation in WIF-B9 cells." Proc Natl Acad Sci USA **102**: 15087 - 15092.

Wakabayashi, Y., P. Dutt, et al. (2005). "Rab11a and myosin Vb are required for bile canalicular formation in WIF-B9 cells." Proc Natl Acad Sci U S A **102**(42): 15087-15092.

Wang, J. T., M. C. Kerr, et al. (2010). "The SNX-PX-BAR family in macropinocytosis: the regulation of macropinosome formation by SNX-PX-BAR proteins." PLoS One **5**(10): e13763.

Ward, E. S., C. Martinez, et al. (2005). "From sorting endosomes to exocytosis: association of Rab4 and Rab11 GTPases with the Fc receptor, FcRn, during recycling." Molecular biology of the cell **16**(4): 2028-2038.

Weisz, O. A. and E. Rodriguez-Boulan (2009). "Apical trafficking in epithelial cells: signals, clusters and motors." J Cell Sci **122**(Pt 23): 4253-4266.

Westlake, C. J., L. M. Baye, et al. (2011). "Primary cilia membrane assembly is initiated by Rab11 and transport protein particle II (TRAPPII) complex-dependent trafficking of Rabin8 to the centrosome." Proceedings of the National Academy of Sciences of the United States of America **108**(7): 2759-2764.

Wiegerinck, C. L., A. R. Janecke, et al. (2014). "Loss of Syntaxin 3 Causes Variant Microvillus Inclusion Disease." Gastroenterology.

Willenborg, C., J. Jing, et al. (2011). "Interaction between FIP5 and SNX18 regulates epithelial lumen formation." The Journal of cell biology **195**(1): 71-86.

Wu, J., D. J. Mariner, et al. (1998). "Production and characterization of monoclonal antibodies to the catenin p120ctn." Hybridoma **17**(2): 175-183.

Yanagisawa, M., D. Huveldt, et al. (2008). "A p120 catenin isoform switch affects Rho activity, induces tumor cell invasion, and predicts metastatic disease." The Journal of biological chemistry **283**(26): 18344-18354.

Yao, X., A. Thibodeau, et al. (1993). "Ezrin-calpain I interactions in gastric parietal cells." The American journal of physiology **265**(1 Pt 1): C36-46.

Yeaman, C., K. K. Grindstaff, et al. (1999). "New perspectives on mechanisms involved in generating epithelial cell polarity." Physiological reviews **79**(1): 73-98.

Yeaman, C., A. H. Le Gall, et al. (1997). "The O-glycosylated stalk domain is required for apical sorting of neurotrophin receptors in polarized MDCK cells." The Journal of cell biology **139**(4): 929-940.

Yu, S., Y. Nie, et al. (2014). "TLR Sorting by Rab11 Endosome in Enterocyte Maintains Intestinal Epithelial-Microbial Homeostasis." The EMBO Journal **In Press**.

Zhang, X. M., S. Ellis, et al. (2004). "Sec15 is an effector for the Rab11 GTPase in mammalian cells." The Journal of biological chemistry **279**(41): 43027-43034.

Zhou, R., L. Zhu, et al. (2005). "Phosphorylation of ezrin on threonine 567 produces a change in secretory phenotype and repolarizes the gastric parietal cell." Journal of cell science **118**(Pt 19): 4381-4391.

Zhu, L., J. Crothers, Jr., et al. (2010). "A possible mechanism for ezrin to establish epithelial cell polarity." American journal of physiology. Cell physiology **299**(2): C431-443.

Zhu, L., R. Zhou, et al. (2007). "High turnover of ezrin T567 phosphorylation: conformation, activity, and cellular function." American journal of physiology. Cell physiology **293**(3): C874-884.

Zuo, X., W. Guo, et al. (2009). "The exocyst protein Sec10 is necessary for primary ciliogenesis and cystogenesis in vitro." Molecular biology of the cell **20**(10): 2522-2529.

Zwaenepoel, I., A. Naba, et al. (2012). "Ezrin regulates microvillus morphogenesis by promoting distinct activities of Eps8 proteins." Molecular biology of the cell **23**(6): 1080-1094.